Titre: Title:	Processing and properties of PLA/thermoplastic starch/montmorillonite nanocomposites
Auteur: Author:	Oscar Henry Arroyo Fernández
Date:	2008
Type:	Mémoire ou thèse / Dissertation or Thesis
Référence: Citation:	Arroyo Fernández, O. H. (2008). Processing and properties of PLA/thermoplastic starch/montmorillonite nanocomposites [Master's thesis, École Polytechnique de Montréal]. PolyPublie. https://publications.polymtl.ca/8312/

UNIVERSITÉ DE MONTRÉAL

PROCESSING AND PROPERTIES OF PLA/THERMOPLASTIC STARCH/MONTMORILLONITE NANOCOMPOSITES

OSCAR HENRY ARROYO FERNÁNDEZ

DÉPARTEMENT DE GÉNIE CHIMIQUE
ÉCOLE POLYTECHNIQUE DE MONTRÉAL

MÉMOIRE PRÉSENTÉ EN VUE DE L'OBTENTION
DU DIPLÔME DE MAÎTRISE ÈS SCIENCES APPLIQUÉES
(GÉNIE CHIMIQUE)
JUIN 2008

Your file Votre référence
ISBN: 978-0-494-46029-0
Our file Notre référence
ISBN: 978-0-494-46029-0

UNIVERSITÉ DE MONTRÉAL

ÉCOLE POLYTECHNIQUE DE MONTRÉAL

Ce mémoire intitulé:

PROCESSING AND PROPERTIES OF PLA/THERMOPLASTIC STARCH/MONTMORILLONITE NANOCOMPOSITES

présenté par: ARROYO FERNÁNDEZ, Oscar Henry
en vue de l'obtention du diplôme de : Maîtrise ès sciences appliquées
a été dûment accepté par le jury d'examen constitué de :

M. FRADETTE Louis, Ph.D., président
M. FAVIS Basil D., Ph.D., membre et directeur de recherche
M. HUNEAULT Michel , Ph.D., membre et codirecteur de recherche
Mme DENAULT Johanne, Ph.D., membre

Dedicado a

Mi padre Oscar, mi madre Matilde

y a mi amada esposa Mariela

ACKNOWLEDGEMENTS

I would like to express my gratitude to my research and thesis director Professor Michael Huneault for providing the opportunity to study under his supervision. I am very grateful for his support, guidance, motivation and great patience since my first day in Canada through the duration of my studies. I certainly enjoyed all conversations with him including the scientific ones. His realistic, precise and optimistic attitude toward scientific research does and holds a positive influence on my vision about research.

I would also like to thank my research director Professor Basil D. Favis for his invaluable support during my work and for his tenacity and enthusiastic during lectures and in research.

My sincere gratitude to other professors, researchers and technical staff of the Industrial Materials Institute, in special to Florence Perrin, Michel Carmel and the Chemical Engineering Department at the Ecole Polytechnique de Montreal for their invaluable help in my research.

I would also like to thank my colleagues and friends in the group Mihaela, Aurelie, Sepehr, Pierre Sarazin, Nick, Zhenyu, Pouneah, Sara, Gang, Prashant, Claire, Pierre, Danut, and Ata. To my friends Claudia, Martha, Farhad, Saeedeh, Samaneh, Antoine, Lilian, Jing Mahasta, Amin, Babak, Gaetan, Jaqueline, Gloria, Hong Bo, Shant, Shima, Camille, Alexander, Jairo, Maryam, Karen, Isabelle, Yolima, Olivier, Cristian, Diego, Beatriz, Judith, Raul for their friendship, help and cooperation during my studies and for the good moments that we share together.

My thanks also go to my mother Matilde for her love and for teaching me that with God, all things are possible. To my father Oscar and my sisters Sheila, Sharon and

Carolina thanks for their faith, love and encouragement during this time even when far away in distance from them. To my parents in law, Lidia and Eduardo Rodriguez for their encouragement as well as my new sister Betsabe. To Camila, Dante, Facundo, Andres, Carlos and Abraham for their support during this time.

My gratitude and love to Mariela, my beloved wife, for her love, care, faith, patience, hope and for never giving up in optimism during this project as a little part of our life.

And to God, and although God is nominee at the end, God will always be first in our lives.

RÉSUMÉ

Cette étude est focalisée sur l'évaluation des propriétés et de la structure de nanocomposites TPS/PLA/MMT en utilisant le PLA greffé avec anhydride maléique comme agent assurant la compatibilité du mélange TPS/PLA et du PLA/MMT. Les mélanges nanocomposites ont été préparés par extrusion en utilisant une extrudeuse à double vis co-rotative et une stratégie d'exfoliation de l'argile dans l'eau.

Les granules d'amidon, le glycérol et le MMT ont été mélangés mécaniquement de façon intensive pour produire une mixture très homogène nommée suspension amidon-MMT. La concentration en glycérol a été fixée tel que dans le TPS obtenu finalement il atteint 36%. Les deux formulations obtenues pour cette étude sont 27%TPS/PLA et 60%TPS/PLA.

Dans toutes les formulations où le MMT a été ajouté dans la suspension initiale d'amidon, les mélanges TPS/PLA, indifféremment s'ils contiennent le PLAg ou pas, ont montré une intercalation partielle dans le MMT. Ce fait a été conclu à partir des spectres obtenus en diffractions des rayons X qui montrent que l'espacement de base entre couches du MMT dans le mélange augmente comparativement au MMT pur. Cette intercalation partielle entre les galeries de l'argile a été observée aussi en technique MET en utilisant des hautes magnifications et ont confirmé les résultats XRD.

Les propriétés mécaniques de nanocomposites on été analysées en utilisant un test de tension standard. Les résultats ont montré que le module d'élasticité et la résistance en traction du PLA et du PLAg atteignaient des valeurs similaires. Pour les mélanges TPS/PLA, des légères augmentations de l'élongation à la rupture ont été observées par

rapport au PLA. L'addition de PLAg comme agent assurant la compatibilité entre le TPS et le PLA a mené à une augmentation de l'élongation à la rupture de 50-60%. L'introduction de 2%MMT naturel dans les mélanges 27%TPS/PLA et 60%TPS/PLA a montré une importante augmentation du module et une légère diminution de la résistance en traction.

La méthode de *Essential work of fracture* (EWF) a été utilisée pour étudier la ténacité des matériaux nanocomposites TPS/PLA. Les résultats obtenus par cette méthode ont montré que la ténacité à la fracture du mélange TPS/PLAg est supérieure à celle du TPS/PLA. Ce résultat est un effet de l'augmentation de l'adhésion interfaciale entre les deux phases engendrée par l'utilisation du PLA greffé, et aussi un effet d'un meilleur transfert de la contrainte entre la matrice PLAg et la phase TPS. L'ajout de 2%MMT dans le mélange TPS/PLA, sans ou avec PLAg, a produit une réduction significative de la ténacité à la fracture.

Des tests en DSC ont été réalisés pour quelques mélanges TPS/PLA et MMT nanocomposites pour étudier l'effet de la présence de la phase TPS et du MMT dans la cristallisation du PLA. Dans les mélanges 27%TPS/PLA et 60%TPS/PLA, l'addition de TPS au PLA a produit une légère augmentation du taux de cristallisation du PLA. Un taux de cristallisation similaire a été observé pour le mélange avec PLAg. Une augmentation supplémentaire du taux de cristallisation du PLA a été produite après l'introduction de 2% de MMT dans les mélanges TPS/PLA. La présence de MMT en concentration très faible et sous forme intercalée ou sous forme d'agrégats a augmenté le

taux de cristallisation du PLA ou PLAg. Le MMT a joué le rôle d'agent de nucléation dans la cristallisation du PLA en augmentant le nombre possible de nucléés.

Des changements dans les transitions thermiques autour de la Tg ont été rapportés pour les mélanges TPS/PLA en fonction du temps. Des échantillons de mélanges TPS/PLA et TPS/PLAg ont été équilibrés à la température de 25°C et une humidité relative de 50% entre 7 et 300 jours.

ABSTRACT

The current study focus on the properties and structure of TPS/PLA/MMT nanocomposites using maleic anhydride grafted PLA as a compatibilizer in TPS/PLA blends and PLA/MMT. The nanocomposites were prepared by melt extrusion using a co-rotating twin-screw extruder and an original water exfoliation strategy.

Dry starch, water, glycerol and MMT were intensively mechanically mixed to produce a homogeneous suspension, known as starch-MMT slurry. The glycerol content was set to 36 wt% relative to the final TPS phase after water was removed. Two TPS formulations were studied 27%TPS/PLA and 60%TPS/PLA.

In all formulations where MMT was added in starch slurry, TPS/PLA blends, with or without grafted PLA, exhibited partial intercalation into the MMT interlayers based on the increment of basal spacing of the MMT compared with basal spacing for the neat MMT illustrated by XRD spectra. This partial intercalation inside the clay galleries was observed by high magnification TEMs pictures in accordance with the XRD results.

The mechanical properties of the nanocomposites were analyzed by a standard tensile test. Results showed the tensile moduli and tensile strength of neat PLA and grafted PLAg reached similar values. For TPS/PLA blends, slight increments in elongation at break were registered with respect to neat PLA. The use of grafted PLAg as a compatibilizer between TPS and PLA showed increment of 50-60% in elongation at break with respect to neat PLA. The addition of 2% wt of natural MMT in 27%TPS/PLA and 60%TPS/PLA showed a significant increment of the tensile moduli with a slight reduction in the tensile strength.

The essential work of fracture (EWF) method was used to study the fracture toughness in TPS/PLA nanocomposites. Results using the EWF method indicated that fracture toughness in TPS/PLAg blends exhibit superior performance than in TPS blended with neat PLA. This behavior can be due to the effect of increment of interfacial adhesion generated by the use of grafted PLA and better stress transfer between the PLAg matrix and the soft TPS phase. The addition of 2% of MMT in TPS/PLA blends containing or not grafted PLA produced a significant reduction of fracture toughness in both cases.

To investigate the effect of TPS phase and MMT on PLA crystallization, DSC scans were performed for some TPS/PLA blends and MMT nanocomposites. In 27%TPS/PLA and 60%TPS/PLA blends, the addition of TPS on neat PLA produced a slight increment of the crystallization rate of PLA. However when TPS was added to the PLAg a similar PLA crystallization rate was found. The addition of 2% MMT in the TPS/PLA blends produced an additional increase in the crystallization rate of PLA. In this case the MMT clay in small amounts, in intercalated or aggregate form, increased the crystallization rate of PLA and PLAg. The clay layers or aggregates increased the number of possible nucleating agents for the crystallization of PLA.

Changes in thermal transitions around Tg in DSC thermograms for TPS/PLA blends, during different time periods, were reported. TPS/PLA and TPS/PLAg blends were aged at 25 °C and 50% relative humidity for periods of between 7 and 300 days.

CONDENSÉ EN FRANÇAIS

L'intérêt pour les polymères produits à partir de ressources naturelles renouvelables est de plus en plus important. Parmi ces composés, peuvent être retrouvés deux bioplastiques très prometteurs et disponibles commercialement : l'amidon thermoplastique (*thermoplastic starch* en anglais, TPS) et le polylactide (PLA).

L'amidon est hydrophile et complètement biodégradable dans l'eau et le sol. Le TPS est produit lorsque l'amidon est rendu non structuré par l'eau, la chaleur et les forces de cisaillement. Le PLA est un polyester aliphatique, thermoplastique biodégradable produit à partir de ressources renouvelables telles que l'amidon de maïs ou de cannes à sucre. Alors que le TPS est un polysaccharide présent à l'état naturel, le PLA requiert une synthèse chimique appelée polymérisation de monomères lactide par ouverture de cycles.

L'étude des polymères nanocomposites est un sujet de recherche croissant. Cet accroissement a fait suite aux résultats encourageants obtenus par Toyota dans les années 80 sur l'amélioration des propriétés mécaniques, de la stabilité thermique, de la température de distorsion à chaud sous charge, la résistance au feu et la perméabilité au gaz observées sur des nanocomposites formés de montmorillonite (MMT) et de polyamide-6. Un des buts des études sur les polymères nanocomposites est d'obtenir une intercalation et exfoliation complètes des couches de silicate dans la matrice de polymères. Ensuite, la surface en contact obtenue peut être jusqu'à 10 000 fois plus importante que pour les systèmes de charges conventionnelles. Une grande surface de contact et un grand rapport de forme (longueur/diamètre) des plaquettes de renforcement sont directement reliés aux améliorations finales des propriétés du nanocomposite.

Les nanotubes de carbone et les nanoargiles sont les nanoparticules les plus fréquemment utilisées afin de renforcer les polymères. La MMT, de l'argile naturel, appartient à la famille des silicates stratifiés. La MMT est caractérisée par une couche d'une épaisseur d'environ 1 nm, par une grande capacité d'échange de cations, par un rapport de forme contenu entre 30 et 1000 et par un module élastique élevé.

Plusieurs études ont permis des progrès sur les nanocomposites de TPS et de PLA utilisant de MMT naturelle (non modifiée) et de MMT modifiée organiquement. Il a été observé que l'addition de MMT naturelle permettait une plus grande dispersion, intercalation et exfoliation dans les composites de TPS/MMT que lorsque des MMT organiquement modifiées étaient utilisées. L'affinité entre les surfaces polaires de MMT et de TPS explique ces résultats. Des résultats opposés ont été trouvés pour les nanocomposites de PLA : à cause d'une incompatibilité entre la nature hydrophile de la MMT et une polarité moindre du PLA, l'utilisation de MMT naturelle ne permet pas une bonne exfoliation.

De plus, une grande dispersion a été observée pour le PLA lorsque des MMT organiquement modifiées ont été utilisées et permettent de former une structure intercalée.

La présente étude se concentre sur les propriétés et la structure de nanocomposites TPS/PLA/MMT utilisant de l'anhydride maléique comme agent comptabilisant dans les mélanges TPS/PLA et PLA/MMT. Les nanocomposites ont été préparés par extrusion en utilisant une extrudeuse à double vis co-rotative et une stratégie d'exfoliation par voie aqueuse originale.

L'amidon séché, le glycérol et la MMT sont mélangés mécaniquement pour produire une suspension d'amidon et de MMT dans un mélange homogène d'eau et de glycérol. Pour toutes les suspensions, le contenu en glycérol était de 36 % en masse relativement à la phase finale de TPS (sans eau). Deux formulations sont étudiées : 27 % TPS/PLA et 60 % TPS/PLA.

La suspension d'amidon/MMT est ensuite incorporée dans l'extrudeuse à double vis par une pompe gravimétrique afin de contrôler le débit massique. Dans la première partie de l'extrudeuse, à 130 °C, l'amidon subi un processus de déstructuration et de gélatinisation. À la fin de la première moitié de l'extrudeuse, l'eau est éliminée par dévolatilisation sous vide, afin d'obtenir un TPS sans eau avant incorporation du PLA, et ceci afin d'éviter la dégradation du PLA par l'eau. Ensuite, l'opération d'intercalation dans la MMT commence pour le TPS et l'eau permet d'augmenter l'exfoliation de l'argile. Du PLA ou du PLAg dans un état fondu, sont ajoutés dans la zone centrale de l'extrudeuse en utilisant une extrudeuse simple vis comme source d'alimentation à 180 °C. Dans la seconde moitié de l'extrudeuse, également à 180 °C, le TPS, le PLA et la MMT sont mélangés pour produire des nanocomposites TPS/PLA/MMT. À la dernière étape d'extrusion, des torons sont formés, refroidis sous l'eau puis formés afin d'obtenir des granules nanocomposites qui pourront être utilisées dans les procédés de mise en forme thermoplastique conventionnels.

La procédure décrite ci-dessus est la procédure standard utilisée dans ce travail de recherche pour la production de nanocomposites. Du PLA et du PLAg ont été mélangés séparément avec du TPS/MMT pour étudier l'effet de l'anhydride maléique sur la

structure des nanocomposites et sur leurs propriétés mécaniques. Du MMT a aussi été mélangé avec du PLA afin de pouvoir comparer les résultats des différentes méthodes.

La morphologie des mélanges de TPS/PLA et de nanocomposites TPS/PLA/MMT a été étudiée en utilisant un microscope électronique à balayage (SEM). La morphologie du mélange TPS/PLA était extrêmement grossière et très faiblement distribuée. L'utilisation de PLA greffé à l'anhydride maléique comme agent de comptabilisation dans les mélanges TPS/PLAg permet de produire une morphologie plus fine et plus homogène, et de procurer une forme sphérique à la phase de TPS. Une morphologie similaire à celle des mélanges TPS/PLA (non comptabilisés) a été observée avec l'addition de 2 % de MMT naturelle dans les mélanges TPS/PLA. Quand du PLAg est ajouté au nanocomposite, la phase de TPS présente une réduction attendue de taille mais moins que celle trouvée dans les mélanges TPS/PLAg. L'addition de 5 % en masse de MMT naturelle dans les mélanges contenant du TPS et du PLA ou du PLAg a conduit aux mêmes observations que celles constatées lors de l'addition de 2 % de MMT dans les mélanges TPS/PLA.

L'augmentation de taille de la phase de TPS lors de l'addition de MMT peut être reliée à l'augmentation de la viscosité du mélange comme la MMT a été ajoutée dans la suspension d'amidon et à la diminution de la déformabilité de la phase de TPS avec la dispersion dans le PLA.

L'intercalation du TPS/PLA dans la MMT et la dispersion de MMT dans les mélanges TPS/PLA a été analysée en utilisant la diffraction par rayons X (XRD), la microscopie électronique a transmission (TEM) et la microscopie a force atomique

(AFM). Dans tous les composés où des MMT ont été ajoutées dans la suspension d'amidon, dans les mélanges TPS/PLA ou TPS/PLAg, une intercalation partielle dans les couches de MMT, basée sur l'accroissement de l'espacement basique du MMT, a été observée comparativement à l'espacement basique du MMT seul, illustré par les rayons X (XRD). Cette intercalation partielle dans les galeries d'argile a été observée sur des photographies obtenues par TEM et sont en accord avec les résultats de XRD. Les photographies ont montrées de larges agrégations d'argile et des empilements de moins de trois couches d'argile.

La faible dispersion de MMT dans la matrice de TPS/PLA et une orientation non préférentielle des agrégations d'argile ont été confirmées par des images obtenues par TEM et AFM. De plus, dans tous les nanocomposites, contenant ou non le PLAg ou même lorsque du MMT a été incorporé dans la phase de PLA, les agrégats de MMT ont été trouvés préférentiellement localisés dans les phases de TPS, ou le long de l'interface du mélange.

Les propriétés mécaniques des nanocomposites ont été analysées par des essais de traction standard. Les résultats ont montré des valeurs similaires pour le module de traction et la résistance à la traction du PLA seul et du PLAg. De plus, les allongements à la rupture des deux nanocomposites sont faibles. L'ajout de 2 % en masse de MMT dans le PLA et le PLAg a conduit à une faible augmentation de module de traction et une réduction de 20 % de la résistance à la traction par rapport au PLAg. Pour les mélanges de TPS/PLA, de faibles accroissements dans l'allongement à la rupture ont été trouvés par rapport au PLA seul. L'utilisation de PLAg comme agent comptabilisant entre TPS et

PLA a montré un accroissement de 50-60 % de l'allongement à la rupture par rapport au PLA seul. L'ajout de 2 % en masse de MMT naturelle dans les composés à 27 % TPS/PLA et à 60 % TPS/PLA a conduit à une augmentation importante du module de traction et à une faible réduction de la résistance à la traction.

D'autre part, l'addition de MMT dans le TPS/PLAg n'a pas montré de variations significatives dans le module de traction et la résistance à la traction. Cependant, une diminution importante de l'allongement à la rupture par rapport aux mélanges TPS/PLAg a été observée. Le MMT rend la phase de TPS plus fragile.

Pour étudier la résistance à la rupture des nanocomposites TPS/PLA, la méthode de *Essential work of fracture* (EWF) a été utilisée. Cette méthode divise l'énergie totale nécessaire pour rupture un spécimen entaillé en deux parties. La première est associée à l'initiation et la propagation de la fissure résultant de la formation de la zone de rupture. L'énergie est considérée comme le travail essentiel de rupture (EWF). L'autre partie est reliée au volume déformé de façon plastique, cette fraction est appelée le travail de rupture plastique ou non EWF et dépend de la taille de la zone de rupture et de l'échantillon testé.

La méthode EWF mesure la surface sous les courbes de charge de déplacement pour un échantillon entaillé avec des variations de longueur des ligaments. En utilisant une expression linéaire fonction de la longueur du ligament pour décrire l'énergie totale impliquée dans le processus de rupture, il est possible de déterminer la valeur d'EWF, pris comme un paramètre intrinsèque dans le matériau. Les résultats utilisant la méthode EWF indiquent que la résistance à la rupture des mélanges de TPS/PLAg est supérieure à

celle des mélanges TPS/PLA. Ce comportement peut être dû à une réduction de la phase dispersée, à l'effet d'accroissement de l'adhésion interfaciale générée par l'utilisation de PLAg et donc à un meilleur transfert de contraintes entre la matrice de PLAg et la phase de TPS plus souple.

L'addition de 2 % de MMT dans les mélanges de TPS/PLA contenant ou non le PLAg a produit une réduction significative de la résistance à la rupture dans les deux cas.

Pour mieux connaître les effets de la phase de TPS et de MMT sur la cristallisation du PLA, des analyses enthalpiques différentielles (DSC) ont été réalisés sur des mélanges TPS/PLA et les nanocomposites de MMT. Les échantillons ont été chauffés à 200 °C avec une vitesse de chauffage de 10 °C/min et ont ensuite été refroidis jusqu'à – 100 °C avec une vitesse de refroidissement de 10 °C/min. Il est attendu que sous ces conditions, le PLA doive rester complètement amorphe, ce qui est vérifié par l'absence de pic de fusion. Il est bien connu que le PLA a un taux de cristallisation très faible à cause de ses chaînes rigides.

Dans les mélanges à 27 % TPS/PLA et à 60 % TPS/PLA, l'addition de TPS sur le PLA seul a produit une faible augmentation du taux de cristallinité du PLA. Cependant, quand le TPS est ajouté au PLAg, un taux de cristallisation similaire a été trouvé.

L'addition de 2 % de MMT dans le mélange TPS/PLA a permis une augmentation additionnelle du taux de cristallinité du PLA. De plus, quand du PLAg a été utilisé avec du mélange à 27 % TPS avec 2 % de MMT, un double pic de fusion a été observé. Ce double pic est peut-être directement relié à la formation de deux types de structures cristallines. Dans ce cas, l'argile (MMT) en petite quantité, intercalé ou sous forme

d'agrégats, augmente le taux de cristallinité de PLA et de PLAg. Dans cette étude, nous avons constaté que les couches d'argile ou les agrégats augmentent le nombre d'agents nucléants pour la cristallisation du PLA.

Cette étude a aussi montré des changements dans les transitions thermiques autour de la température de transition vitreuse (Tg) dans les thermogrammes de DSC pour les mélanges de TPS/PLA. Les mélanges de TPS/PLA et de TPS/PLAg ont été conservés à 25 °C et avec 50 % d'humidité durant des périodes de 7, 15, 45 et 300 jours. Dans tous les cas, un pic endothermique relié à l'excès d'enthalpie de relaxation a été détecté autour de Tg. Le pic endothermique a augmenté avec un accroissement du temps de conditionnement conséquemment à une élévation de l'excès d'enthalpie de relaxation. L'augmentation avec le temps de l'excès d'enthalpie de relaxation a été associée au vieillissement physique du PLA et dépend du temps et de la température de conditionnement.

TABLE OF CONTENTS

LIST OF TABLES

LIST OF FIGURES

NOMENCLATURE

TPS = thermoplastic starch

MMT = montmorillonite

EWF = essential work of fracture

PNCs = polymer nanocomposites

SEM =scanning electron microscope

TEM = transmission electron microscope

AFM = atomic force microscope

LEFM = linear elastic fracture mechanics

U = total potential energy of the system

U_o = the elastic energy of the uncracked specimen

U_a = the energy consuming by introduction the crack in specimen

U_γ = the surface energy or energy consuming by the development of the new crack surfaces

a = one half crack length in cracked specimen

B = the specimen thickness

$4aB$ = the total surface crack area in cracked specimen

γ_s = specific surface energy

$E = E^*$= elastic modulus

σ = applied stress at specimen

υ =Poisson's ratio

K = stress intensity factor

σ_c = critical stress

$a^{1/2}$ = square root of the critical size of crack length

K_I = stress intensity factor under loading mode I

K_{IC} = critical stress intensity factor under loading mode I

K_{IIC} = critical stress intensity factor under loading mode II

K_{IIIC} = critical stress intensity factor under loading mode III

G = strain energy rate

G_I = strain energy rate under loading mode I

R = resistance force

Sy = internal stress

EPFM = elastic plastic fracture mechanics

CTOD = crack tip opening displacement

Γ = J integral contour path

W' = strain energy density

T_i = the stress vector

u_i = displacement vector

ds =increment along a contour surrounding a crack tip

J_{IC} = represents the point at which the plastic deformation occurs (plastic yielding) during the crack propagation

Δa = increment in crack length

U_P = potential energy

d_c = displacement path

σ_y = yield stress

σ_{max} = local stress strength

IFPZ = inner fracture process zone

OPZ = outer plastic zone

W_F = total energy of fracture

W_E = essential work of fracture

W_P = plastic work of fracture

w_E = the specific fracture work per unit of new produced area

w_P = the specific plastic deformation work

w_F = the specific total work of fracture

w_{Eini} = specific essential work of crack initiation

w_{Etotal} = total specific essential work of fracture

DDENT = deeply double edge notched tension specimen

DSENT = deeply single edge notched tension specimen

SENB = single edge notched bend specimen

DCNT = deeply centre notched tension specimen

CEC = cation exchange capacity

β = shape factor related to the geometry of plastic zone

l = ligament length

t = thickness specimen

δ = CTOD inside of the fracture process zone

δ_{ini} = critic CTOD related with the crack initiation

r_p = radius of the plastic zone

$\bar{\sigma}, \bar{\varepsilon}$ = true stress and strain respectively

$\bar{\varepsilon}_n, \varepsilon_n$ = true and engineering strains during the necking of material

HDT = heat distortion temperature

PLA = polylactide

PLAg = maleic anhydride grafted polylactide

LLDPE = Linear Low Density Polyethylene

LDPE = low density polyethylene

HDPE = high density polyethylene

PA66 = polyamide 66

PET = polyethylene terephthalate

PEO = polyethylene oxide

PP = polypropylene

PVA = polyvinyl alcohol

PC = polycarbonate

EPR = epoxy polymer resins

PE = polyethylene

EVA = polyethylene-co vinyl acetate

PCL = polycaprolactone

PBS = polybutylene succinate

PEG = polyethylene glycol

PBT = polybutylene terephthalate

ABS= acrylonitrile butadiene styrene

PVP = polyvinyl pyridine

SEBS = styrene-ethylene-butylene-styrene

HMWPE = high molecular weight polyethylene

LMWPE = low molecular weight polyethylene

UHMWPE = ultra high molecular weight polyethylene

PETG = polyethylene terephtalate glycol

PEEK = polyetheretherketone

BOPET= biaxial oriented polyethylene terephthalate

PEN = Polyethylene naphthalate

PEI = polyethyleneimine

PI = polyimide

PVC = polyvinyl chloride

HIPS = high impact polystyrene

ELPP = elastomeric polypropylene

EPBC = ethylene–propylene block copolymers

EPR = Ethylene propylene rubber

PPC = polypropylene carbonate

PB = polybutadiene

PA = polyamide

POE = polyoxyethylene

TPNR = thermoplastic natural rubber

CHAPTER 1

INTRODUCTION AND OBJETIVES

1.1 Introduction

Biobased polymers and polymer nanocomposites are two materials that are nowadays getting attention in the polymer field.

The quest for novel biobased polymers is seen as a potential solution to the ever increasing worldwide demand for fossil resources and the imminent scarcity of petroleum reserves. This situation requests the exploration of new viable alternatives to produce novel polymeric materials developed from renewable sources instead of petroleum. New biodegradable bio-based polymeric materials based on renewable resources are being commercially produced as an alternative to petroleum based polymers. Among these bio-based polymer materials, Polylactide (PLA) and Thermoplastic starch (TPS) are promising materials.

On the other hand, the fabrication of polymer nanocomposites is an attractive and interesting topic in the polymer science domain. These nanocomposites are attractive due to molecular interactions involving nanoparticles in their different shapes and origins and polymeric matrices. The required nanoparticles concentration, typically less than 5% are used to produce improvements in thermal, mechanical and flexural properties in comparison to the neat polymer. The nanocomposites have an important density advantages over conventional fillers such as talc, glass fiber, calcium carbonate, mica,

which are usually used at much higher loadings. It is therefore possible to produce light weight products with improved properties such as the ones cited above; and at the same time, offers exclusive potential for others applications such as biomaterials.

All types of nanoparticles are being incorporated in dispersive manner in a polymer matrix including nanofibers, nanotubes, nanowhisker, nanolayers such as layered silicates that will be used in this study and nanodots. Enhanced storage modulus, tensile and flexural properties, increase in heat distortion temperature, decrease in flammability and gas permeability, and increase in biodegradability rate (Sinha Ray & Okamoto (2003b)). are among the properties typically sought with the use of layered silicates in nanocomposites (Mai & Yu (2006))

The current work will build on these findings in order to explore the processing and properties of MMT nanocomposites based on the compatibilized TPS/ PLA blends. The different steps of the study included the addition of nanoclays platelets as reinforcing phase, the injection molding of standard coupons followed by the mechanical and thermal characterization and the microstructure characterization to assess the blend morphology and clay exfoliation.

Nanoclays as reinforced phase are extensively used due to the good results showed when mixing them with several types of polymers. (LeBaron et al. (1999)) (Alexandre & Dubois (2000)) (Sinha Ray & Okamoto (2003b)) (Mai & Yu (2006)). The remarkable results on the improvement of mechanical properties in polyamides (PA) (Okada & Usuki (2006)), e.g. the enhancement of elastic moduli, suggests nanoclays

might have a similar effect in TPS/PLA blends. In addition, the use of clay platelets is attractive, because the clay platelets have high elastic moduli and have a natural origin.

1.2 Polymer Nanocomposites

The first studies on layered silicates intercalation in polymer matrices started in the 60s. Results back then were unsuccessful, in part because of high concentrations of clay, similar to conventional composites, resulting in nanocomposites with a ceramic character.

Nowadays, at least 500 papers are being published each year on polymer nanocomposites (Okada & Usuki (2006)). This boom was caused in part to the publication in 1986 of the encouraging results on Polyamide-6 nanocomposites (Okada et al. (1988)). In this first successful work, thermal and mechanical properties of Polyamide-6 were improved with the addition of small amounts montmorillonite. Following the same line of research, several polymer matrices were used in the production of nanocomposites including: polyethylene vinyl alcohol, PVA, and polyvinyl pyridine, polycarbonate (PC), epoxy polymer resins (EPR), polypropylene (PP), polyethylene (PE) and polyethylene-co-vinyl acetate (EVA), etc. (Sinha Ray & Okamoto (2003b)) (Utracki (2004)) (Mai & Yu (2006))

Among biodegradable polymers Polylactide (PLA) (Mai & Yu (2006)), and Thermoplastic starch (TPS), polycaprolactone (PCL) (Kalambur & Rizvi (2005)) (Luduena et al. (2007)), aliphatic polyester (Lee et al. (2005)) (Lee et al. (2002)), polyhydroxy butyrate (PHB) (Sanchez-Garcia et al. (2008)) and polybutylene succinate

(PBS) (Ray et al. (2003)) (Shih et al. (2007)) have been used in investigations on nanocomposites.

The intercalation phenomenon was used and studied approximately 160 years ago. The first studies involved the partial or total intercalations of metals into graphite (Herold et al. (1980)) (Guerard et al. (1986)). In the 60s, other host layered materials, such as metal phosphorous chalcogenides, lamellar oxide halides, vanadyl, niobyl and layered minerals were used. Among these last materials, the montmorillonite and beidellite were host materials.

In polymer nanocomposites, the interactions are produced at the molecular level. Molecular interactions are formed by the insertion of molecules of a guest specimen, in our case macromolecules, into the empty spaces between the layers of a layered specimen (host lattice). During the molecular intercalation, the expansion or translation of layers of host specimen along the perpendicular direction to the layers, plane xy, is typical. The expansion distance is related to the molecular dimension of the guest molecule. The success in the intercalation process was expressed in the following general directives (Capkova & Votinsky (2000)). The interaction between host and guest specimens must be stronger than the interactions among the guest molecules and the solvent (if used). The surface of the layered host must have active sites or groups or has a polar nature. In addition the host interlayer distance must have a minimal value to accommodate guest molecules or have a weak interaction among host layers.

Numerous mechanisms involved in molecular intercalation have been proposed. Only some of the possible interactions studied are presented below (Votinský et al. (1992)):

a) Layered complexes intercalation: the intercalation of the guest is achieved by the formation of coordination bonds. The guest molecules act as donors. The coordinate bond includes a complicated harmonization of polyhedron of electropositive atoms of the host layer. In these interactions, weak Lewis bases are involved to form very stable compounds. These physical systems are based on the function of a guest to act as donor and acceptor at the same time.

b) The intercalation in this case is based on two sub-anchoring mechanisms. The first is the formation of hydrogen bonds. A part of the guest molecules are anchored by hydrogen bonds between the oxygen atoms of the oxo-anion of the host. In the second mechanism, guest molecules are anchored by a coordinate bond with the most electronegative atoms of guest layer.

c) Another type of intercalation is produced when guest molecules are anchoring using a total electron transfer from the layered host specimen to stabilization of guest-host compound by an ionic bond involving guest cations and the negative charges from host layers.

d) Very stable intercalations involving very weak van der Waals's forces between host lattice and guest molecules were found in some systems such as iodine molecules intercalated in lattice of tellurium. The interlayer distances correspond to Van der Waals's bond.

e) The intercalation mechanics, frequently found in systems involving layered minerals, is produced by proton transfer. Protons are transfer from the layered host to the guest molecules. The guest molecule admits protons from hydroxyl groups of the layered

host. The interaction between cation and negative layers involved in this kind of intercalation has an electrostatic nature. This is possible when the mechanism involved in polymer nanocomposites contains layered silicates. The intercalation can be expressed in term of electrostatic interactions with the following reaction:

$$\text{Host (OH)} + \text{Guest} \rightarrow \{\text{Host (O)}\}^{-} + \{\text{Guest (H)}\}^{+}$$

where in our case the host will be MMT and the guest will be the PLA and TPS. The montmorillonite as a type of layered silicate contains active hydroxyl groups on its surfaces. (Rozin et al. (1974))

1.2.1. Types of Nanocomposites

Figure 1.1 shows three types of composites for layered silicate materials. If the polymer chains are not capable to penetrate or intercalate between the silicate layers, a conventional or micro composite is produced, and thus the properties reached are different and lower in comparison to when partial or fully exfoliation is achieved. (Hussain et al. (2006))

1.2.1.1 Intercalated Nanocomposites

For intercalated nanocomposites, the polymer chains are inserted inside of silicate galleries in a crystallographically regular fashion. The amount of layered silicate inside the polymer matrix is independent of its structural arrangement. The properties of these nanocomposites are similar to ceramic materials.

1.2.1.2 Exfoliated Nanocomposites

In exfoliated nanocomposites, the silicate layers are completely dispersed into the polymer matrix, singles clay platelets are separated and the separation distance depends of amount of silicate in the nanocomposites.

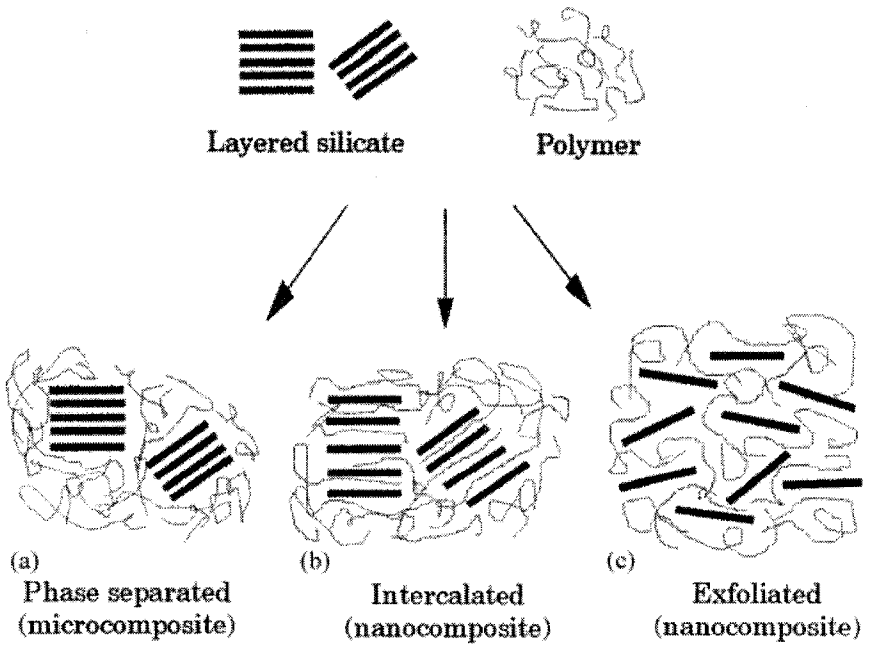

Figure 1.1 Different types of composites: microcomposites, intercalated nanocomposites and exfoliated nanocomposites. (Sinha Ray & Okamoto (2003b))

1.2.2 Preparation Methods of Nanocomposites

There are many methods available for clay introduction in a polymer matrix. The polar nature of MMT and non polar nature for the usual polymers play a critical role when choosing the best-suited strategy for a given polymer-montmorillonite combination. The following are three general and available methods to prepare nanocomposites. All of them have their inherent advantages and disadvantages.

1.2.2.1 Solution Intercalation of polymer or pre-polymer

The polymer or pre-polymer is solubilized (on a solvent system) (Figure 1.2) and then the silicate layers are added. The layered silicate is swollen in a solvent, such as water, chloroform, methanol, toluene or other solvent. When the polymer and layered silicate solutions are mixed, the polymer chains intercalate or diffuse and displace the solvent within the interlayer of the silicates. Finally the solvent is removed by drying under vacuum or direct heating and the intercalated structures remains resulting in a nanocomposite. Solution intercalation methods are mostly used for polar polymers soluble in polar solvents. Nevertheless, non-polar polymer matrices such as polyethylene and polyimide can also be used with this method when combined with other solvents and the use of organically modified montmorillonite. The main advantage of this method is the possibility to process polar polymers with natural montmorillonite. However, this method can be unsuitable for a large scale. This is due to the large amount of solvents to achieve dispersed and intercalated nanostructures. (Sinha Ray & Okamoto (2003b)) Polymer composites of polyethylene vinyl acetate (Strawhecker & Manias (2000)), polyethylene oxide (Shen et al. (2002)) (Ke & Stroeve (2005)) and polyvinyl alcohol (Hussain et al. (2006)) were obtained by this method.

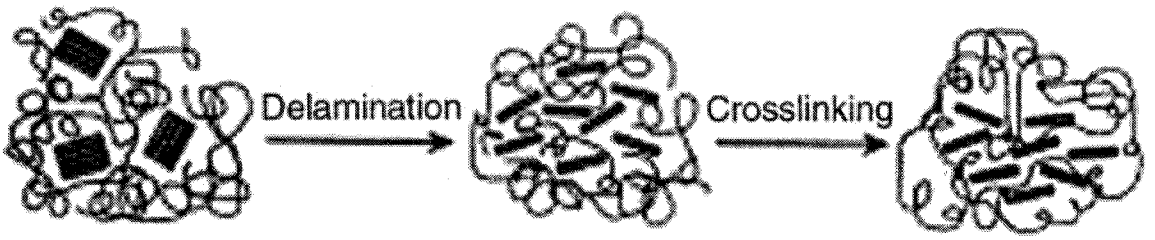

Figure 1.2 Nanocomposites prepared by intercalation of polymer in solution. (Sinha Ray & Okamoto (2003b))

1.2.2.2 In situ intercalative polymerization method.

This method is very similar to the solution intercalation method. In this case, the use of polymers is changed by a monomer and an initiator or catalyst. The in situ polymerization method induces the exfoliation of the clay into the growing polymer matrix. (Okada et al. (1988)). In the same way as solution intercalation, this method was mainly developed for polar monomers that can intercalate into the clay interlayers. (Hussain et al. (2006))

The layered silicate is swollen within a solution of monomer-polymer. (Figure 1.3). The polymerization occurs inside the intercalated layered galleries. In this method, the polymerization can be initiated either by heat or by radiation, by the diffusion of a suitable initiator, or by an organic initiator. Caprolactam and montmorillonite were produced under this method (Sinha Ray & Okamoto (2003b)). The addition of an acid surfactant as polymerization initiator was necessary to allow the polymerization-interaction processes. Other polymer systems such as polyurethane composites (polyol and cyanate are polar monomers) were produced using this technique but in this case

without any surfactant and initiating the polymerization thermally. (LeBaron et al. (1999))

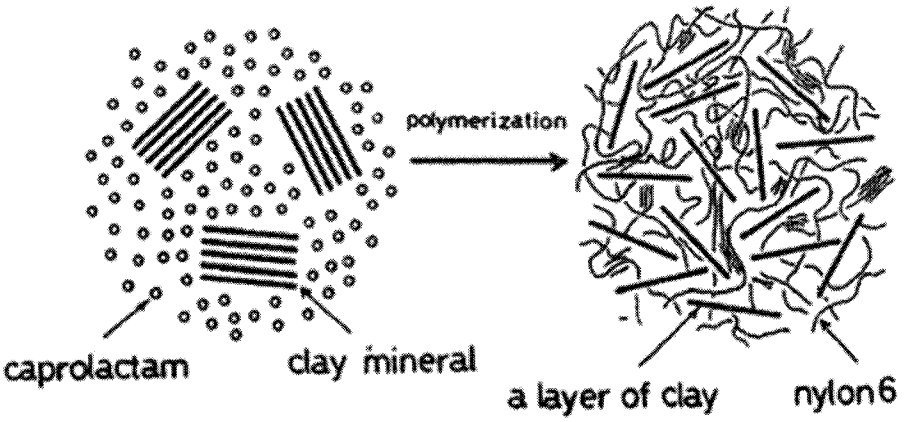

Figure 1.3 Schematic diagram of synthesis of polyamide-6 (PA6) and clay nanocomposites. (Sinha Ray & Okamoto (2003b))

1.2.2.3 Melt intercalation method

This method involves the annealing of a polymer in static or under shear conditions and then the mixing of the melt polymer and layered silicates. The first studies were reported in 1993 using PS and an organically MMT (A.Vaia et al. (1993)). The PS/MMT nanocomposite showed partial intercalated structures, although the montmorillonite was not completely exfoliated. Nowadays, the melt intercalation method has become the standard for the production of polymer nanocomposites in industrial scale

The melt intercalation method has more advantageous than previous ones. It is environmentally benign due to the absence of organic solvents. In addition, it can be adapted to several types of polymer matrix, polar or non-polar. It allows the use of

polymers which were previously not suitable for in situ polymerization or solution intercalation. Also, it is compatible with current industrial processes, such as extrusion, roll mill, blenders and injection molding. The use of this method is limited by the use of a compatibilizer or modified clay for most polymer matrices. This means an increase in the cost of production of nanocomposites. Furthermore, the addition of surfactants and other compatibilizers can degrade the overall properties of the polymer matrix. (Frankowski et al. (2007))

1.2.3 Nanocomposites Proprieties

1.2.3.1 Thermal Stability.

The inclusion of clay into the polymer matrix enhances the overall thermal stability of the nanocomposites. Clay acts as an insulator or heat barrier, and mass transport barrier to the volatile products generated by the heat of decomposition. Besides, the clay addition supports the creation of layer of char after thermal decomposition.

Usually, to study the thermal stability of nanocomposites, a thermo gravimetric analysis (TGA) is performed. The degradation of the material was measured as loss of weight due to oxidative or non-oxidative degradation of the material. The addition of MMT in polymer matrices (PS,PCL) (Zhu et al. (2001)) (Lepoittevin et al. (2002)) , high impact polystyrene (HIPS), poly (styrene-co-acrylonitrile) (SAN), acrylonitrile-butadiene-styrene (ABS), polymethyl methacrilate (PMMA), polypropylene (PP), polyethylene (PE),poly(ethylene-co-vinylacetate) (EVA), epoxy resin (ER)and polyurethane (PU) (Mai & Yu (2006)) showed enhancement of the thermal stability.

The opposite behavior was showed when MMT was added to a synthetic biodegradable aliphatic polyester (BAP) (Lim et al. (2002)). The thermal degradation temperature and rate increased with the addition of up to 15 wt% of MMT. In this case, the clay acts as heat shield at the first moment. Then, the accumulated heat in the stacks of silicate layer, acts as heat source to accelerate the thermal degradation of the system. In consequence, the heat barrier effect would result in a reverse thermal stability of the nanocomposites.

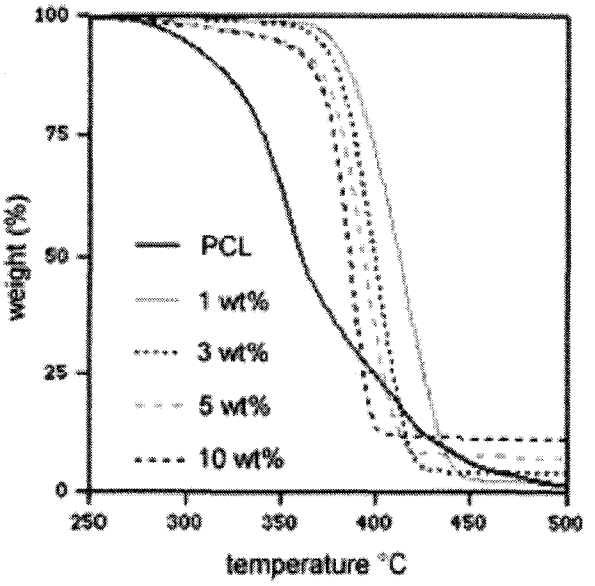

Figure 1.4 Effect of the clay loading over the thermal stability in PLC nanocomposites. (Lepoittevin et al. (2002))

1.2.3.2 Mechanical Properties.

The incorporation of lows amount of clay (< 5%wt) in several polymeric systems shows remarkable improvement in elastic modulus and tensile strength (Figure 1.5) (Tjong (2006)) e.g. PP (Liu & Wu (2001)), (LeBaron et al. (1999)) .The main reason

relies in the strong interactions between matrix and silicate layers, in some cases (PA6/MMT) via formation of hydrogen bonds. (Figure 1.6)

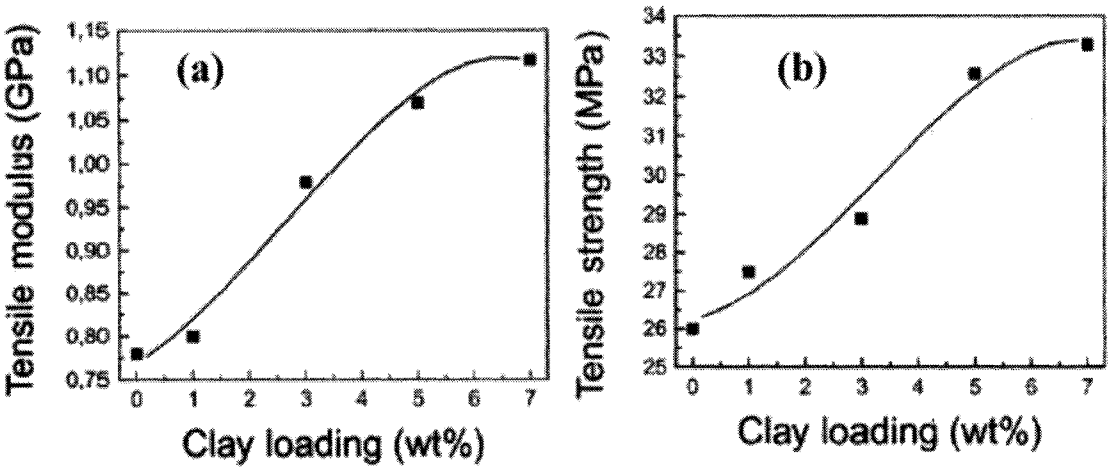

Figure 1.5 The effect of clay loading over a) elastic modulus and b) tensile strength in a nanocomposites (Sinha Ray & Okamoto (2003b))

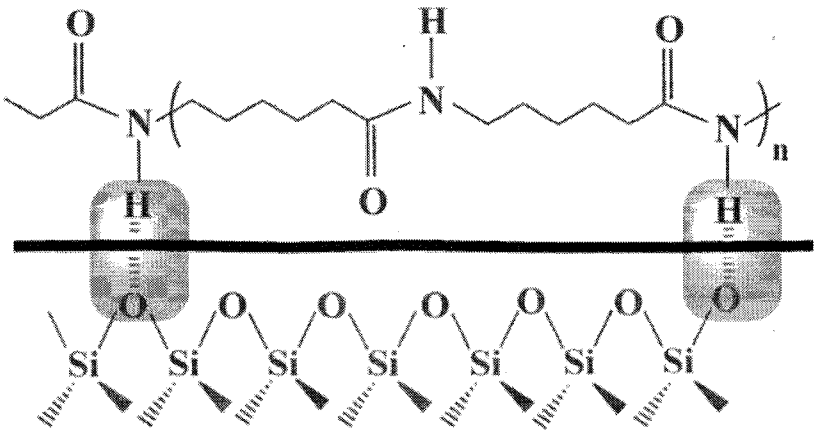

Figure 1.6 schematic illustration of formation of hydrogen bonds in PA6/MMT (Sinha Ray & Okamoto (2003b))

The improvement in terms of flexural and Young moduli of nanocomposites materials also relies on the degree of dispersion into a polymer matrix and high aspect

ratio of the clay. The widely known Halpin-Tsai (Equations 1.1 and 1.2) (Halpin & Kardos (1976)) can be useful to understand the effect of adding clay on the elastic modulus.

$$E_c = E_m\left(\frac{1+\xi\eta V_f}{1-\eta V_f}\right) \qquad (1.1)$$

$$\eta = \frac{\left(\frac{E_f}{E_m}\right)-1}{\left(\frac{E_f}{E_m}\right)+\xi} \qquad (1.2)$$

Where E_c is the modulus of the nanocomposite, E_m is the modulus of the polymer matrix, E_f is the modulus of the montmorillonite, V_f is the volume fraction of MMT and ζ is the shape factor of MMT. The shape factor was approximated assuming twice the aspect ratio. The high aspect ratio of MMT was established to be around 100-150.

Based on the Halpin-Tsai equation, the higher moduli is reached, when the higher aspect ratio or shape factor of MMT are found. Equation 1.1 also shows the effect of clay concentration on the mechanical properties of the nanocomposites. When MMT concentration is low, the possibilities of reaching a better degree of platelets distribution are high. On the other hand, by increasing the clay concentration, the MMT could not be well dispersed and the MMT platelets should interact mutually, losing the effect of high aspect ratio and then reducing the mechanical performance of the nanocomposite material. In this case the material obtained is a micro rather than a nanocomposite. (Hbaieba et al. (2007))

1.2.3.3 Gas barrier Properties

The addition of silicate layers increases the barrier properties (gas permeability), in comparison to conventional composites, by creating a tortuous path like a maze (Figure 1.7) that retards the motion of gas molecules through the polymer matrix. For example the addition of 2% of MMT in a polyimide matrix reduced in 10 times the water vapor permeability of the final nanocomposite. (Sinha Ray & Okamoto (2003b))

In conventional polymer composites, the addition of filler does not increase the barrier properties or permeability of the final material because the distance between filler particles is larger than in gas molecules. In nanocomposites, when the nanoparticles are well dispersed, the gas molecules can not easily diffuse through the polymer matrix because the molecules must be in contact with the impermeable silicate layers increasing the effective volume of material through which the gas molecules must diffuse, resulting in a decreased rate of diffusion.

The control of gas permeability of polymer nanocomposites has large applications as packaging and membranes. This control can be obtained by formation of a tortuous path, mentioned above. (Bharadwaj (2001))

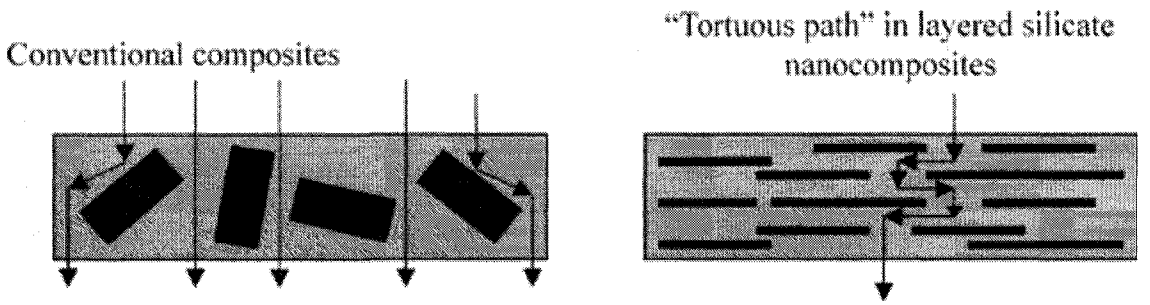

Figure 1.7 The increment of gas permeability in nanocomposites is due to formation of tortuous path. (Sinha Ray & Okamoto (2003b))

1.2.3.4 Optical transparency

In fully exfoliated nanocomposites, the optical transparency was not affected by addition of MMT. This is due to a highly dispersion of MMT in the polymer matrix in individual layers. The average montmorillonite layer thick is around 1nm, and the typical lateral sizes are 50-1000 nm. These dimensions did not affect the pass of visible light through the material. In PVA/MMT nanocomposites showed the optical transparency was similar than in the case of pure polymer. (Sinha Ray & Okamoto (2003b))

1.3 PLA/TPS Blends

The first attempts to blend dry starch with PLA showed a low interfacial adhesion between phases and lead to poor mechanical properties highlighting the need for some interfacial modification (Ke & Sun (2001)). The first TPS/PLA blends (Martin & Averous (2001)) also showed relatively poor properties (e.g. low elongation at break) in comparison with neat materials because of their coarse morphology. This also indicated high interfacial tension between both phases.

Zhang and Sun (Zhang & Sun (2004)) worked using dry granulate starch blended with PLA, but this time using maleic anhydride (MA) as an in situ compatibilization agent. The PLA/Starch/MA showed an improvement in interfacial adhesion and better mechanical properties principally in tensile strength, but the elongation at break remained in a very low range, below 5%.

Huneault and Li (Huneault & Li (2007)) prepared TPS/PLA blends compatibilized using PLA grafted with maleic anhydride (PLAg). The PLAg was obtained by free-radical grafting of maleic anhydride in the melt state in a separate compounding step. When the TPS and PLAg were mixed, reaction between the maleic anhydride grafts and the OH- groups of starch reacted leading to in situ production graft copolymers of starch and PLA at the interface. The ductility and elongation at break were greatly improved; elongation values of 100-200% were obtained. The TPS phase was better dispersed and more homogeneously distributed due to the reduced interfacial tension between phases.

1.4 TPS and PLA Nanocomposites

1.4.1 TPS Nanocomposites

The reinforcement of TPS with montmorillonite has already been a matter of study (Fischer & Fischer (2001)) (Park et al. (2002)) (Wilhelm et al. (2003)) (Park et al. (2003)) (Huang et al. (2004)) (Chen & Evans (2005)) (Ma et al. (2007)) (Yu et al. (2007)). In most cases, the intercalation is carried out during melt-extrusion or in a solvent prior to casting of thin films. (Fischer & Fischer (2001)) made the first attempt to intercalate TPS inside several types of clay with adequate concentrations of plasticizer.

In the patent literature, it is claimed that suspensions of MMT or smectite clay in water or in mixtures of water and other plasticizers can be compounded with dry starch to produce TPS nanocomposites with improved mechanical properties. (Fischer & Fischer (2001)). Park and co-workers prepared TPS pellets and later blended them with clays. (Park et al. (2002)) (Park et al. (2003)) They showed that the use of natural MMT lead to superior dispersion in TPS than the use of organically modified MMT with ammonium cations in the gallery.

Tensile strength and elongation at break were both increased by more than 20% when adding the natural MMT while the vapor transmission rate was decreased by 35% compared to the neat TPS. The thermal stability was also slightly enhanced. Partial exfoliation was found. The best results observed with natural MMT were explained by the affinity between the polar surfaces of MMT and TPS.

Wilhelm et al (Wilhelm et al. (2003)), using a film casting method and Chen and Evans (Chen & Evans (2005)) worked on TPS/hectorite systems and suggested that part of the glycerol molecules, used as starch plasticizers, migrated inside the interlayer of hectorite. Interactions with formation of H-bonds between hydroxyl groups in the clay surface, glycerol, starch and water were also suggested. Intercalated structures were created with variable interlayer distances; large distances were obtained when relatively low clay content (5% wt.) and an excess of glycerol were used. This translated in an increase in stiffness, elastic modulus and thermal stability and in the reduction of the elongation at break in presence of the clay.

Ma and co-workers used sorbitol instead of glycerol as starch plasticizer in a TPS-MMT system (Ma et al. (2007)). The interlayer distance was improved reaching 2.07 nm in comparison to 1.8 nm when using glycerol. Once again, the tensile strength and Young modulus were improved by 200% and 325% respectively when 10% wt of MMT was added, but the elongation at break dropped by 30% with respect to the neat TPS control.

One phenomenon sometimes encountered in TPS-based materials is the starch recrystallization (also called retrogradation). This is due to the formation of H-bonds between starch macromolecules and is typically accelerated by the presence of humidity. It is usually not desired since it leads to embrittlement of the TPS. Since this phenomenon is related to long-term diffusion of the plasticizer out of the material and its replacement by water, it could be expected that the addition of clay platelets, by decreasing permeability and by disrupting the re-crystallization mechanism, would improve the TPS stability. This has been confirmed for glycerol-plasticized TPS (Huang et al. (2004)) and for water-plasticized TPS (Yu et al. (2007)). However it may not be the case for all plasticizers. Chen and Evans, (Chen & Evans (2005)), associated cracking marks on TPS-MMT composites to recrystallization. The plasticizer was undisclosed in that study but it was noted that recrystallization of starch in the nanocomposites was decreased by the use of plasticizer with stronger hydrogen bonds with starch.

Ultrasonic mixing prior to extrusion-blending was investigated as a means to improve the dispersion and exfoliation of natural MMT and natural hectorite in water suspensions (Yu et al. (2007)). Large MMT interlayer distances, up to 6.2 nm were found after using 30 min of sonication time. However, these distances decreased rapidly in the

final TPS-MMT compound to values between 1.2 and 2.4 nm. Good exfoliation was achieved at low clay concentration over a relatively narrow window of operating parameters and of plasticizer composition in MMT clay. The cation exchange capacity of the clay appeared to be an important factor during exfoliation. Overall, ultrasonically treated samples produced similar results in terms of exfoliation and of mechanical properties in comparison with conventionally mixed TPS-clay samples.

1.4.2 PLA Nanocomposites

PLA based nanocomposites were also prepared by melt processing (Ogata et al. (1997)) (Pluta et al. (2002)) (Maiti et al. (2002)) (Sinha Ray et al. (2002)) (Paul et al. (2003)).

Ogata and co-workers (Ogata et al. (1997)) reported the first PLA nanocomposites prepared by the solvent-cast method where MMT was modified using distearyldimethylammonium chloride. The MMT dispersion, in form of tactoids, was poor and only the Young modulus of the final nanocomposites was slightly improved. Pluta and co-workers (Pluta et al. (2002)) prepared PLA nanocomposites using natural and organo-MMT. The results showed natural MMT does not lead to exfoliation in PLA because of the incompatible hydrophilic nature of MMT with PLA (Pluta et al. (2002)) (Paul et al. (2003)) . Sinha Ray and co-workers (Sinha Ray et al. (2002)) (Sinha Ray et al. (2003)) worked with MMT modified with trimethyl octadecylammonium cation (C^3C_{18}-MMT). The oligo-polycaprolactone (o-PCL) was added in very low concentrations as compatibilizer to produce better parallel stackers and to increase the flocculation due to hydroxylated edge-edge interaction of MMT layers. The MMT dispersion in the PLA

matrix was satisfactory producing intercalated material. However, a full delamination of MMT layer was not reached and MMT aggregates were present. The materials showed improvements in flexural and storage modulus, gas barrier property and heat distortion temperature (HDT). HDT was increased from 76°C for neat PLA to 111° C for PLA loaded with 7% of C^3C_{18}-MMT. The rate of biodegradability was also enhanced.

Polyethyleneglycol (PEG) can be added in PLA to increase its elongation at break and its impact resistance. When Na-MMT was added to PEG-plasticized PLA, the interlayer distance increased from 1.2 nm to 1.7 nm since PEG was preferentially intercalated in natural MMT (Paul et al. (2003)). Similar results were obtained with or organo-modified MMT but better thermal resistance was found in this case. This was explained by PLA hydrolysis at high temperature, caused by hydrated Na^+ cations of Na-MMT, by polarity differences between PLA and Na-MMT, and by the preferential intercalation of PEG in interlayers of natural MMT.

Maiti et al. (Maiti et al. (2002)) prepared Clay-PLA nanocomposites by melt extrusion using different clays (smectite, MMT and an synthetic mica). Phosphonium salts were used to modify the clay surfaces. The miscibility between these organic modifiers and PLA was determined by the higher chain length of phosphonium salt. After this modification, mica (2.4 nm) and MMT (2.1 nm) exhibited higher values of interlayer distance. However, better values in storage modulus and gas barrier property were produced adding smectite (1.8nm) due to higher interactions between smectite with PLA and better dispersion present, overcoming then the effect of higher interlayer distance showed in mica.

As a result, the use of organically-modified layered silicates using cloisite 30B or other organo-modified MMT has been preferred. (Krikorian & Pochan (2003)) (Di et al. (2005)) (Kubies et al. (2006)) (Pluta (2006)) In some cases, it has lead to a clear intercalation and moderate dispersion of stacked silicate platelets and tactoids without achieving a fully exfoliation of individual silicates platelets. These nanocomposites showed improvements in mechanical and flexural properties, furthermore reducing the gas permeability.

1.5 Water as intercalation-exfoliation agent

Due to the hygroscopic character of natural clays, several studies have focused on the use of water as an intercalation/exfoliation agent. The use of starch slurries is more compatible with the thermoset polymers fabrication. Low molecular weight precursors can be more readily mixed with a clay slurry than a molten high viscosity thermoplastic polymer. For example, exfoliation in water has also been explored in water-based curable silicone emulsions. In this case, a surfactant was reacted with clay in water prior to mixing the clay suspension with the silicone emulsion. (Ma et al. (2005)). Similarly in another study, Na-MMT was exfoliated in water using stirring and sonication; water was then replaced as suspending media by acetone to form an acetone-clay slurry. A surfactant was added to modify the clay surface prior to mixing the slurry with a curable epoxy resin. The epoxy was cured after removing the acetone by evaporation resulting in exfoliated MMT/Epoxy nanocomposites (Wang et al. (2005)).

Similarly, clay can be exfoliated in water in water-based monomer emulsions prior to polymerization of thermoplastic materials. This idea has been explored for laponite clay

(Herrera et al. (2004)) and for MMT. In the second case, Na-MMT has been mixed with monomer emulsion to produce composites with Polymethyl methacrylate (PMMA) (Lee & Jang (1996)) and polystyrene (PS) (Noh & Lee (1999)). In these studies, ion-dipole bonding was proposed as the main driving force responsible to intercalate and attach the polymers chains to the clay surfaces.

Mixing a clay water slurry to a high molecular weight polymer is more challenging in terms of mixing and technological requirements. One route consists in using hydrophilic or water-soluble polymers where the polymer solution intercalates the clay prior to water removal. This was achieved in water-soluble Polyvinyl alcohol (PVA)(Strawhecker & Manias (2000)). The PVA was dissolved and later mixed with MMT slurry to produce a film by casting. The elastic modulus was doubled upon addition of 5% wt. of Na-MMT. Of course, water-solubility is not a common property for most polymers. In the case of non-water soluble polymers, the water must rapidly be replaced by the polymer matrix to stabilize exfoliated structure upon water removal. This complicates the interface modification strategy but is also more challenging from a technical point of view since the water must also be maintained in the system at elevated temperatures to prevent premature evaporation and then rapidly removed from the system to provide water-free materials. For this reason, polymer melt-extruders are the most sensible choice to provide the required closed environment as well as supplying a high level of mixing and the potential to remove the water at a high rate through devolatilization in a continuous fashion. The first successful water-assisted clay exfoliation in a molten polymer was reported into a polyamide 6 matrix (Hasegawa et al. (2003)). The main appeal for

assisting exfoliation with water was that it could be a way to prepare polyamide nanocomposites without the need to chemically modify the clays prior to the compounding step. In the reported method, the clay was suspended into water and this suspension was pumped at mid-extruder into the molten polyamide. The water was later removed in the last third of the extrusion process through devolatilization under vacuum to provide a water-free material at the end of the compounding step. Surprisingly, the use of a high water concentration did not induce significant hydrolysis of the polyamide. Homogeneous dispersion and high exfoliation were found. The mechanical properties showed improvements and were similar to those obtained when using organo-MMT. For reasons that were left unexplained by the authors, only the heat deflection temperature was not as high as those obtained with the organoclay. Using a variation of this extrusion method, it was also shown that polyamide 6-MMT blends could be prepared by mixing polyamide 6 and dry MMT in the first stage of a twin-screw compounding extruder and then adding water at the middle of extruder to assist the clay exfoliation step. Again the excess water was removed by a devolatilization stage near the end of the extruder (Yu et al. (2005)). Although mechanical properties were improved with this variant, the dispersion and exfoliation were better when the clay was fed to the process as a suspension in water.

Water-assisted exfoliation was also investigated in natural Na-MMT/PP composites (Kato et al. (2004)). As in the work of Yu et al., all ingredients except water were first melted and mixed in the first section of the twin-screw extruder. The water was pumped at mid-extruder and removed by devolatilization before the end of the compounding

process. Best exfoliation was found when adding two compatibilizers to the mixture: octadecyl trimethyl ammonium chloride and maleic anhydride grafted PP.

1.6 Objectives

The main objectives of this work are 1) to investigate the water-assisted dispersion/exfoliation of natural MMT clay in polylactide/thermoplastic starch blends, 2) to investigate the effect of interface modification using PLAg on the nanocomposites microstructure and 3) to examine the relation between the nanocomposites microstructure and its mechanical behavior. Twin-screw extrusion was used to prepare the nanocomposites using the best compounding practices. The microstructure was characterized using state-of-the-art SEM, TEM, AFM microscopy and X-Ray diffraction. Mechanical properties were examined using standard tensile testing and the EWF methodology to finely probe the fracture resistance. Thermal properties were probed using standard DSC techniques on samples freshly molded as well as on samples aged up to 300 days.

CHAPTER 2

FRACTURE MECHANICS IN POLYMERS

2.1 Fracture Mechanics in Polymers

The fracture of polymers is defined as a partial disintegration due to the formation of new surfaces. Loads, internal or external, provoke deformation in the specimen and enable the development of some damage that leads to the disintegration of the material. (Kinloch & Young (1983))

There are two clear stages in the fracture process. The first one is called initiation or activation of flaw or defects, the growth of the crack step does not appear during this time. (Kinloch & Young (1983)) This stage is irreversible and appears after the mechanical reversible deformation of the polymer matrix. The second stage is related to the growth of the initial deformed zone, the increment of the initial crack size, and the increase of the velocity of crack propagation. The crack propagation finishes when the crack size causes mechanical instability and leads to the final brakeage of the specimen.

The crack behavior depends on the properties of the polymer matrix, specimen geometry and the conditions during the loading. (Kinloch & Young (1983)). In general, the polymer materials and their cracks can be classified as fragile or ductile. Materials with ductile behavior are associated with the presence of large plastic deformation before crack instability appears, large amount of energy dissipation and large deformation which takes place over a relative long time period. The yielding process before final breakage is always present in ductile failure. In contrast, brittle materials are characterized by low

energy dissipation, small deformation and lower presence of plastic deformation. The breakage in this type of materials is unexpected and catastrophic. The crack velocity is high in this case.

Cracks are also classified by propagation's velocity. High crack propagation rates are directly related with high stress field at the crack tips, then the specimen shows rapidly instabilities to finally produce a specimen breakage. In low propagation rates, the crack shows a stable and uniform growth where loading is continuous and gradually applied on the specimen.

Fracture mechanics is a very complex process that involves the nucleation and growth process of cracks with presence of dislocations, flip banding or other phenomena. (Broek (1984)) The geometry of specimens, temperature, force loading mode and speed and other environmental conditions also affect the fracture process. It can be assumed that all materials have initial and inherent defects in the form of inclusions, cracks, voids, etc. These defects can originate from a second phase added to the major phase, to debonding in composites, to fabrication defects or to fatigue cracks or creep cracks. The defects affect the mechanical performance of the materials decreasing the permissible loading capacity of them. The types of fracture found in a material can be associated with the imperfections present in it prior to failure. Defects such as dislocations, crazes, shear banding, precipitates and interstitial substitutional atoms are mainly discovered in ductile fracture while large defects such as cracks, surface scratches, inclusions and sharp notches in brittle fracture.

In polymers, there are two main mechanisms for crack production. (Roesler et al. (2007)) (Kinloch & Young (1983))

The first mechanism is known as crazes formation or crazing (Figure 2.1). Crazes are microscopically lengthened cavities of ~ 1 μm to 10 μm thicknesses and ~ 10 μm to 1000 μm of diameter. These individual cavities are connected by fibrils (Figure 2.2) which are made from several polymer chains with diameters of 10 nm to 100 nm. The fibrils take a volume fraction between 10 to 50% into an individual craze.

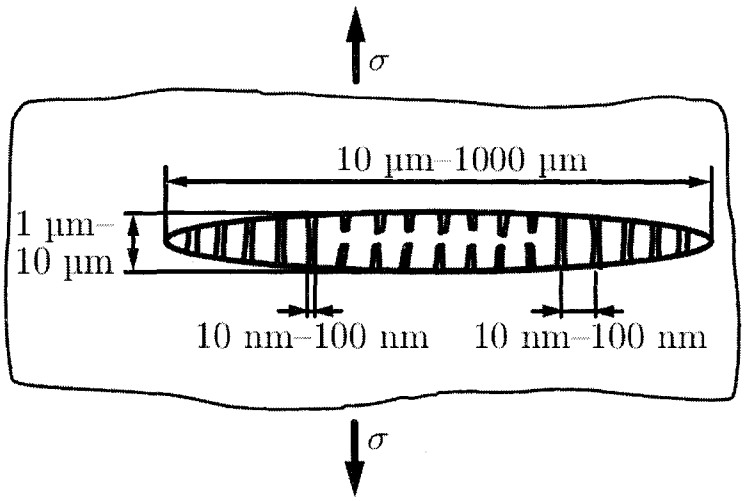

Figure 2.1. Micro-structure of a craze. (Roesler et al. (2007))

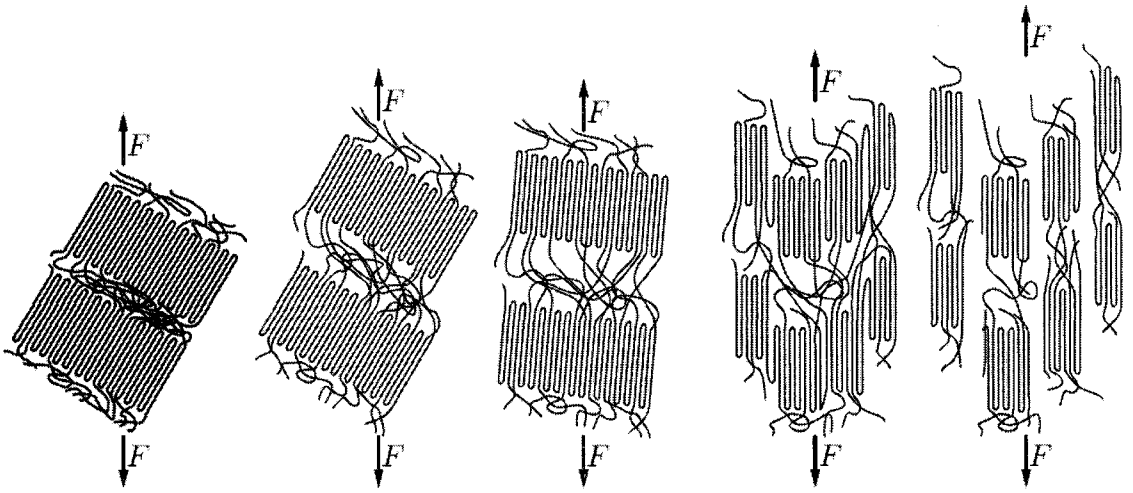

(a) Initial stage (b) Lengthening amorphous regions (c) Rearrangement of crystalline regions (d) Separation into blocks (e) Formation of microscopic fibres (microfibrils)

Figure 2.2. Schematic representation of the plastic deformation process of a semi-crystalline thermoplastic. (Roesler et al. (2007))

The craze's length size is independent of the applied load. However, at high loads the number of crazes increases. The effect of the temperature in the craze's size is clear; an increase of temperature raises the craze's length. Craze formation (Figure 2.3) results from surface defects such as impurities, scratches or small cavities. The cavities have a few nanometers of length. Those defects caused stress on the material which then is plastically deformed generating fibrils and crazes. The craze's growth originates the fracture of the polymer.

Craze mechanics is a characteristic present in amorphous polymers such as polyethylene terephthalate (PET), polystyrene (PS), polypropylene (PP), polymethylmethacrylate

(PMMA), polycarbonate (PC) and high impact polystyrene (HIPS) (Kausch et al. (1983)) (Jang et al. (1985)) (Bucknall (2007))

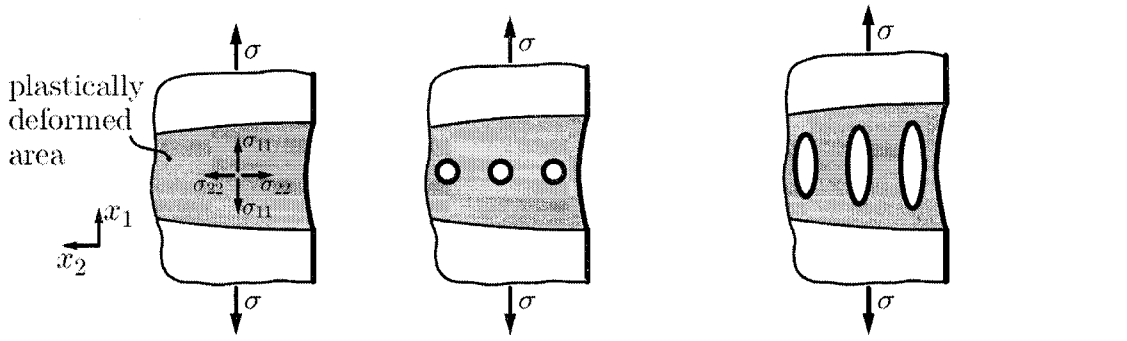

(a) Local necking (b) Formation of cavities (c) Extension of cavities

Figure 2.3 Development of a craze by formation of cavities (Roesler et al. (2007))

Crazes should not be though of as micro cracks. In zones with crazes, the fibrils increase the fracture toughness. Thus, the strength of the material in that zone is only slightly reduced in comparison to the unloaded material.

The second mechanism of plastic deformation in polymers is known as shear yielding. The shear yielding mechanics is based on the formation of shear bands. (Roesler et al. (2007)) (Kinloch & Young (1983)) Shear bands are created by a large plastic deformation becoming mainly visible under compression loads. The polymer chains are stretched and aligned under shear forces to form the shear band region (Figure 2.4) The convergence of some shear bands produces a crack. The shear bands appears at 45° and 60° with respect to loading direction

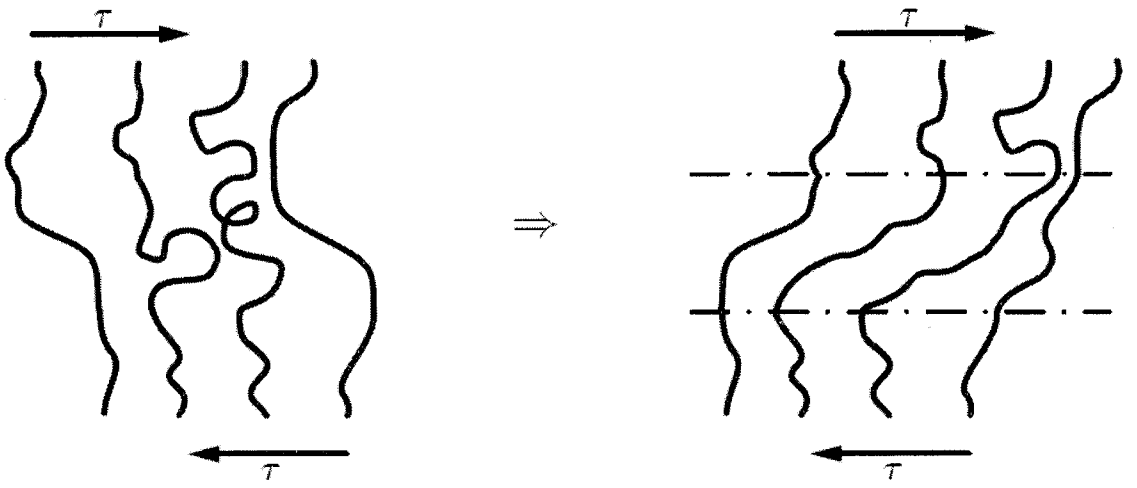

Figure 2.4 Formation of a shear band by local stretching and contracting of polymer chains. (Roesler et al. (2007))

2.1.1 Fracture Mechanics in Polymer Composites

The addition of diverse types of particles as a reinforcement phase into a polymer matrix increases the tenacity and toughness of the neat polymer. The polymer composites show enhancement resistance to crack propagation by increasing the energy dissipated during the fracture process. (Roesler et al. (2007))

The incorporation of particles permits increase the plastic volume deformed at the crack tip, generating new fracture surfaces and acting as barriers for the crack fronts, increasing the energy needed to propagate a crack.

The same mechanics for plastic deformation in polymers, crazing and shear yielding are present also in the deformation of polymer composite. However additional mechanics as crack-pinning (Figure 2.5) or cavitation (Kinloch & Young (1983)) are characteristic in polymer composites. In the crack-pinning mechanics, the addition of rigid particles

interacted with the crack front and the polymer matrix. In the crack-pinning, the crack length and shape is increasing by the pinning and bowing process, then the formation of tails at the rear of the particles and finally the reunification of crack front was produced. Thus the energy need to the fracture process is increasing and the fracture toughness is improved. (Kinloch & Young (1983))

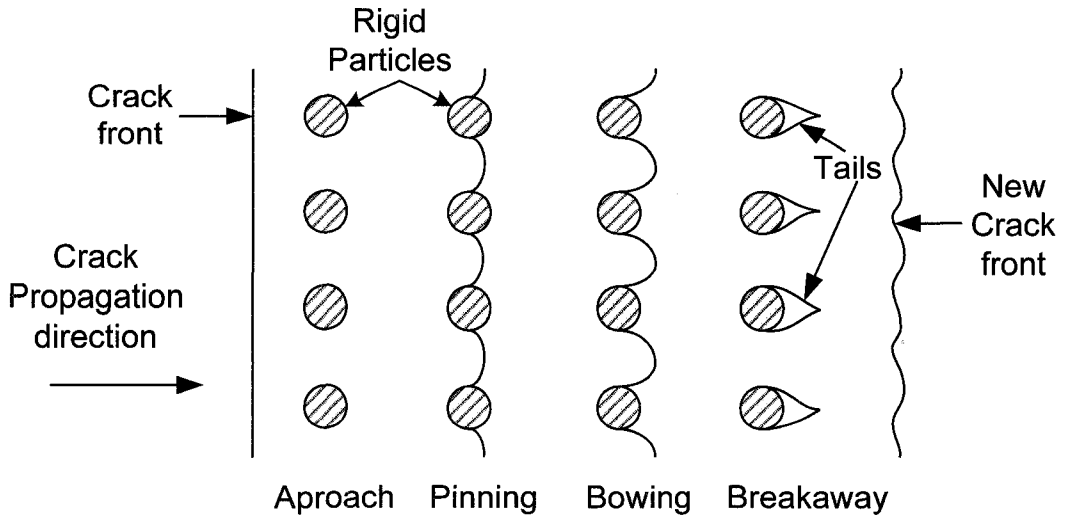

Figure 2.5 Schematic representations of the crack-pinning mechanics. Adapted from (Kinloch & Young (1983))

2.2 Fracture toughness in Polymers

The fracture toughness is an intrinsic material property that quantifies the capacity of a material to absorb energy during the fracture process. Therefore, the fracture toughness can be used as a reference to compare different materials.

The loading modes are important in fracture mechanics; they are associated with relative crack face displacement for a cracked specimen. These modes are also known as crack propagation modes and are denoted as mode I, II and III. (Figure 2.6)

Mode I: The tensile or opening mode.

Mode II: The in-plane shearing or sliding mode.

Mode III: The anti-plane shearing or tearing mode.

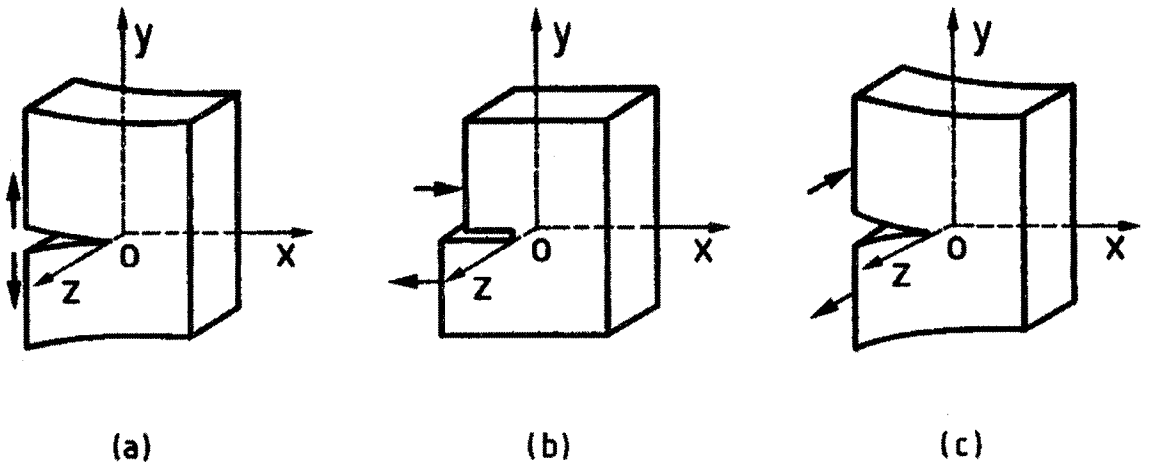

Figure 2.6 Three independent loading modes of crack extension. (a) opening: mode I, (b) sliding or shearing: mode II , and (c) tearing: mode III. (Gdoutos (2005))

2.3 Linear Elastic Fracture Mechanics (LEFM)

This theory is based in the assumption that the materials are linear, elastic and isotropic. The presence or pre-existence of flaws type crack-like is a condition for crack initiation and later crack propagation process. The energy involved in the crack propagation and thus the increase of cracked surface is assumed as energy of fracture. The LEFM achieve

to relate the stress field, magnitude and distribution near to crack tip with loads applied distant from crack, and crack shape and size.

2.3.1 Griffith's Theory: Energy Approach

The first studies in this topic were presented by A. A. Griffith (1921) and were followed by numerous others (Gdoutos (2005)) (Kinloch & Young (1983)) (Perez (2004)) (Broek (1984)) (Bui (2006)) . The first criteria for crack propagation in solids used the idea of the transformation of energy between elastic energy in surface energy. The stress intensity factor was derived from the direct relation between the extension of the crack and the creation of new surfaces at the faces of crack.

Griffith calculated the total potential energy of the system, using an infinite plate, in loading mode I, (Figure 2.7 a) containing a through-thickness crack of length 2a under tensile load. The total potential energy was expressed in the following equation. (Perez (2004)).

$$U = U_o - U_a - U_\gamma \qquad (2.1)$$

Where U is the total potential energy of the system, U_o is the elastic energy of the uncracked specimen, U_a is the energy consuming by introduction the crack in specimen and U_γ is the surface energy or energy consuming by the development of the new crack surfaces. Griffith studies showed that fracture is related to the consumption of potential energy and that the same proposal can be applied for a plate with defined dimensions (Figure 2.7 b) obtaining the following equation (Perez (2004))

$$U = U_o - \frac{\pi\beta a^2\sigma^2 B}{E} - 2\left(2aB\gamma_s\right) \qquad (2.2)$$

Where a is one half crack length , B is the thickness, $4aB$ is the total surface crack area, γ_s is specific surface energy, E is the elastic modulus, σ is applied stress, υ is Poisson's ratio, $\beta=1$ for plane stress and $\beta=1-\upsilon^2$ for plane strain.

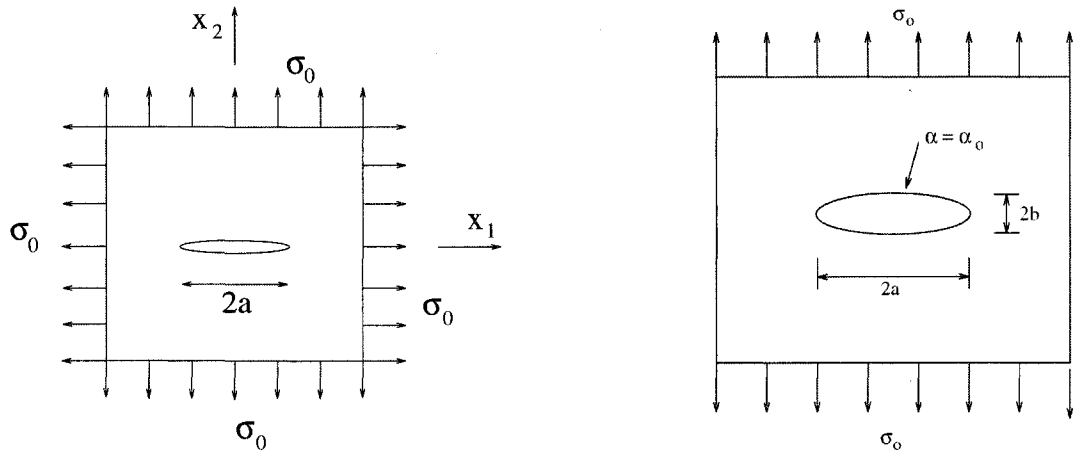

Figure 2.7 a) Infinite plate containing a crack of length 2a under stress at infinity. (b) Large plate containing an elliptical hole.

If equation 2.2 is partially derived in terms of crack length and then equal to zero ($dU/da=0$). It is obtained an expression for critical crack size and for total surface energy.

$$a = \frac{(2\gamma_s)E}{\pi\beta a\sigma^2} \qquad (2.3)$$

$$2\gamma_s = \frac{\pi\beta a\sigma^2}{E} \qquad (2.4)$$

By rearranging equation 2.4, the expression for stress intensity factor (K_I), for this particular geometry is as follows:

$$K_I = \sigma\sqrt{\pi a} = \sqrt{\frac{(2\gamma_s)E}{\beta}} \qquad (2.5)$$

The stress intensity factor, K, corresponds to the amplitude of the crack tip stress singularity.

$$\sigma_c = \sqrt{\frac{(2\gamma_s)E}{\beta\pi a}} \qquad (2.6)$$

Griffith work also showed that when the stress reached the critical stress, σ_c, the crack propagation process started.

The stress intensity factor (K) can be used to describe the driving forces to crack a specimen. When the critical value of K_I is reached, this is denoted as (K_{IC}). K_{IC} is taken as a material property known as fracture toughness. The fracture toughness can be explained as the resistance to crack extension. K_{IC} is used to compare different materials in presence of driving forces to crack them. K_{IC} implies, in brittle fracture,

The second derivative with respect to the crack length of equation 2.2 gives us an expression that indicates that the crack always has a tendency to grow and propagate inside this unstable system.

2.3.2 Critical and strain energy release rate

Equation 2.6, developed by Griffith, is derived on the assumption of brittle fracture without presence of plastic deformation. Researches E. Orowan (1950) and later G. R. Irwin (Kinloch & Young (1983)) (Perez (2004)) (Bui (2006)) introduced terms related with the plastic deformation. They observed the presence of plastic deformation for tested metal and polymer specimens. Orowan showed that the energy consumed during the

fracture process is much grater than surface-elastic energy assumed by Griffith. Orowan introduced a term relative to plastic deformation using as a reference the Griffith energy approach. Therefore equation 2.6 is modified as shown in equation 2.7

$$\sigma_c = \sqrt{\frac{2E\left(\gamma_s + \gamma_p\right)E}{\beta\pi a}} \qquad (2.7)$$

Where γ_P is the plastic deformation energy, this term was explained as plastic strain work γ_P during the fracture process. G. R. Irwin (1950) incorporated both energy terms γ_S and γ_P into a single expression G, as shown in equation 2.8

$$G_I = 2\left(\gamma_S + \gamma_p\right) \qquad (2.8)$$

$$G_I = \frac{\pi a \sigma^2}{E/\beta} \qquad (2.9) \qquad \text{or in terms of stress}$$

$$\sigma = \sqrt{\frac{EG_I}{\beta\pi a}} \qquad (2.10)$$

Irwin developed an expression to quantify the total elastic-plastic strain energy under tension loading called also strain energy rate G and G_I for the loading mode I. (Perez (2004)). The strain energy release rate G_I represents the energy consumed or supplied by the body elastic energy and external loads per unit length along the crack edge to create and increase the new fracture surface area. In the same way, as the stress intensity factor reaches a critical value, G_{IC} is known as the critical energy release rate during the fracture process.

Combining equations 2.5 and 2.9, we obtain a relation between intensity factor and energy release rate. Equation 2.11 was developed for plane stress state and equation 2.12 for the plane strain state case.

$$G_I = \frac{K_I^2}{E} \qquad (2.11)$$

$$G_I = \frac{K_I^2\left(1-\upsilon^2\right)}{E} \qquad (2.12)$$

K_{IC} and G_{IC} are two of the most standard parameter used to quantify the toughness of materials before fracture.

Irwin proposed that materials should be considerer as completely elastics up to the uniaxial tensile yield stress σ, after that the plastic effect starts. This model described the extension of crack tip plasticity as shown in Figure 2.8 in addition Irwin worked on the crack-opening displacement at the crack tip (δ) and the corrections to plastic zone size, r_p.

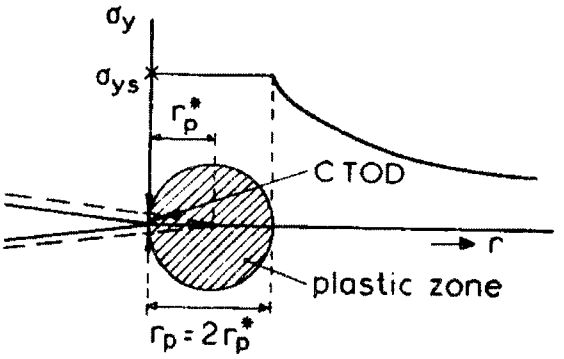

Figure 2.8 Irwin model to plastic zone at the crack tip (Broek (1984))

2.4 Elastic Plastic Fracture Mechanics (EPFM)

Linear elastic fracture mechanics (LEFM) is based on materials that do not reach yielding during the fracture process. This assumption is only applied for materials that show brittle fracture. For most polymers and for some other materials, this hypothesis is unpractical and unrealistic to the study of polymer toughness. In consequence, the stress intensity factor K, basic concept in LEFM, is not adequate to describe the problem.

Polymer systems are characterized by semi-ductile, ductile or rubber behavior. The LEFM's principles have no validity for polymers since they can not be consider as a linear solid body, and they present high plasticity at the crack tip. Then, it is necessary to extend the initial analysis considering the contribution of energy dissipation by plastic deformation.

There are some approaches to explain the Elastic Plastic Fracture Mechanics (EPFM). Two of the most important models used are the J-Integral (J_{IC}) and crack-tip opening displacement (CTOD).

The experimental procedure to measure J_{IC} consists in performing tests to achieve stable crack growths during certain lengths (Δa) and using several geometric identical specimens with the same crack length a.

The crack resistance curves (J_{IC} vs Δa) are plotted and J_{IC} is defined as a point where the slope changes dramatically. Besides, its versatility, J-contour integral method lacks of precision when determining and measuring the extremely tiny increments of length crack (Δa).

The crack tip opening and tip displacement (CTOD) is also used to measure the fracture toughness of materials that show elastic plastic, plastic or transitions from ductile to brittle behavior. (Gdoutos (2005)) (Broek (1984)) (Wang (1996))

During the transition from the sharp crack tip to blunt tip due to plastic deformation process, a finite radius is produced at the crack tip. The radius and the crack-opening displacement at the crack tip (δ) were estimated and developed by Irwin's model.

It is possible to relate the critical CTOD with the J-contour integral. However this relation is not simple because CTOD as a parameter is not independent from specimen geometry and it depends on deformation field at the crack tip. This approach assumes a uniform deformation process. However, in polymers, the deformation is not homogeneous. For this reason the use of this method to derivate values of fracture toughness in polymer materials is limited.

2.5 Essential Work of Fracture (EWF)

As previously mentioned, the J-contour integral and CTOD criterions present limitations, such as lack of precision during the measuring of crack length (a and Δa) in the J- contour integral case, and the assumption of homogeneous plastic deformation during the fracture process for polymer specimens (Gdoutos (2005)). Those restrictions make difficult the study of fracture toughness in polymers or in polymer nanocomposites.

Based on this previous work and using the principles derived by Broberg (Broberg (1968)) (Broberg (1975)) (Broberg (1982)) the theory of the essential work of fracture (EWF) was developed. An experimental method based on the EWF theory was developed to study the fracture behavior initially in ductile metals. Cotterrell and Reddel (Cotterell

& Reddel (1977)) revised and modified this first EWF method. In addition, they proposed the equivalence between the CTOD and the theoretical zero ligament length used in this method. Mai and Cotterrell (Mai & Cotterell (1986)) applied for the first time the EWF method in polymers. They tested specimens of polyamide 66 (PA66), HIPS and two grades of HDPE showing the applicability of EWF in polymers and relating the results obtained with the J-contour integral. Also the EWF method was tested in PET (Mouzakis et al. (2000)) and contrasted with the CTOD method and showed a bad agreement in the results between both methods.

For ductile behavior materials, Broberg used a specimen containing a central notch and proposed that the plastic zone at the crack tip involve in the fracture process can be divided into two zones. The internal zone is called inner fracture process zone (IFPZ) or fracture zone and the second zone is called outer plastic zone (OPZ) or plastic zone. These two zones share deformations related with the plasticity flow or plastic deformation. Broberg assumed that the energy dissipated inside the fracture zone is constant and it should be assumed as a material property.

On the other hand the plastic zone is not constant. It depends on the specimen geometry, loading mode and the ligament length (l). (Broberg (1968)) (Cotterell & Reddel (1977)) (Mai & Cotterell (1986))

The EWF method relies on concepts of energy to describe the mechanics of fracture in notched specimens. The EWF method assumes that the total energy (W_F) involved in the fracture of a notched specimen can be also divided into two parts. One part is associated with the propagation of the crack, resulting in the formation of a new fractured

area. This energy is designated as the essential work of fracture EWF (W_E) and it is associated with fracture zone (IFPZ). The other part is related to the volume being plastically deformed, this fraction is called the plastic work of fracture (W_P) or non-EWF and it depends of the specimen geometry and process zone. In addition the plastic work of fracture is related with plastic zone (OPZ)

The total work of fracture can be described using the following general expression:

$$W_F = W_E + W_P \qquad (2.13)$$

The energy associated with W_E is related to the surface created during the fracture process. Then W_E is proportional to the fracture area. On the other hand, W_P is directly proportional to the ligament length squared and depends on the volume of plastic zone. These assumptions were experimentally corroborated using polymer specimen Nylon 66 (PA66), (Mai & Cotterell (1986)) PP, (Karger-Kocsis (1996)) and LLDPE. (Mai & Powell (1991))

Procedures and data analysis for the EWF method is more practical than for the J-contour integral, CDTO and other parameters. Therefore, the EWF method is more commonly used to test the fracture toughness in polymers. However the EWF is not recognized as a formal standard test for polymers by ASTM or other organisms while for metals, it is a standard test. The total energy W_F can be also expressed in terms of specific total energy (w_F) and graphically W_F can be expressed as the area under a load displacement curve such as the one shown in Figure 2.9:

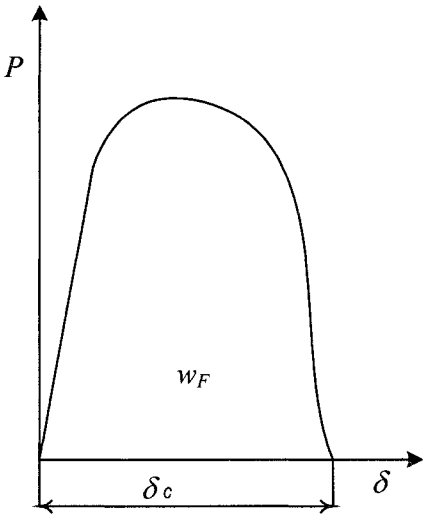

Figure 2.9 Typical load displacement curve.

The following expressions were developed from the general equation 2.13

$$W_F = \int_0^{\delta_c} P d\delta = w_F l t \qquad (2.14)$$

Where l is the length of ligament, t is the thickness of the notched specimen.

Equation (2.14) which is based on the previous assumptions can be rewritten in terms of specific values.

$$W_F = w_E l t + w_P \beta l^2 t \qquad (2.15)$$

Where β is a shape factor related to the geometry of plastic zone, w_E is the specific fracture work per unit of new produced area, and w_P is the specific plastic deformation work or specific non-essential work per unit of plastically deformed volume. By dividing equation 2.15 by the nominal fractured area, we obtain a linear expression in function of the ligament length l to express the specific total work of fracture (w_F).

$$w_F = w_E + \beta w_P . l \qquad (2.16)$$

Then, it is possible to determine the value of w_E and βw_P from equation 2.16 by obtaining data for various ligament length l.

Based on the assumption that w_E is a constant and characteristic of a material and that w_F and β are independent of ligament length (Cotterell & Reddel (1977)); an experimental method was developed to derive these parameters. The experimental method requires the use of films or thinner sheets expected with this requirement to work under plane-stress conditions. The specimens, containing one lateral notch (DSENT) or double lateral notches (DDENT) are tested under tension. The test is accomplished by varying different ligament lengths. Using the data from tension is possible to plot different load displacement curves varying the ligament length as shown in Figure 2.9. The shape of these curves depends of the geometry of the tested specimen and the mechanical behavior observed during the test. Figure 2.10

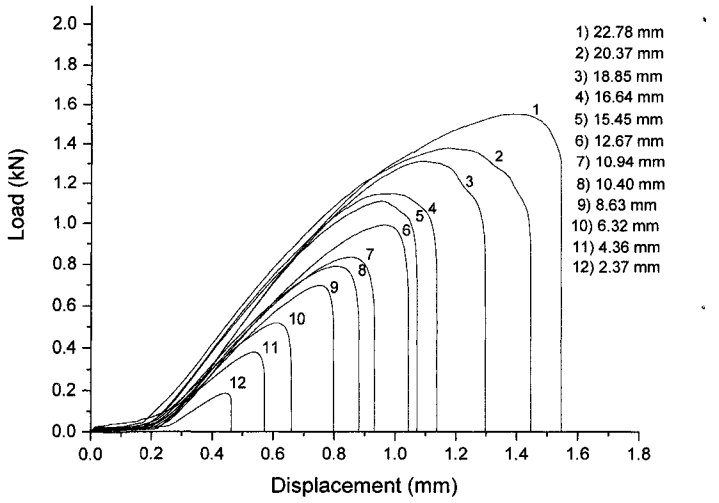

Figure 2.10 Load displacement curves for different ligament lengths for 27TPS/PLA

The specific energy related with the fracture process (w_E) is calculated as the area under the load displacement curves and later divided by the fracture area. It is possible to

plot these energy values against their respectively ligament length value using equation 2.16. This procedure is show in the Figure 2.11

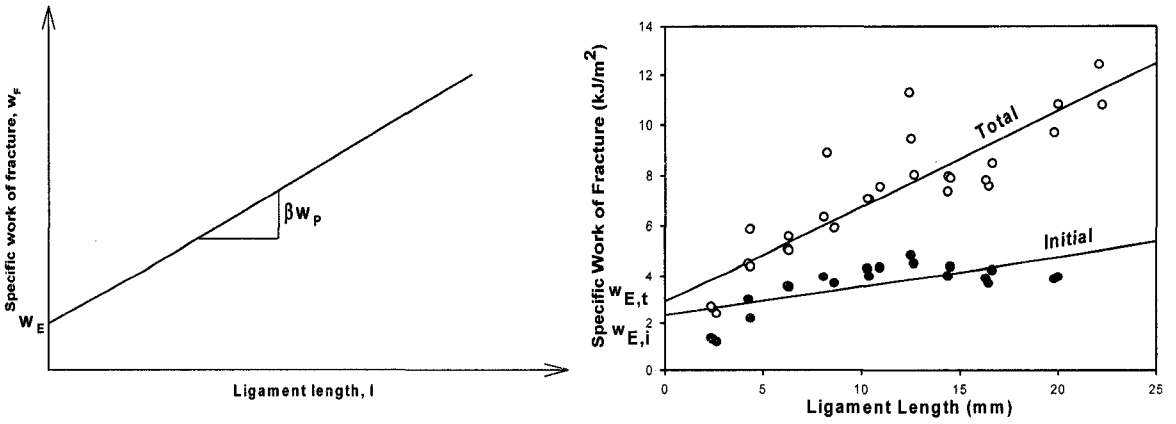

Figure 2.11 Theoretical definition of specific EWF using the equation 2.16 (right) and the experimental determination of the specific EWF (left).

The geometries of the specimens used in EWF method are the same for polymers and metals. Some of these geometries are showed in Figure 2.12. The most used specimen geometries are the deeply single edge notched tension (DSENT) and the deeply double edge notched tension (DDENT). Other possible specimen geometries include the deeply centre notched tension specimen (DCNT) (Mai & Powell (1991)), single edge notched specimen bend (SENB) tested in PA6,6/PP blends (Wong & Mai (1999)), and less commonly, the trouser specimen to simulate the loading mode III. All these geometries were tested in polymers. Among all these specimens, the DDENT specimen shows some advantages such as the achievement of total specimen collapse and a better repeatability of results (Moore et al. (2001))

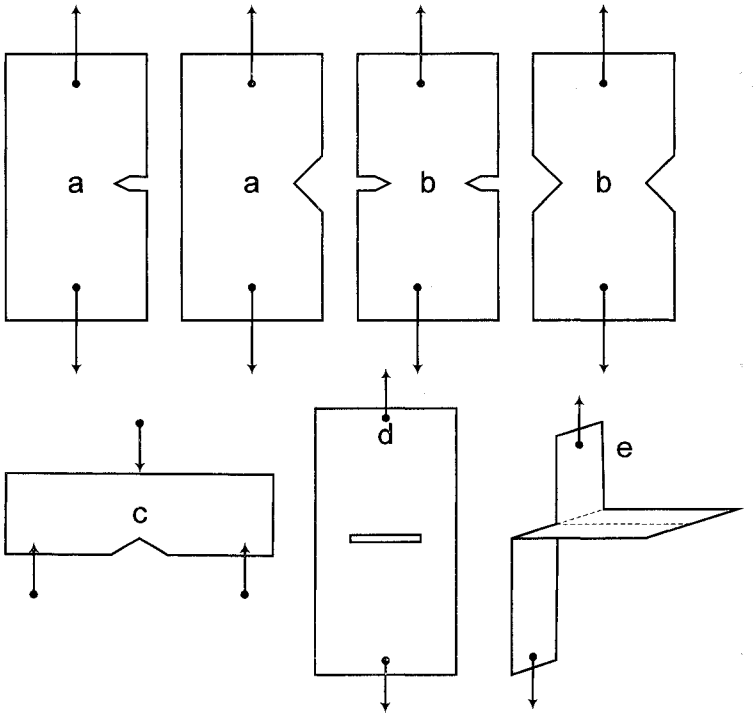

Figure 2.12 Schematic of specimens used in EWF method. a) DDENT specimen. b) DSENT c) SENB d) DCNT d) Trouser tension. Adapted from (Mai & Cotterell (1985))

In our study, we choose to use the DDENT specimens for the advantages mentioned previously. The geometry and dimensions of the DDENT used was shown in Figure 2.13.

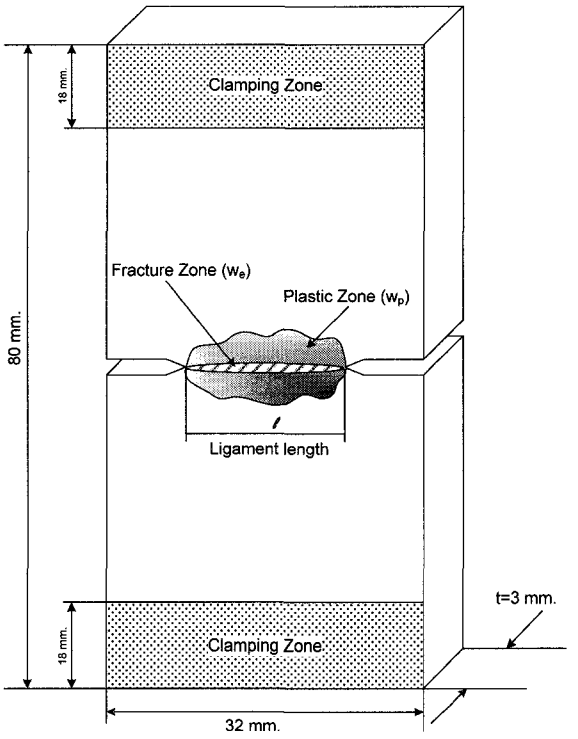

Figure 2.13 Geometry of double deeply notched tension specimen (DDENT) shows the ligament length and the schema of fracture and plastic zone shape.

The EWF method is not yet considered an international standard for polymers. Nevertheless, since 1993, the European structural integrity standard (ESIS) proposed preliminary protocols for the application of the EWF method for polymers. The ESIS protocol has been revised in several occasions. Among these revisions, it is found that the experimental method to determinate the β parameter and therefore w_P from βw_P was discarded due to difficulties in measuring the boundaries of the plastic zone (Moore et al. (2001)) (Moore et al. (2001)) The experimental method of EWF, thought the last years, was modified, revised and developed by the European Structural Integrity Standard (ESIS)

A committee designed by the ESIS established some minimal conditions and restrictions for the validity of this technique. (Clutton (2000)) (Moore et al. (2001)) Three conditions are needed to warrant the quality of the results obtained.

The first is about the ligament length, as we can see in Figure 2.14. The figure shows a region where the ligament lengths show a linear relationship, important to be in agreement with the linear equation 2.16. Based on this restriction, complete development of the crack tip plasticity before the crack propagation is assumed. (E.Clutton (2001)) (Moore et al. (2001)) (Mai & Cotterell (1986)) (Hashemi (1993b)) (Hashemi (2000b))

The ESIS T4 group proposed the following limits for the ligament length

$$3t < l < \min(W/3, 2r_p) \qquad (2.17)$$

Where l is the ligament length, W is the specimen's width, and r_p is the radius of the plastic zone. The restriction of $l < W/3$ is used to avoid the edge effects produced at the plastic zone. On the other hand $l < 2r_p$ was established as a condition to reach a total plastic collapse of the ligament. The determination of r_p is based on the model used to describe the plastic zone .(Paton & Hashemi (1992)) (Hashemi (1997))

The other limit was established for plane stress conditions. The lower limit $l > 3t$ was established for this objective.

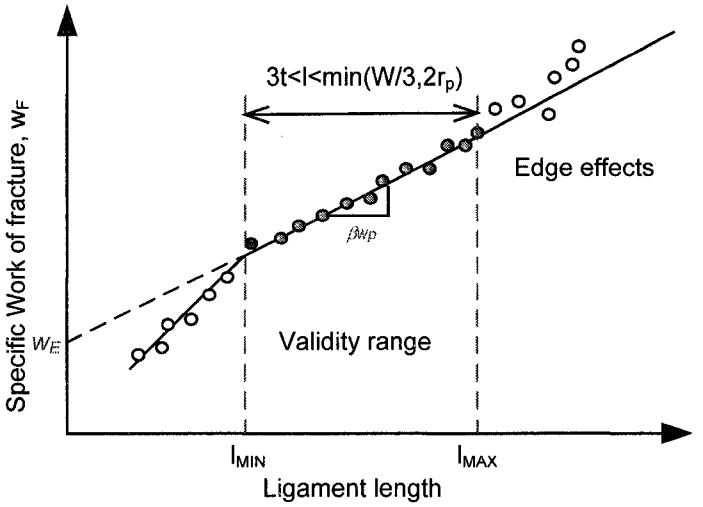

Figure 2.14 Linear region for the ligament length validation.

The second restriction for the EWF method is established in the following way. The local stress strength (σ_{max}) registered for the DDENT specimens varying the ligament lengths (Figure 2.15) must be lower or equal to 1.15 yield strength (σ_y) of the material in the standard uniaxial tensile test at an equivalent EWF test speed. (Hashemi (2000c)) (Hashemi (2000a))

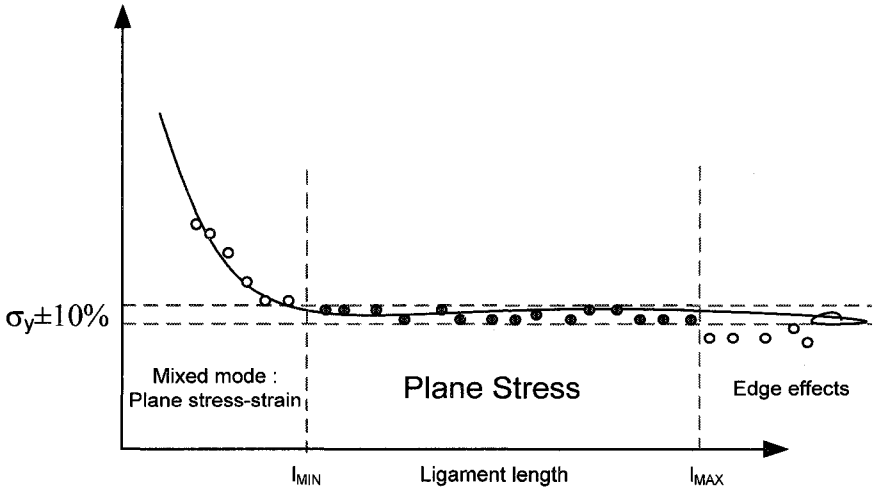

Figure 2.15 Validation of data by comparison with maximum strength based on the Hill's theory of plasticity.

Figure 2.15 shows the variation of local stress strengths along different ligament lengths. High values of the local stress strengths for low ligament lengths were found when a mixed mode was achieved. Based on the theory of plasticity proposed by R. Hill, (1950) (Mouzakis et al. (2000)), it is assumed that stress plane state is present when the variation of the local stress with the ligament length is minimal or when a plateau is reached. However the plane stress state also can be reach above the plateau predicted by Hill.

The T4 ESIS committee proposal does not define a minimal ligament length; however it was proposed a range of valid ligament lengths using as a rule the maximal variation of the local stress strength with respect to the yield strength of the material (equation 2.18). (Clutton (2000)) (E.Clutton (2001))

$$0.9 \leq \frac{\sigma_{max}}{\sigma_y} \leq 1.1 \qquad (2.18)$$

Both limits are not exacts, however this range is used to avoid or minimize to work under a mixed mode, plane strain-strain, when $\sigma_{max} > 1.1\ \sigma_y$ and to reach a total yield along the ligament before the final fracture for high values of ligament or in other works when $\sigma_{max} < 0.9\ \sigma_y$.

The final requirement is self similarity of the load displacement curves for the different ligament lengths. The similar shape of these curves is one of the prerequisites adopted also for the ESIS. An example of the self similarity was shown in Figure 2.10. Although the main objective is the definition of w_E, the specific plastic deformation work or specific non-essential work, w_P, is defined implicitly by the term βw_P. The w_P as

previously mentioned is not a property of the materials. However it provides information about the energy dissipation process during the plastic deformation and fracture of material that the parameter w_E does not take into account.

It is worth mentioning that until now it was not possible to separate w_P, from the expression βw_P. The first attempts of the T4 ESIS group to determinate the values of β based on the plastic zone shape such as diamond, circular, elliptical and other variations were taken into account until the ESIS protocol was published in 1993. In the next ESIS protocol this practice was discarded because of the inaccuracy of the methods used to describe the plastic zone border, measure of the implicated areas and problems in the repeatability of results. In Figure 2.16 it is shown the development of the plastic zone' shape during the EWF test. There, it is possible to notice the difficulty on defining the plastic zone shape. (Fig. 2.16 a to d).

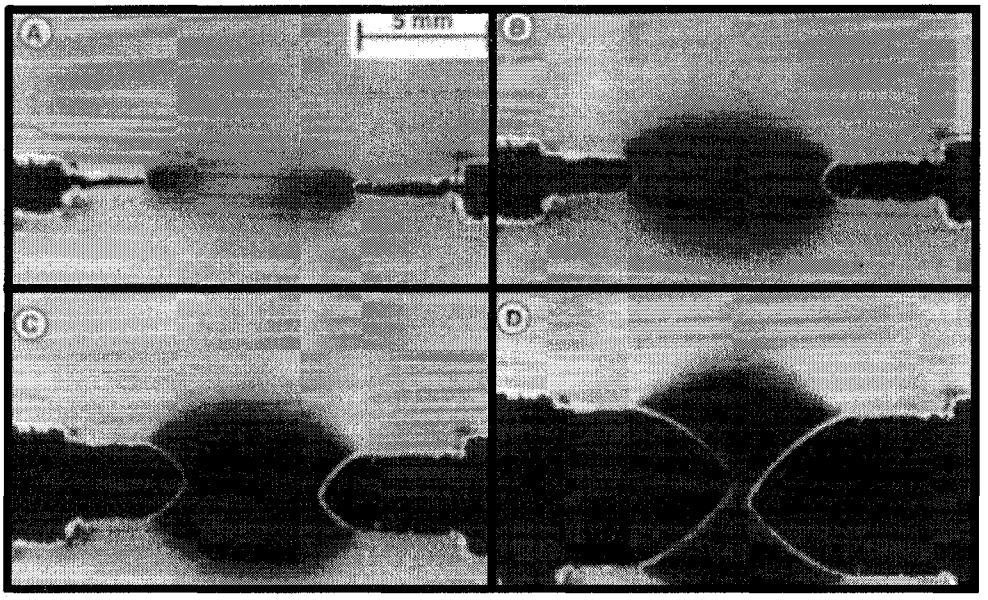

Figure 2.16 Infrared thermographic pictures of DDENT specimen of β-modification of isotactic polypropylene. (Karger-Kocsis (1996))

The whole energy involved in the fracture process can be represented as the area under the load displacement curves. However the mode of partition of the energy involved in the individual process of initiation and propagation was subject of study.

Cotterell and Mai suggested the specific essential work of crack initiation (w_{Eini}) should have a value lower than w_E and w_{Eini} was independent of ligament length and depended of a critical CTOD. (Mai & Cotterell (1986)). By using the load displacement curves (Figure 2.17 a) it was possible to divide the area under the curve based on the point where the crack propagation started. From this point a straight line parallel to the linear portion of the load displacement curve was used to delimit the energy involved in the crack initiation. The δ_{ini} is the critic CTOD related with the crack initiation. This model was successful contrasted in polyamide 66 but not with HDPE. (Mai & Cotterell (1986)) (Mai et al. (1987)). A similar partition for the crack initiation was proposed by Karger-Kocsis et al and devolped by Hashemi (Mouzakis et al. (2000)) (Hashemi (2000a)). In this case the straight line from the crack initiation point is perpendicular to the x-axis (Figure 2.17 b). In our study, this second approach was used to limit the energy involved with the crack initiation.

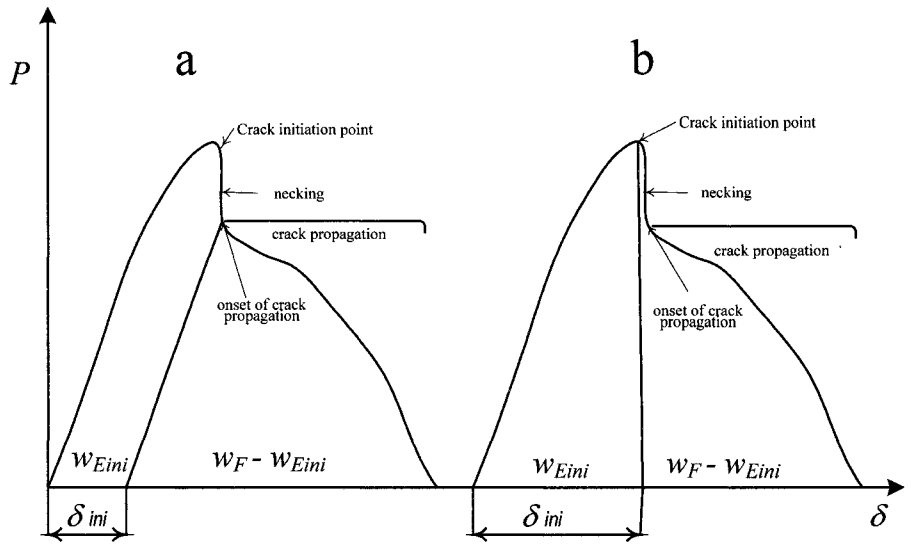

Figure 2.17 Energy partitioning of the fracture process using load displacement curves a) model proposed by Mai and Cotterell. b) model proposed by Karger-Kocsis Modified from (Mai & Cotterell (1986)) (Ferrer-Balas et al. (1999))

2.5.1 Essential Work of Fracture in Polymer and Polymer Nanocomposites

The EWF method was tested with good results to describe the fracture toughness in several polymeric systems such as polyethylene terephthalate PET (60.kJ/m^2), polycarbonate PC (32.kJ/m^2), polybutylene terephthalate PBT (30.kJ/m^2), polyether-ether ketone PEEK (54.7 kJ/m^2), polyetherimide PEI (40.8 kJ/m^2), polyimide PI (66.25 kJ/m^2), polyethylene naphthalate PEN (51.3 kJ/m^2), cellulose acetate CA (13.8 kJ/m^2) (Hashemi (1997)), Polypropylene carbonate copolymer (PPC) (11.kJ/m^2) (Fung et al. (2004)), amorphous copolyester (COP) (36.11.kJ/m^2)(Barany et al. (2003))

Fracture toughness shows to be independent of gauge length (40-120 mm) when using polypropylene homopolymer samples. However, the effect of crosshead speed or strain

rate influenced the values of w_E., 2 to 100 mm/min in iPP, (Ferrer-Balas et al. (1999)), 1, 10, 70, 100 mm/min in ultra high molecular weight polyethylene UHMWPE, (Ching et al. (2000)) 5, 50, 500 mm/min in PA6 (Yamakawa et al. (2004)) and 0.0001 to 3 m/s in iPP and ethylene-propylene rubber/iPP blends (Grein et al. (2003)) and based on the resuts, the quasi-static test conditions was recommended.

The effect of specimen geometry using DDENT, CT and SEN specimens in polybutylene terephthalate (PBT)/PC, ABS/PC, (Jingshen & Yiu-Wing (1996)) PA66, and PE (Mai & Cotterell (1986)), PBT (Hashemi (2000a)) showed similar values of fracture toughness and thus w_E is a material's constant, independent of specimen geometry.

Fracture toughness showed also to be independent of temperature, in certain ranges, when specimens of PC were tested under temperatures from 20° to 120°C (Hashemi & Williams (2000)). However, in samples of polybutylene terephthalate (PBT) (Hashemi (2000c)), w_E decreased from 33.4 kJ/m^2 (25 to 80 °C) to 27.51 kJ/m^2 when the test temperature was 100 °C. Similar behavior was found in PA66/TiO_2 , PA66/SiO_2 , PA66/Al_2O_3 (Zhang et al. (2006)) when test temperatures above 80 °C were used.

The effect of aging time (0 to 50 days) on the fracture toughness was studied on copolyester resins (Chun-Hsin & Nairn (1998)) resulting in good stability of the toughness properties during the test time.

The effect of thickness on the EWF was observed with specimens of thickness 125, 150, 175, 190, 250, 350 and 500 μm using a polyester (Hashemi (1993a)), PC (Hashemi (1993b)) polyether-ether ketone (PEEK) (Hashemi & Yuan (1994)), and PBT (Hashemi (2000a)) 0.5, 1 and 1.5 mm in polyethylene terephthalate glycol (PETG) (Poon et al.

(2001)), 1.6 and 3.2 mm in PA6 (Yamakawa et al. (2004)), 3, 5, and 9 mm in PP and ABS specimens (Fasce et al. (2001)) and 12.5 mm in HDPE (Kwon & Jar (2007)) showed a good linear fit to calculate the w_E , however high w_E values were found using smaller thickness specimens than larger ones. A mixed state, plain strain/strain state related with bigger thickness can explain this difference.

The loading modes I and II, tension and shear modes were compared using polyacrylonitrile butadiene styrene (ABS) samples. The results showed variations of at least 2.5 times in w_E under shear mode than in conventional tension mode. (Kwon & Jar (2005))

The EWF method was also effectively used to test the interface adhesion between PP and PA (Lauke & Schueller (2001)) using DDENT specimens, where each half of the DDENT specimen contained one material.

The EWF method was tested using polymer composites such as PP/$CaCo_3$. (Gong et al. (2005)) The results showed that the addition of 10% of $CaCo_3$ slightly decreased the fracture toughness of the composite, however the incorporation of 20 and 30% of $CaCo_3$ resulted in the lost of toughness ability in a half in comparison with the pure PP.

The fracture toughness of nanocomposites was also measured using the EWF method. The addition of 2 and 4% MMT in HDPE/SEBg (Tjong & Bao (2007)) showed similar performance to neat HDPE, however the w_E of nanocomposites showed reduced values in comparison with grafted HDPE. PP/organo-MMT nanocomposites (Bureau et al. (2006)) (Bureau et al. (2004)) were also tested, the results showed that the addition of 2%

of clay decreased the w_E in comparison with pure PP. However the addition of 2% clay and PP-g-MA in the PP matrix showed an enhanced fracture toughness of nanocomposites. In PP/MMT/SEBS-gMA (Tjong et al. (2005)) showed that the addition of MMT (2 and 4% of organically modified MMT) causes a decrease of fracture toughness. However, increasing the content of SEBS-g-MA (from 5 to 20%wt.) reduces this behavior. Other system studied was a polyethylene-co-methacrylic acid ionomer/MMT (Yoo et al. (2007)). The incorporation of MMT (4 to 10% wt) on this polymer matrix decreased the toughness properties in comparison with the neat polymer. However, when only 2% of MMT was added, an enhancement in fracture toughness was found.

CHAPTER 3

MATERIALS AND PHYSICAL PROPERTIES

3.1 Thermoplastic Starch

Starch is present as an energy reserve in many crops such as corn, wheat, potatoes, etc. Starch's granules (Figure 3.1) are a mixture of two polysaccharides known as amylose and amylopectin. (Figure 3.2) It naturally occurs as water-insoluble granules with a diameter of 1-50 microns. The proportion of amylose and amylopectin is related with starch origin. Starch is completely biodegradable in soil and water and has a hydrophilic character due to the presence of hydroxyl groups on the macromolecular chains.

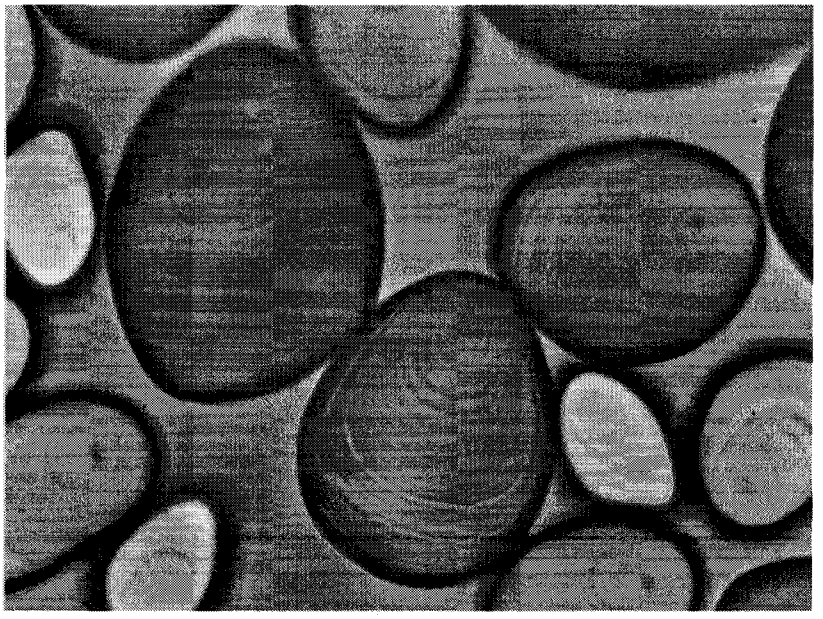

Figure 3.1 Optical micrographs of whole potato starch granules (Bastioli (2005))

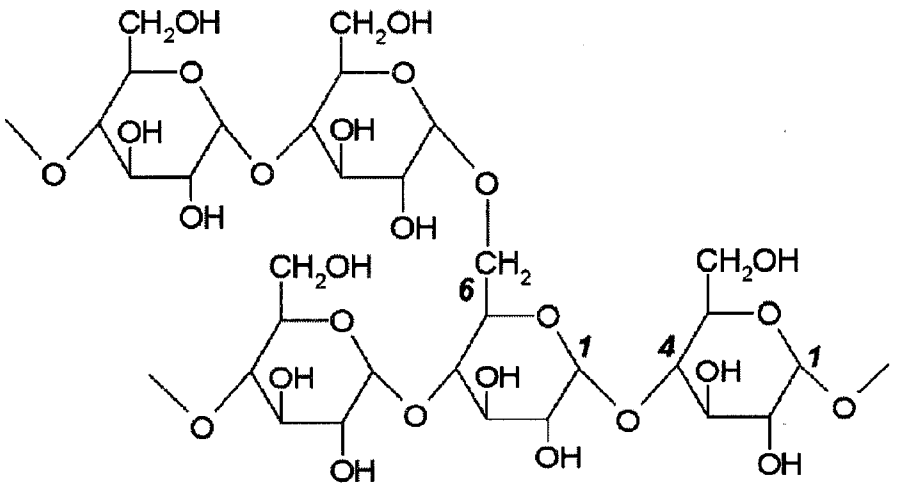

Figure 3.2 Molecular structure of amylopectin (Poutanen & Forssell (1996))

Native starch is not a thermoplastic material per se. Thermoplastic starch (TPS) is produced by gelatinizing the starch granules in the presence of a plasticizers under shear and at temperature above 100°C. After gelatinization, TPS becomes a completely amorphous material. (Figure 3.3)

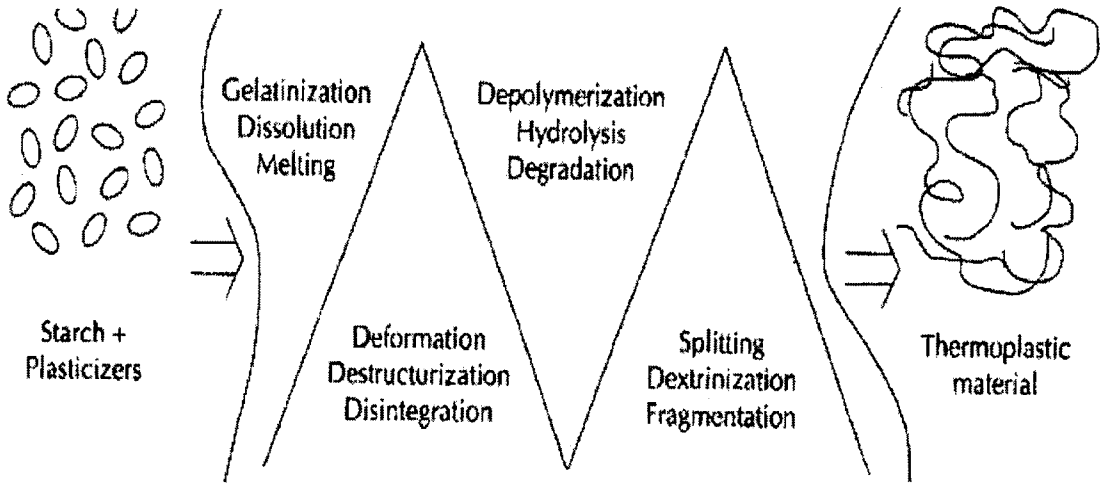

Figure 3.3 Processing of TPS by extrusion (Van Soest et al. (1996))

If starch is plasticized only with water, the starch will recrystallize over in time resulting a embrittlement (Van Soest et al. (1996)). The other problem encountered with water-plasticized starch is its dimensional stability since the water content in the material will be very sensitive to the humidity and temperature level. One first step toward decreasing this dependency is by using high boiling point plasticizers such as glycerol which is more stable. The second step is to blend TPS with a hydrophilic polymer. TPS has been blended with low density polyethylene (LDPE) (Rodriguez-Gonzalez et al. (2003)) (Rodriguez-Gonzalez et al. (2003)) (Favis et al. (2003)), PLA(Martin & Averous (2001)) (Huneault & Li (2007)) and polycaprolactone (PCL) (Shin et al. (2004)).

3.2 Polylactide

PLA is a biobased thermoplastic polymer obtained using a chemical synthesis process (Figure 3.4), more specifically by ring opening polymerization of lactide, a lactic acid cyclic dimer. (Figure 3.5) The lactic acid is derived from bacterial fermentation of dextrose obtained from corn starch. PLA is a linear aliphatic polyester and has similar physical, mechanical and optical properties to polyethylene terephthalate (PET). As a result PLA is an appropriate alternative as a food packing material. (Auras et al. (2005)). PLA has been blended with other polymers such as, poly(ε-caprolactone) (Semba et al. (2006)), poly (R)-3-hydroxybutyrate, poly(ethylene oxide) and poly(vinyl acetate) (Mehta et al. (2005)), poly(propylene carbonate) (PPC), poly(para-dioxanone) (PPD), Polyhydroxyalkanoate (Anderson et al. (2008)) to obtain less brittle and more flexible materials while keeping the PLA strength.

An interesting feature of PLA structure is related to the stereochemistry of its monomer. There are both L and D forms of lactic acid. The crystallinity of PLA, and in turn its physical properties, can be readily modified by varying the chemical composition in terms of L-and D- isomer during its synthesis. (Garlotta (2001)) Commercially available PLA generally comprise a major part of the L-LA component which is more easily produced using biotechnological processes. In this context, the D-LA content is used to disrupt the crystallization of the L-LA and control the final crystalline content of the material. Some of physical and mechanical properties of PLA are summarized respectively in Tables 3.1 and 3.2.

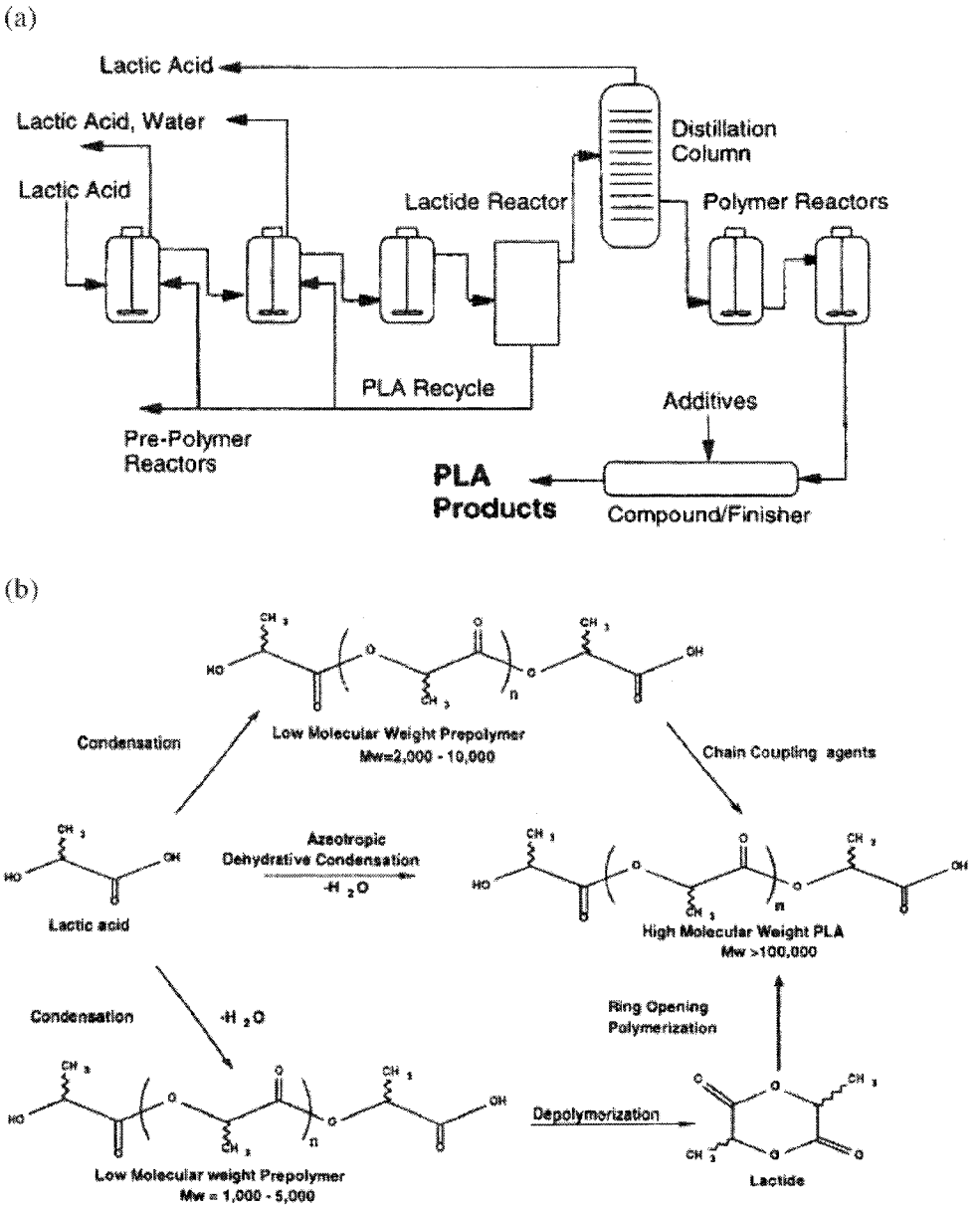

Figure 3.4 a) Cargill commercial manufacturing process of PLA (b) Manufacturing routes of polylactic acid (Sinha Ray & Okamoto (2003a))

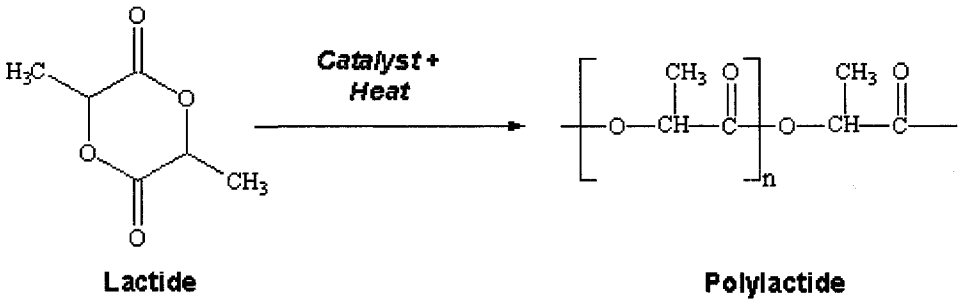

Figure 3.5 Ring-opening polymerization of lactide to polylactide.

Table 3.1 Some physical properties of PLA (Marks (1999))

PROPERTY	UNITS	CONDITIONS	VALUE
Degree of crystalline X_c	%	D-PLA	Semicrystalline
		L-PLA	0-37
		D,L-PLA	Amorphous
Density ρ	gcm^{-3}	P(L-co-DL)LA	
		Amorphous	1.248
		Single crystal	1.290
Heat of fusión ΔH_f	kJ mol^{1}	L-PLA complete crystalline	146
		L-PLA fiber	
		As extruded	2.5
		After hot-drawing	6.4
Heat capacity C_p	$JK^{-1}g^{-1}$	L-PLA of	
		M_v = 5,300	0.60
		M_v = (0.2-6.91) x 10^5	0.54
Glass transition temperature T_g	K	L-PLA of various molecular weights	326-337
		D,L-PLA of various molecular	323-330
Melting point T_m	K	D-PLA injection-molded, M_v = 21,000	444.4
		L-PLA of various molecular weights	418-459

Table 3.2 Mechanical properties of PLA (Marks (1999))

PROPERTY	UNITS	CONDITIONS	VALUE
Tensile strength	MPa	L-PLA film or disk, M_w = (0.5-3) x 10^5	28-50
		L-PLA melt-spun fiber	Up to 870
		L-PLA solution-spun fiber from D,L-PLA film or disk, M_w = (1.07-5.5) x 10^5	29-35
Tensile modulus	MPa	L-PLA film or disk, M_w = (0.5-3) x 10^5	1,200-3,000
		L-PLA melt-spun fiber	Up to 9200
		L-PLA solution-spun fiber from	
Flexural storage modulus	MPa	L-PLA film or disk M_w = (0.5-3) x 10^5	1,400-3,250
		D,L-PLA film or disk, M_w = (1.07-5.5) x 10^5	1,950-2,350
Shear strength	MPa	L-PLA pin	54.5
Shear modulus	MPa	L-PLA melt-spun monofilament	1,210-1,430
Bending strength	MPa	L-PLA pin	132
Bending modulus	MPa	L-PLA pin	2,800
Elongation at yield	%	L-PLA film or disk, M_w = (0.5-3) x 10^5	3.7-1.8
		D,L-PLA film or disk, M_w = (1.07-5.5) x 10^5	4.0-3.5
Elongation at break	%	L-PLA film or disk, M_w = (0.5-3) x 10^5	6.0-2.0
		L-PLA fiber spun from toluene	12-26
		L-PLA melt-spun fiber, M_v = 1.8 x 10^5	25
		D,L-PLA film or disk, M_w = (1.07-5.5) x 10^5	6.0-5.0

3.3 Layered Silicates: Clay Structure

The surface properties and structure of the clay involve the final the properties of the nanocomposites. Also the chemical treatment and different procedures used to prepare the composites produced nanocomposites with different properties.

Different types of clays and other natural materials, have been used in polymer as reinforced polymer matrix.

Layered silicates are inorganic materials that are layered in crystal structure. Most of layered silicates are part of 2:1 phyllosilicates family (Figure 3.6). Natural clays like montmorillonite, saponite and hectorite, and synthetic silicates such as mica, kenyaite and

magadiite belong to the layered silicates family. Layered silicates have layer thickness around 1nm and high aspect ratio in a range of 30 to 1000. (Krishnamoorti et al. (1996))

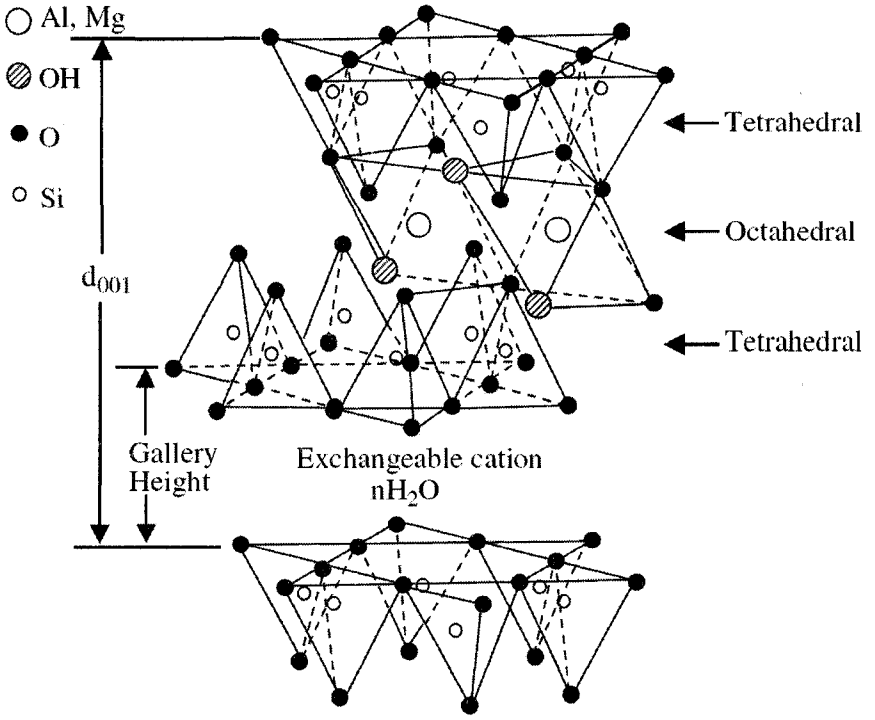

Figure 3.6 Structure of 2:1 smectite clays. (Chen & Evans (2006))

Desirable characteristics in layered silicates are their ability to exfoliate in single layers while dispersed in a polymer matrix. Their capability of reaction or exchange on the silicate surface with guest cations is decisive to reach a stable intercalation. The use of clay platelets is attractive, because they have a high elastic moduli between 178 and 265 GPa. (Chen & Evans (2006)) that can readily be put to profit because of the very high aspect ratio of the particulates in their exfoliated form.

Montmorillonite, saponite and hectorite (Table 3.3) which belong to smectite family are the most commonly used in nanocomposites due to their high cation exchange

capacity and high aspect ratio. When the layered silicates are well dispersed inside a polymer matrix in single or dual platelets, the contact surface between the mineral and the polymer is a thousands time higher than in conventional composites. This big disparity in reactive-contact surface is responsible for the improved properties of the nanocomposites.

Table 3.3 Chemical formula and characteristic parameter of commonly used 2:1 phyllosilicates. (Sinha Ray & Okamoto (2003b))

2:1 phyllosilicates	**Chemical Formula**	**CEC (meq/100 g)**	**Particle length (nm)**
Montmorillonite	$M_x(Al_{4-x}Mg_x)Si_8O_{20}(OH)_4$	110	100-150
Hectorite	$M_x(Mg_{6-x}Li_x)Si_8O_{20}(OH)_4$	120	200-300
Saponite	$M_xMg_6(Si_{8-x}Al_x)Si_8O_{20}(OH)_4$	86.6	50-60
M, monovalent catión; x, degree of isomorphous substitution (between 0.5 and 1.3).			

The typical structure of layered silicates consists of silicate layers. The lamellar structure consist in aluminum octahedral layers, tetrahedral silica layers and exchangeable cations between layers to satisfy overall balance. The stacking layers are regularly organized leaving a gap called the Van der Waals'gap, interlayer or gallery.

The charges generated during the balance and counterbalance inside silicates galleries produce a moderate surface charge, cation exchange capacity (CEC). The values of CEC expressed in mequiv/100 gm are the average values of all silicate layers. Two general structural arrangements in layered silicates are observed: the tetrahedral and octahedral substituted structures. The layers are held through electrostatic and hydrogen-bonding

interactions. The surface of tetrahedral substituted layered silicates is negatively charged, for this reason the interaction between polymer and silicates is easier than octahedral case. (Sinha Ray & Okamoto (2003b)) (Tjong (2006))

For the case of montmorillonite, classified as a dioctahedral clay, arrangements of two fused silica tetrahedral sheets confine an edge-share octahedral sheet of aluminum or magnesium hydroxide. Isomorphic substitution of SiO_4 with $(AlO_4)^-$ and $(AlO_6)^{-3}$ with $(MgO_6)^{-4}$ inside the layers causes a surplus of negative charges. This unbalance of charges is compensated with additional cations, alkali metal and alkaline earth, such as Na^+ and Ca^{2+} situated at interlayers. Molecules of water are linked with these cations. For this reason, montmorillonite has a hydrophilic character.

Natural layered silicates cannot always be used to produce polymer nanocomposites because of the large interfacial forces between the polar mineral and the less polar polymer surface. Then, some form of compatibilization to produce nanocomposites with a high exfoliation degree. Only few polymers can react with natural layered silicates without any interfacial modification. For example, natural montmorillonite contains hydrated Na^+ ions. Because of this particular aspect, it can only compatible with hydrophilic polymers such as polyethylene oxide (PEO), polyvinyl alcohol (PVA) and thermoplastic starch, poly(3-hydroxybutyrate) (Sanchez-Garcia et al. (2008)), anhydride-cured epoxy (Wang et al. (2007)) (Chiu et al. (2007)).

In this study, montmorillonite with commercial name Cloisite Na+® provided by Souther clay products were used. Some physical properties of this commercial MMT are presented in (Table 3.4

Table 3.4 Some physical properties of Montmorillonite Cloisite® Na+ (Souther-Clay-Products (2008))

Physical Properties	
Specific Gravity	2.86 g/cc
Bulk Density	0.1994 g/cc
Loss On Ignition	7.00 %
Dry Particle Sizes:	2.00 μm; 10%
	6.00 μm; 50%
	13.0 μm; 90%
Moisture Content	2.00 %
Cation exchange capacity (CEC)	92.6 meq/ 100g
X-Ray Diffraction d-Spacing (001)	11.7 Angstroms
Color	Off White

For the hydrophobic polymers, the usual strategy is to modify the hydration characteristic of layered silicates to produce a compatible reactive exchange surface with polymers. Usually the organic modification of layered silicates is performed by ion-exchange reactions with cationic surfactants such as primary, secondary, tertiary and quaternary alkyl ammonium cations. Another method is to modify the interfacial properties of the polymers by grafting the polymer chains with reactive functional

groups. These reactive groups should be compatible with the natural or modified layered silicate surface.

The function of the alkylammonium in organo-treated clays (Figure 3.7) is to decrease the surface energy of the silicate layer, so that the polymer chains can be anchored to the silicate surfaces and in this way increase a basal distance in layered silicate. This kind of modification also produces functional groups on silicate surface that can react with the polymer chains or use these reactive groups as initiators during the intercalation-polymerization process. (Vaia et al. (1994)) (Tjong (2006))

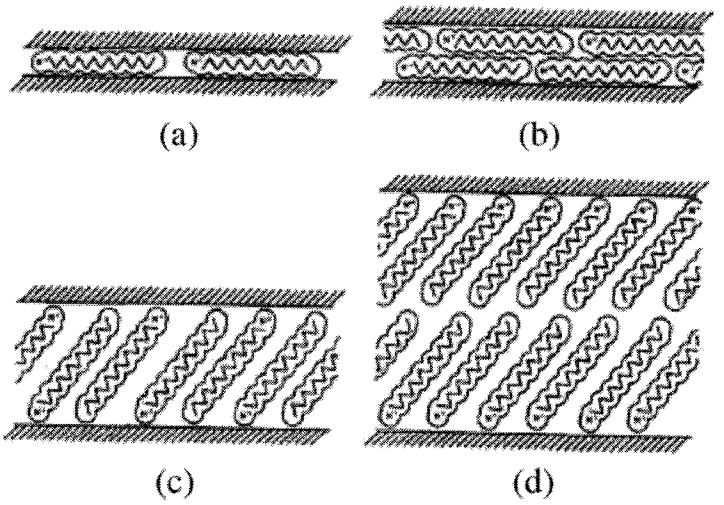

Figure 3.7 Arrangements of alkyl ammonium ions in layered silicates. Hatch areas are silicate layers (Vaia et al. (1994))

CHAPTER 4

PROCESSING AND CHARACTERIZATION OF TPS/PLA/MMT NANOCOMPOSITES

This chapter is focused on the processing, equipments and techniques used to prepare and study of nanocomposites based on TPS/PLA blends.

4.1 Processing of TPS/PLA/MMT Nanocomposites

A Leistritz 34 mm co-rotating twin-screw extruder was used to prepare the compounds. The process configuration and screw configuration are shown in Figure 4.1 and Figure 4.2.

The starch incorporation and gelatinization method was based on the technique developed by (Rodriguez-Gonzalez et al. (2003)) (Favis et al. (2003)) (Favis et al. (2005)) and later adapted for PLA/TPS compatibilization by Huneault and Li (Huneault & Li (2007)).

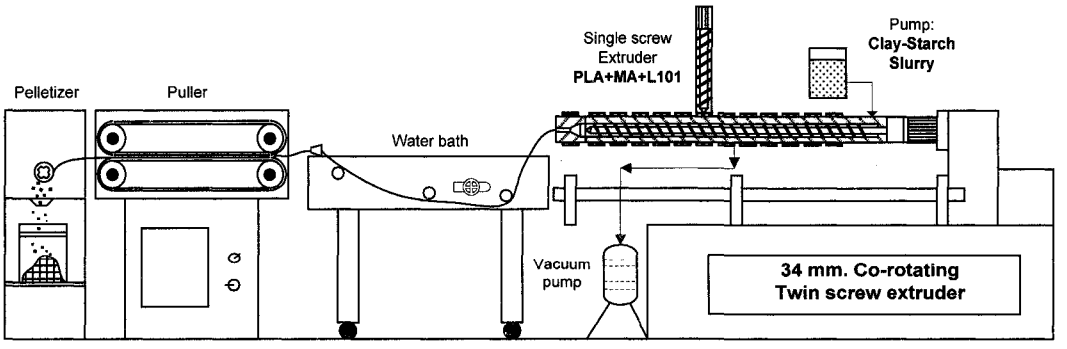

Figure 4.1 Setup used to processing TPS/PLA/MMT nanocomposites.

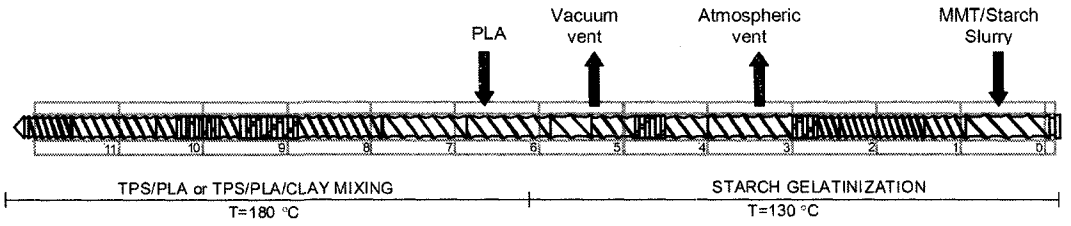

Figure 4.2 Twin-screw process configuration for TPS/PLA blending and TPS/PLA/MMT nanocomposites.

Dry starch, water, glycerol and MMT were intensively mechanically mixed to produce a homogeneous suspension, known as starch-MMT slurry. For all suspensions, glycerol content was set to 36 wt% relative to the final TPS phase after water was removed. Two TPS formulations were studied 27%TPS/PLA and 60%TPS/PLA.

The starch-MMT slurry was incorporated within a twin-screw extruder by a gravimetric pump to better control of the mass flow at the hopper of twin-screw extruder. In the first part of the extruder, at 130°C, the starch passed thought destructuration and gelatinization processes. In the first half of the extruder, water was removed by vacuum devolatilization to obtain a water-free TPS prior to PLA incorporation and to avoid PLA degradation by water. Then TPS starts the intercalation process in MMT and water was expected to enhance the clay exfoliation. PLA or PLAg in molten state was added at mid-extruder using a single-screw extruder as a side feeder at 180°C. In the second half of the extruder, also at 180°C, the TPS, PLA and MMT were intensively mixed to produce TPS/PLA/MMT nanocomposites. At the end-extruder a strand die was used, later water-cooled, and the TPS/PLA/MMT nanocomposites were pelletized.

4.2 Morphological characterization

4.2.1 SEM Characterization

Scanning electron microscopy (SEM) was carried out to examine the morphology of the TPS/PLA blend and nanocomposites. The SEM analysis was done using a JEOL JSM-6100 scanning electron microscope operated at 15 kV. The samples surfaces were microtomed at -100° C from tensile bars. Then, the TPS phase was selectively extracted by placing the samples in HCl 1M solution for 3 hours. The specimens were then dried for at least 12 hours prior to microscopic examination.

4.2.2 TEM Characterization

Transmission electron microscopy (TEM) was performed using a high resolution JEM-2011 TEM operating at 200 kV. The samples were cryo-ultramicrotomed from injected tensile bars in thin sections at -100° C using a diamond knife.

Atomic force microscopy (AFM) was carried out using a Digital Instrument Nanoscope IV scanning microscope (Veeco Metrology Group) operated in tapping mode. Phase imaging mode was used to differentiate between the different phases present in the nanocomposites and in the TPS/PLA blends.

4.2.3 X-Ray Diffraction

X-ray diffraction measurements (XRD) were performed to investigate the intercalation and exfoliation of MMT clay. XRD was performed using a Bruker Discover 8 diffractometer with CuKα radiation at 40 mA and 40KV. To determine the degree of

exfoliation and intercalation, small angles between 0.8° and 10° were scanned. The Bragg's law ($k=2d_{001}\sinh_{001}$) was used to determinate the clay interlayer distance d_{001}.

4.3 Mechanical properties.

4.3.1 Tensile Test

ASTM Type I samples were injection-molded using a 30t Boy injection molder. The melt temperature was 180°C and the mold temperature was set to 30°C. The tensile measurements were carried out according to ASTM D638. Precise initial strain measurement for Young modulus calculations were obtained using clip-on gauge extensometers. The crosshead speed for the tests was 5 mm/min. Reported values are the average obtained from five samples.

4.3.2 Toughness Fracture

The toughness fracture test was executed using the European Structural Integrity Society (TC4) protocol. (E.Clutton (2001)) The samples were deeply double edge notched tensile (DDENT) specimens (shown in Figure. 5.2) with nominal dimensions of 32 mm x 80 mm x 3 mm. The DDENT samples were machined out of 3mm thick rectangular bars that were injected at 180°C. The notches were created using a milling machine. The root tips were carried out by hand using a fresh razor blade into the notch roots.

Thirty samples for each set were tested. The ligament length, defined as the distance between notches, was varied between 3 and 21 mm. A longitudinal video extensometer was used to measure the specimen deformation.

4.4 Thermal analysis

Differential scanning calorimetric (DSC) was performed using TA instruments Q2000 equipment at heating and cooling rates of 10°/ min. The data reported in this study was collected from the second heating runs.

CHAPTER 5

PROCESSING AND PROPERTIES OF PLA/THERMOPLASTIC STARCH/MONTMORILLONITE NANOCOMPOSITES

5.1 Presentation of the article

The objective of this article is to study the processing of polymer nanocomposites by melt reactive extrusion. Thermoplastic starch (TPS) and Polylactide (PLA) were the natural and biodegradable polymers used in this study. Natural montmorillonite (MMT) was added to the TPS/PLA blends as a reinforcing phase.

Two TPS concentrations, 27 and 60% in TPS/PLA, and two loading concentrations of MMT, 2 and 5 % wt. in TPS/PLA/MMT, were evaluated in this research.

Morphology studies were performed for the TPS/PLA blends and for the TPS/PLA/MMT nanocomposites. Fracture toughness was tested in the blends using the EWF method. The influence in the fracture toughness with the addition of MMT inside the TPS/ PLA blends was also analyzed. In addition, tensile and fracture toughness properties of TPS/PLA blends and nanocomposites were investigated.

Nanocomposite structure, exfoliation and dispersion of MMT in the TPS/PLA blends were analyzed using X-Ray diffraction, transmission electron microscopy and atomic force microscopy.

This article has been submitted for revision to the Polymer Composites.

5.2 Processing and properties of PLA/thermoplastic starch/montmorillonite Nanocomposites.

O. H. Arroyo[1,2], M. A. Huneault[1*], B. D. Favis[2], M.N. Bureau[1]

[1]Industrial Materials Institute, National Research Council of Canada
75, de Mortagne, Boucherville, QC, J4B 6Y4
[2]Department of Chemical Engineering, Ecole Polytechnique de Montréal (CREPEC),
Québec, Canada H3C 3A7

Abstract

Thermoplastic starch (TPS) and polylactic acid (PLA) were compounded with natural montmorillonite (MMT) using a twin-screw extrusion process to investigate the structure and properties of these nanocomposites and to examine the use of water to enhance clay exfoliation. Tensile and essential work of fracture measurements were performed on standard dumbbell shape samples and on double notched samples to determine the effect of MMT and PLA/TPS interfacial modification on the mechanical and fracture properties of the materials. The nanocomposite structure was investigated using X-Ray diffraction, transmission electron microscopy and atomic force microscopy. Differential scanning calorimetric analysis was performed on the materials to determine the effect of TPS and MMT on PLA crystallization and physical aging. It was found that the thermoplastic starch can intercalate the clay structure and that the clay was preferentially located in the thermoplastic starch phase or at the blend interface. This led to an improvement in tensile modulus and strength and to a reduction in fracture toughness.

Keywords: Thermoplastic starch; Polylactide; MMT; Nanocomposites; Fracture toughness.

***corresponding author**: Michel A. Huneault (michel.huneault@cnrc-nrc.gc.ca)

5.2.1 Introduction

Thermoplastic starch (TPS) and polylactic acid (PLA) are two biobased materials that hold a promising future for the fabrication of compostable plastic articles. Thermoplastic starch is obtained through plasticization and gelatinization of starch. Because of its hygroscopic nature, thermoplastic starch is typically blended with another hydrophobic polymer [1] [2] [3]. PLA is also biobased but is obtained by a synthetic route. It is a linear aliphatic polyester that has physical, mechanical and optical properties similar to polyethylene terephthalate (PET) and has already been adopted in a small number of packaging applications. Compared to PET however, it suffers from lower temperature resistance, higher gas permeability and brittleness. This has prompted efforts in blending PLA with impact modifiers and/or fillers as means to improve its property balance. The first attempt to blend PLA with starch involved dry-starch granules [4] [5] [6] [7] [8] but resulted in very brittle materials. Recently however, it was shown that blending of PLA with thermoplastic starch (rather than dry-starch particulates) and a suitable compatibilizer could lead to homogenously-dispersed materials with high elongation at break [9].

The addition of nanoclays to form a polymer nanocomposite is another means to modify the property balance of a material. The addition of 2-5 wt% of exfoliated clays can lead to improvements in thermal, mechanical and flexural properties in comparison to the neat polymer [10] [11] [12] . The reinforcement of TPS with montmorillonite has already been a matter of study [13] [14] [15] [16] [17] [18] [19] [20] . In most cases, the intercalation is carried out during melt-extrusion or in a solvent prior to casting of thin

films. It was generally observed that the use of natural MMT leads to superior dispersion in TPS than the use of organically modified MMT. Several authors have reported advances on PLA nanocomposites using natural (unmodified) and organically-modified MMT [21] [22] [23] [24] [25] [26] [27] [28] [29] [30] . In this case, better MMT dispersions were found using organically-modified MMT.

Due to the hygroscopic character of natural clays, several studies have focused on the use of water as an intercalation/exfoliation agent especially in curable systems. The use of clay slurries is more compatible with thermoset polymer fabrication since this usually involves low molecular weight precursors that can be readily mixed with clay to form a suspension. For example, exfoliation in water has been explored in water-based curable silicone emulsions [31], curable epoxy resins [32] and monomer emulsions to produce composites with polymethyl methacrylate (PMMA) [33] and polystyrene (PS) [34]. Mixing a clay suspension to a high molecular weight polymer is more challenging in terms of mixing and technological requirements. One route consists in using hydrophilic or water-soluble polymers where the polymer solution intercalates the clay prior to water removal. This was achieved in water-soluble polyvinyl alcohol (PVA)[35]. In the case of non-water soluble polymers, the water must rapidly be replaced by the polymer matrix to stabilize the exfoliated structure upon water removal. Successful water-assisted clay exfoliation in a molten polymer was reported into a polyamide 6 matrix [36]. The main appeal for assisting exfoliation with water is that it could be a way to prepare polyamide nanocomposites without the need to chemically modify the clays prior to the compounding step. In the reported method, the clay was suspended into water

and this suspension was pumped at mid-extruder into the molten polyamide. The water was later removed in the last third of the extrusion process through devolatilization under vacuum to provide a water-free material at the end of the compounding step. Using a variation of this extrusion method, it was also shown that the blends could be prepared by mixing polyamide 6 and dry MMT in the first stage of a twin-screw compounding extruder and then adding water at the middle of extruder to assist the clay exfoliation step. Again the excess water was removed by a devolatilization stage near the end of the extruder [37]. Although mechanical properties were improved with this variant, the dispersion and exfoliation were better when the clay was fed to the process as a suspension in water. Water-assisted exfoliation was also investigated in natural Na-MMT/PP composites [38].

The current study investigated the properties and structure of TPS/PLA/MMT nanocomposites prepared by twin-screw extrusion using an original water exfoliation strategy. Natural montmorillonite was added to the starch slurry in the hope that the clay exfoliation will occur during the intensive mixing of the starch-water-glycerol slurry. The study investigated the extent of clay intercalation/exfoliation, the selective localization of clay platelet within the PLA and TPS blend phases, and finally the mechanical properties and physical aging of these nanocomposites.

5.2.2 Experimental

5.2.2.1 Materials

The PLA (grade 2002D) was obtained from NatureWorks LLC. It is a semi-crystalline extrusion grade material with a *D*-Lactic acid content around 4%. Wheat starch, Supergel 1203 was supplied by ADM. Water and glycerol were used as starch plasticizers. Natural montmorillonite, Cloisite Na^{+}, supplied by Southern Clay Products, was used as reinforcing phase. The maleic anhydride grafted PLA, PLA-g-MA, was prepared using 2% maleic anhydride (MA) and 0.25% peroxide initiator 2,5-dimethyl-2.5-di(t-butylperoxy) hexane (Luperox 101, L101) provided by the Aldrich Company.

5.2.2.2 Processing

A Leistritz 34 mm co-rotating twin-screw extruder was used to prepare the compounds. The process configuration is shown in Figure 5.1. The starch incorporation and gelatinization method was based on the technique developed by Rodriguez-Gonzalez et al. [39] [40] [41] and later adapted for PLA/TPS compatibilization by Huneault and Li [9]. It consisted in feeding starch in suspension in a water-glycerol mixture in the feed hopper of the twin-screw extruder. Water was removed by vacuum devolatilization in the first half of the extruder prior to PLA incorporation. The PLA was added at mid-extruder using a single-screw extruder as a side feeder. In the current study however, clay was added to the starch suspension with the expectation that water will enhance the clay exfoliation. As a reference, clay was also introduced into the PLA to compare the two methods. The first half of the twin-screw extruder was set to 130°C in order to carry-out

starch gelatinization in presence of water and glycerol. The second half of the extruder used to mix the PLA/TPS mixture was operated at 180 °C. The blends were extruded using a strand die, water-cooled and pelletized. In all composites, the glycerol content was set to 36 wt% relative to the TPS phase. Since water is removed from the material, all compositions are given on a water-free basis.

5.2.2.3 Morphological characterization

Scanning electron microscopy was carried out to examine the study the TPS/PLA blend morphology. The SEM analysis was done using a JEOL JSM-6100 scanning electron microscope operated at 15 kV. The samples surfaces were microtomed at -100° C from tensile bars. Then, the TPS phase was selectively extracted by placing the samples in a HCl 1M solution for 3 hours. The specimens were then dried for at least 12 hours prior to microscopic examination.

Transmission electron microscopy (TEM) was performed using a high resolution JEM-2011 TEM operating at 200 kV. The samples were cryo-ultramicrotomed from injected tensile bars in thin sections at -100° C using a diamond knife.

Atomic force microscopy (AFM) was carried out using a Digital Instrument Nanoscope IV scanning microscope (Veeco Metrology Group) operated in tapping mode. Phase imaging mode was used to differentiate between the different phases present in the composites and in the TPS/PLA blends.

X-ray diffraction measurements (XRD) were performed to investigate the intercalation and exfoliation of MMT clay. XRD was performed using a Bruker Discover

8 diffractometer with CuKα radiation at 40 mA and 40KV. To determine the degree of exfoliation and intercalation, small angles between 0.8° and 10° were scanned. The Bragg's law ($k=2d_{001}\sinh_{001}$) was used to determinate the clay interlayer distance d_{001}.

5.2.2.4 Tensile property measurements

ASTM Type I samples were injection-molded using a 30t Boy injection molder. The melt temperature was 180°C and the mold temperature was set to 30°C. The tensile measurements were carried out according to ASTM D638. Precise initial strain measurement for Young modulus calculations were obtained using clip-on gauge extensometers. The crosshead speed for the tests was 5 mm/min. Reported values are the average obtained from five samples.

5.2.2.5 Essential work of fracture (EWF)

The EWF method was initially developed for metals but has later been adapted to the study of nanocomposites [42] [43] [44] [45]. In the EWF method, load-displacement curves are obtained for various double-notched specimens in which the distance between opposing notches is varied. This distance is known as the ligament length *l*. The specific total work of fracture (w_F) is given by.

$$w_F = w_E + \beta w_P l \qquad \text{(eq. 1)}$$

where β is a shape factor related to the geometry of the process zone, w_E is the fracture work per unit of area, and w_P is the plastic deformation work per unit volume. It is then possible to determine the value of w_E from data obtained for various ligament lengths l. The test was executed using the European Structural Integrity Society (TC4) protocol [46]. The samples were deeply double edge notched tensile (DDENT) specimens (shown in Figure 5.2) with nominal dimensions of 32 mm x 80 mm x 3 mm. The DDENT samples were machined out of 3mm thick rectangular bars that were injected at 180°C. The notches were created using a milling machine. The root tips were carried out by hand using a fresh razor blade into the notch roots. Thirty samples for each set were tested. The ligament length, l, was varied between 3 and 21 mm. A longitudinal video extensometer was used to measure the specimen deformation. The crosshead speed was set to 1 mm/min, to generate quasi-static loading conditions. There are three conditions established in the EWF protocol to determine the validity of a test. First the deformation must occur in a plane stress state. The protocol establishes a range of ligament length (l) to ensure that this condition is satisfied. The criteria is that $3t < l < \min(W/3, r_p)$, where t is thickness of sample, W is width of sample and r_p is plastic zone size [46] [47] [48]. The second condition is that all yield strength data must be within 10% of the average value of yield stress measured. The third condition is the self-similarity criteria which states that the load-displacement curves obtained for the various ligament lengths must have similar shapes. All EWF data reported in this paper satisfy these criteria.

After the EWF test, the fracture surfaces of the DDENT specimens were analyzed by scanning electron microscope (SEM). The fractographic observations were useful to

determine the possible failure mechanics and the organization of the phases during fracture.

5.2.2.6 Thermal analysis

Differential scanning calorimetric (DSC) was performed using TA instruments Q2000 equipment at heating and cooling rates of 10°/ min. The data reported in this study was collected from the second heating runs.

5.2.3 Results and discussion

5.2.3.1 TPS/PLA Blend Morphology

The first level of morphological investigation consisted in evaluating the TPS/PLA blend morphology and the effect of clay addition on the blend morphology. Figure 5.3 presents SEM micrographs of microtomed surfaced in which the TPS phase has been selectively extracted to improve the contrast. Micrographs are presented for 27 and 60%TPS blends, for clay concentration of 0, 2 and 5%, with and without maleic anhydride grafted PLA (PLAg). The morphology of control blends without PLAg were extremely coarse and poorly distributed. The morphology changed dramatically when PLAg was added. The TPS phase decreased from 5-40 μm to the 1-3 μm range for the 27%TPS blend and to the 2-5 μm range for the 60%TPS blend. The distribution were more homogeneous and the TPS phase presented a spherical shape, as reported previously [9]. The addition of 2% wt. of MMT clay without PLAg lead to morphologies fairly similar to that of uncompatibilized TPS/PLA controls. When PLAg was added to

the composite, the TPS phase size was reduced as expected but not to the same extent as for the compatibilized controls. Similar micrographs were obtained when 5% MMT was added instead of 2%. The slight increase in TPS phase size upon MMT addition may be associated with an increase in the blend viscosity ratio. Since the clay is added in the starch slurry, it is expected to be preferentially located in the TPS phase. The MMT will therefore increase the viscosity of the minor phase and decrease its deformability in the dispersion process.

5.2.3.2 Dispersion of Natural Montmorillonite in TPS/PLA

The intercalation and exfoliation of the MMT clay was investigated using X-ray diffraction as well as with transmission and atomic force microscopy (i.e. TEM, AFM). The XRD spectra for TPS/PLA-MMT nanocomposites are shown in Figure 5.4. The XRD spectrum of neat Na^+ was measured as a reference. It shows a peak at $2\theta=9^o$ indicating a basal spacing $d_{001}$of 1.08 nm. The basal spacing of the MMT was shifted to 1.83 nm in 27%TPS blends and in the 60%TPS/PLAg blend. Weaker peaks indicative of basal spacing of 1.48 nm and 3.13 nm were found for the 60%TPS/PLA system. Therefore, there is intercalation into the MMT interlayers in all the formulations. The fact that similar diffraction peaks were observed for different TPS concentration and also using PLA or PLAg supports the assumption that it is the hydrophilic TPS phase and probably part of glycerol [15] [16] [17] [18] that are being intercalated into the MMT clay galleries.

Low and high magnification TEM images of TPS/PLA composites are presented in Figure 5.5. Partial intercalation inside the clay galleries can be observed in the high magnification TEMs in accordance with the XRD results. In all the TPS/PLA blends, large clay aggregates were present while few MMT stacks formed by 3 or less clay layers were located around the large aggregates. In general, there was not any preferential orientation of these large clay aggregates and clay stacks. The materials therefore presented a mixed variety of structure including agglomerates, intercalated structures and some exfoliated layers. Similar clay distributions were found in high TPS content blends and in the blends made using the PLAg. This indicates that the PLAg was effective in reducing the TPS phase size but did not have a significant effect on the MMT dispersion. One potential reason for this lack of effect may be that the clay platelets remained in the TPS phase without ever interacting directly with the PLA phase.

To verify this assumption, low magnification TEM micrographs were taken to determine the global distribution of the MMT. Also, to further our understanding on this topic, additional experiments were carried out where the MMT was introduced in the PLA phase prior to mixing with the TPS instead of in the starch-water suspension. Figure 5.6 presents TEM micrographs for the nanocomposites based on the 27%TPS/PLA (or PLAg) blend. In the left column, the MMT was incorporated in the starch suspension using the process described in the Experimental section. The MMT is thus intimately mixed with the TPS phase prior to TPS/PLA mixing. The micrographs for the case where the MMT was first mixed in PLA are presented in the right column for the same compositions. The contrast between the TPS and PLA was sufficient to

discriminate the two materials. It is clear from the left-column micrographs that when the MMT platelets were introduced first in the TPS phases, they remained in the TPS phase and did not cross the PLA/TPS interface. When the MMT was introduced in the PLA, an interesting result was obtained. The MMT platelets to a large extent migrated toward the TPS phase and entered it rather than staying in the PLA phase. Clay aggregates were located along the TPS/PLA interface. This trend was verified in all blends regardless of whether PLA or PLAg was used. Thus, the strong affinity between natural montmorillonite and the hydrophilic thermoplastic starch phase were sufficient to create this segregation effect. The preferential concentration of the MMT platelet within the TPS phase or at the interface contributed to reduce the total interfacial energy of the blend. Even in the case where the MMT was added to PLA, the convective forces present in the extruder enabled the particles to migrate and sometimes cross the blend's interface therefore reaching their lowest interfacial energy state.

To corroborate these findings on the location of MMT platelets, the nanocomposites surface were examined by atomic force microscopy (AFM). Figure 5.7 presents the AFM micrographs for the same formulations as Figure 5.6. Phase imaging in tapping mode was used to obtain contrast based on the surface hardness. The scanned zone presented in each picture has a 2μm x 2μm area. The dark zones are the TPS phase while the brighter zones are the PLA and MMT clay. There is a sharp contrast between the TPS and PLA phase. Within the TPS phases, the brighter irregular shaped platelets are the MMT phase. The MMT was found in the TPS phase regardless of the initial phase in which it was introduced. MMT was not detected in the PLA matrix. Similar results

were found for the blends containing 60%TPS. This confirms that the MMT tends to stays in the TPS phase and even to migrate from the PLA to the TPS phase when it is introduced in the PLA phase.

5.2.3.3 Tensile Properties

The tensile properties of TPS/PLA and TPS/PLAg with and without MMT are presented in Table 1, in which the properties of PLA, PLAg and MMT/PLA are reported for reference purposes. PLA and PLAg showed a similar high modulus, strength and low elongation at break typical for these polymers. MMT/PLA showed a slight increase in modulus and a 20% reduction in tensile strength, with similar low elongation at break. MMT/PLAg showed similar increase in modulus and low elongation at break, but maintained their tensile strength with respect to PLAg. This different trend in tensile strength for PLA and PLAg reveals the effect of particle-matrix affinity.

Addition of soft TPS into PLA or PLAg led to, as expected, reductions in modulus and strength; 27%TPS showed tensile modulus over 2 GPa, while the one for 60%TPS blends was around 1.3 GPa, close to typical polyolefin values. TPS/PLA showed marginal increases in elongation at break, while TPS/PLAg had elongation at break of the order of 50-60%. The use of PLAg instead of PLA with TPS thus enabled to maintain interesting tensile properties as it improved stress transfer between the soft minor phase and the rigid matrix.

MMT addition to 27%TPS/PLA and 60%TPS/PLA resulted in increases in tensile modulus respectively of 13% (to 3.34 GPa) and 53% (to 2.21 GPa), while tensile strength was only marginally affected (respectively -5 MPa and +5 MPa); in both cases elongation at break was decreased in the 5-15% range. It is noteworthy that since the MMT is introduced in the TPS and preferentially remained in that phase, the TPS phase in the 60%TPS blends is less concentrated in MMT than in the 27% blend for a same overall MMT concentration. This may have enabled a higher relative fraction of exfoliation in the 60%TPS blends. This higher exfoliation degree in turn could explain the greater MMT relative effect on modulus observed with the 60%TPS blends. Addition of MMT in TPS/PLAg did not lead to important variations in tensile modulus when added at 2% but increased it when used at 5%. In all cases, the addition of MMT led to considerable reductions in elongation at break. This was expected because the TPS phase is embrittled by MMT [16] [17] [18] [19] [20].

The small changes, especially for the 27%TPS blends, and limited effect of the TPS/PLA interface modifier may be explained by the preferential location of the MMT in the TPS phase described earlier. The PLAg decreases the interfacial tension between the PLA and TPS phases but cannot interact much with the MMT particles located within the TPS phase. The preferential location in the TPS also explain the higher modulus and strength enhancement observed in the blends where the TPS is forming the major phase (i.e. at 60%TPS).

5.2.3.4 Essential Work of Fracture

The load-displacement curves for the 27%TPS/PLA composition with and without PLAg and MMT are presented in Figure 5.9. Similar curves (not shown) were obtained with the 60%TPS/PLA nanocomposites. Two important observations can be made. The first one is that the obtained data satisfied the self-similarity criteria, *i.e.* the stress amplitude increased with the ligament size but that the overall shape of the stress-strain curve remained the same. The second general observation is that all materials investigated in this study exhibited a relatively brittle behavior, *i.e.* initiation energy was significantly greater than the propagation energy. In order to compare the different materials, the specific work of fracture was plotted as a function of ligament size and is reported in Figure 5.5. The fracture initiation energy is represented by the solid data points. In order to calculate the overall energy involved in the breakup, the total energy is also presented using the open symbols. As expected, the specific work of fracture increased linearly with the ligament length. The crack initiation energy w_E and the propagation/deformation βw_P term defined earlier were obtained from the Y-axis intercept and from the slope of curve. The values of $w_{E,ini}$ and $w_{E,tot}$ as well as the non-EWF term βw_P and correlation coefficient (r^2) are reported in Table 5.2. As observed from the curves in Figure 5.10, the data variability r^2 is within an acceptable range ($r^2 > 0.78$). Results obtained for pure PLA and of pure PLAg are also presented in Table 5.1. Both polymers showed a very small non-EWF term (βw_P), resulting in a small coefficient of linearity (expressed as correlation coefficient r^2) and indicating that little plastic deformation occurred, which raises doubts that plane stress conditions fully developed

upon EWF testing. However, in the absence of EWF values reported in the literature for PLA and PLAg, the EWF values obtained for these materials will be used for comparison purposes herein.

Results in Table 5.2 first indicate that PLAg has lower $w_{E,ini}$ and $w_{E,tot}$ values than PLA, probably as a result of its lower molecular weight. Results from 27%TPS/PLA show that TPS addition in PLA led to a considerable reduction in both $w_{E,ini}$ and $w_{E,tot}$ while βw_P increased dramatically. 27%TPS addition in PLAg on the contrary did not lead to such a reduction in $w_{E,ini}$ and $w_{E,tot}$ values but lead to a similar increase in βw_P values. A similar but less pronounced trend was noted upon 60%TPS addition in both PLA and PLAg. It should be reminded that, in the compatibilized case, a much finer dispersed particle size was found as shown earlier. This resulted in less severe stress concentration sites in the rigid/brittle matrix, leading to voids that form at higher loads. Furthermore, the improved TPS-PLA interfacial adhesion resulted in increased fracture toughness and ductility in TPS/PLAg blends as a result of increased stress transfer between the PLAg matrix and the soft TPS domains.

Results in Table 5.2 also indicate that 2%MMT addition in both 27%TPS/PLA and 27%TPS/PLAg reduced significantly their $w_{E,ini}$ and $w_{E,tot}$ values, and their βw_P values, with the exception of $\beta w_{P,tot}$ of 27%TPS/PLAg/2%MMT that increased by approximately 30%. MMT addition in these cases led to reduced fracture toughness. When 2%MMT is added to 60%TPS/PLA or 60%TPS/PLAg, a different trend was noted:

$w_{E,tot}$ and $\beta w_{P,tot}$ values all increased significantly, showing that MMT addition resulted in an improved fracture toughness.

5.2.3.5 Fracture Surface Analysis

SEM observation of surfaces fractured in the EWF test was carried out to understand the fracture toughness data obtained for TPS/PLA blends and nanocomposites. The fracture surfaces of the 27%TPS/PLA blend series are showed in Figure 5.8. As expected, 27%TPS/PLA showed large voids, formed at TPS domains (> 10 μm), that grew and coalesced upon loading as a result of matrix fibrils stretching and tearing, until final fracture. In this case, final fracture occurred at reduced EWF values with respect to PLA as a result of poorly-bonded, large TPS domains within the brittle matrix. This fracture surface can be compared to the fracture surface of 27%TPS/PLAg at the same magnification. The latter figure indicates that fracture occurred again by void formation at the minor phase followed by matrix stretching and tearing, but it also indicates that considerably more voids were observed on the fracture surface, that they were considerably smaller and that matrix stretching and tearing was reduced significantly. Also, the stronger TPS-PLAg interface enabled matrix-particle stress transfer, which led to both phases contributing to bear the load during the tests. Once formed, the extension of the crack process zone, is highly limited, as shown by low matrix stretching and tearing, therefore lower non-EWF.

MMT addition in TPS/PLA blends (Figure 5.6c) promoted the formation of numerous microvoids and tearing fibrils and lamellar ligaments. In some cases, MMT platelets were

visible in the voids on the fracture surface. In general, fibrillation appeared more intense in 27%TPS/PLA/2%MMT than in 27%TPS/PLA, but did not result in higher non-EWF, probably due to the reduced mobility of polymer chains and thus a more limited ability to be deformed plastically. In turn, this decreased the resistance to crack propagation. Similar observations were made for polyamide 6-MMT [49]. The fracture surface of 27%TPS/PLAg/2%MMT showed features similar to those observed for 27%TPS/PLA/2%MMT, in support of their similar EWF and non-EWF.

5.2.3.6 Effect of MMT on PLA Crystallization

Because of its rigid backbone, PLA has a low crystallization rate. A common way to increase the crystallization rate is to add nucleating agents to initiate crystallization at higher temperature and to add plasticizers to enhance PLA chain mobility [50]. It is therefore interesting to investigate the effect of the TPS phase and of the MMT on PLA crystallization. Figure 5.11 presents DSC heating scans at +10 °C/min for various TPS/PLA blends and MMT nanocomposites. All samples had been previously heated to 200 °C and then cooled to -100 °C at a cooling rate of 10 °C /min. In these conditions, the PLA remained completely amorphous as revealed by the absence of melting peak. However when TPS was added to PLA, a weak crystallization exotherm was detected in the 110-135 °C range followed by a melting endotherm at 145 °C. Thus, the TPS phase increased the crystallization rate of PLA. Almost no crystallization peaks was present when the TPS was added to the PLAg. The addition of TPS did not have any effect on the crystallization of PLAg. Similar results were found for 60%TPS blends. In this case, the

peaks are weaker since the blends contain a smaller concentration of crystallizable PLA. The addition of 2% MMT in the TPS/PLA blends produces a further increase in the crystallization rate of PLA. For the 27%TPS blends with MMT, similar crystallinity levels were found. In all the formulations a double or a broad melting peak (double peak merged) was observed. This double peak has been reported before and is related to the formation of two types of crystalline structures [51]. MMT clay in small amounts increased the crystallization rate of PLA and PLAg. We assume that the clay layers or aggregates increased the nucleation density for the crystallization of PLA as reported previously for MMT/PLA and MMT/PET nanocomposites.[28] [52].

5.2.3.7 Changes in Physical and Mechanical Properties with time

The embedded graph in Figure 5.12 shows typical DSC thermograms of TPS/PLA blends aged at 25 °C and 50% relative humidity for periods of 7, 15, 45 and 300 days. In all cases, an endothermic peak related to the excess enthalpy of relaxation was observed right around the glass transition temperature. The endothermic peak increased with an increase in storage time as result of an increase in the excess enthalpy of relaxation. Similar results were found for TPS/PLAg blends (not shown here). This peak has been associated with the physical aging of PLA and was shown to depend on aging time and storage temperature [53]. In the main graph of Figure 5.12, the area of the excess enthalpy relaxation peak of the PLA/TPS blends as function of aging time is compared to that reported for PLA. For neat PLA, obtained from Cai et al [53], the excess enthalpy increased rapidly during the first 30 days. The PLA blended with TPS or the one blended

with dry-starch reported by Wang et al [54] shows a similar behavior to that of the neat PLA. However, for the PLA in compatibilized blends and composites the excess enthalpy peak reaches a lower value.

In order to verify the potential effect of aging on the mechanical stability of the investigated materials, their tensile properties were measured 300 days after their injection molding. Results are presented in Table 5.2 along with the as-molded properties already discussed. For PLA and its nanocomposites, the elongation at break and elastic moduli were similar while the tensile strength was slightly increased after 300 days of storage. For the TPS/PLA blends and nanocomposites, tensile properties were almost unchanged after 300 days. The use of PLAg as compatibilization agent and the addition of MMT clay as a reinforcing did not affect the blend stability either. All changes are within the experimental uncertainty related to the tensile testing and to the residual humidity present in the materials at the time of testing. The property evolution of materials comprising thermoplastic starch, due to plasticizer migration or to starch retrogradation, is often emphasized as a potential drawback of starch-based blends. In the investigated blends and composites however, the stability of mechanical properties was not an issue over a period of 300 days. It can be postulated that the growth of the excess enthalpy of relaxation observed by DSC either has no significant effect on PLA properties and that the TPS particles are sufficiently well encapsulated in the PLA matrix to prevent changes in plasticization or significant increase in humidity level.

5.2.4 Conclusions

Na-Montmorillonite (MMT) Clay can be successfully incorporated into PLA/TPS blends through a water suspension to produce TPS/PLA/MMT nanocomposites. In the investigated composites, the clay particulates showed a greater affinity for the TPS phase. Therefore, the clay incorporated in the TPS phase remained in it while clay incorporated into the PLA phase migrated to the blend interface or even crossed the interface into the TPS phase. The addition of MMT clay increased the tensile modulus of the materials. This was most noticeable in TPS rich blends since the tensile modulus of the TPS is much lower than that of PLA. The fracture toughness and elongation at break decreased with the addition of clay. It was postulated that the clay preferentially located at the blends interface could reduce the interaction between the PLA and TPS phases in compatibilized blends resulting in lower stress transfer from the PLA matrix to the TPS dispersed phase. The addition of MMT produced a slight increase in PLA non-isothermal crystallization. Finally, it was shown that the TPS/PLA blends and the TPS/PLA/MMT composites have stable mechanical properties over a period of 300 days.

ACKNOWLEDGEMENTS

The authors would like to acknowledge the financial support of Canada's Natural Science and Engineering Research Council and of the Canadian Biomass Innovation Network.

5.2.5 References

1. X.-L. Wang, K.-K. Yang and Y.-Z. Wang, *Polymer Reviews*, **43**, 385 (2003).

2. L. Avérous, *Polymer Reviews*, **44**, 231 (2004).

3. S. Kalambur and S.S.H. Rizvi, *Journal of Plastic Film and Sheeting* **22**, 39 (2006).

4. S. Jacobsen and H.G. Fritz, *Polym. Eng. Sci. (USA)*, **36**, 2799 (1996).

5. D. Carlson, L. Nie, R. Narayan and P. Dubois, *J. Appl. Polym. Sci.*, **72**, 477 (1999).

6. T. Ke and X. Sun, *J. Appl. Polym. Sci.*, **81**, 3069 (2001).

7. J.F. Zhang and X. Sun, *Biomacromolecules*, **5**, 1446 (2004).

8. O. Martin and L. Averous, *Polymer*, **42**, 6209 (2001).

9. M.A. Huneault and H. Li, *Polymer*, **48**, 270 (2007).

10. P.C. LeBaron, Z. Wang and T.J. Pinnavaia, *Appl Clay Sci*, **15**, 11 (1999).

11. M. Alexandre and P. Dubois, *Mater Sci Eng R Rep*, **28**, 1 (2000).

12. A. Okada and A. Usuki, *Macromol. Mater. Eng.*, **291**, 1449 (2006).

13. H. Fischer and S. Fischer, *World Intellectual Property Organization Patent WO 01/68762 A1*, (2001).

14. H.M. Park, X. Li, C.Z. Jin, C.Y. Park, W.J. Cho and C.S. Ha, *Macromol. Mater. Eng.*, **287**, 553 (2002).

15. H.M. Wilhelm, M.R. Sierakowski, G.P. Souza and F. Wypych, *Carbohydr Polym*, **52**, 101 (2003).

16. H.M. Park, W.K. Lee, C.Y. Park, W.J. Cho and C.S. Ha, *J. Mater. Sci. (UK)*, **38**, 909 (2003).

17. M.F. Huang, J.G. Yu and X.F. Ma, *Polymer*, **45**, 7017 (2004).

18. B. Chen and J.R.G. Evans, *Carbohydr Polym*, **61**, 455 (2005).

19. X. Ma, J. Yu and N. Wang, *Macromol. Mater. Eng.*, **292**, 723 (2007).

20. L. Yu, K. Dean and W. Dong Yang, *Compos. Sci. Technol. (UK)*, **67**, 413 (2007).

21. N. Ogata, G. Jimenez, H. Kawai and T. Ogihara, *J Polym Sci Part B*, **35**, 389 (1997).

22. M. Pluta, A. Galeski, M. Alexandre, M.A. Paul and P. Dubois, *J. Appl. Polym. Sci.*, **86**, 1497 (2002).

23. M.A. Paul, M. Alexandre, P. Degee, C. Henrist, A. Rulmont and P. Dubois, *Polymer*, **44**, 443 (2003).

24. S. Sinha Ray, P. Maiti, M. Okamoto, K. Yamada and K. Ueda, *Macromolecules*, **35**, 3104 (2002).

25. P. Maiti, K. Yamada, M. Okamoto, K. Ueda and K. Okamoto, *Chem. Mater.*, **14**, 4654 (2002).

26. S. Sinha Ray, K. Yamada, M. Okamoto and K. Ueda, *Polymer*, **44**, 857 (2003).

27. V. Krikorian and D.J. Pochan, *Chem. Mater.*, **15**, 4317 (2003).

28. Y. Di, S. Iannace, E. Di Maio and L. Nicolais, *J Polym Sci Part B*, **43**, 689 (2005).

29. D. Kubies, J. Scudla, R. Puffr, A. Sikora, J. Baldrian, J. Kovarova, M. Slouf and F. Rypacek, *Eur Polym J*, **42**, 888 (2006).

30. M. Pluta, *J Polym Sci Part B*, **44**, 3392 (2006).

31. J. Ma, Z.Z. Yu, H.C. Kuan, A. Dasari and Y.W. Mai, *Macromol. Rapid Commun.*, **26**, 830 (2005).

32. K. Wang, L. Wang, J.S. Wu, L. Chen and C.B. He, *Langmuir*, **21**, 3613 (2005).

33. D.C. Lee and L.W. Jang, *J. Appl. Polym. Sci.*, **61**, 1117 (1996).

34. M.W. Noh and D.C. Lee, *Polymer Bulletin*, **42**, 619 (1999).

35. K.E. Strawhecker and E. Manias, *Chem. Mater.*, **12**, 2943 (2000).

36. N. Hasegawa, H. Okamoto, M. Kato, A. Usuki and N. Sato, *Polymer*, **44**, 2933 (2003).

37. Z.Z. Yu, G.H. Hu, J. Varlet, A. Dasari and Y.W. Mai, *J Polym Sci Part B*, **43**, 1100 (2005).

38. M. Kato, M. Matsushita and K. Fukumori, *Polym. Eng. Sci. (USA)*, **44**, 1205 (2004).

39. F.J. Rodriguez-Gonzalez, B.A. Ramsay and B.D. Favis, *Polymer*, **44**, 1517 (2003).

40. B.D. Favis, F. Rodriguez-Gonzalez and B.A. Ramsay, *U.S. Patent 6, 605, 657*, (2003).

41. B.D. Favis, F. Rodriguez-Gonzalez and B.A. Ramsay, *U.S. Patent 6,844,380*, (2005).

42. M.N. Bureau, F. Perrin-Sarazin and M.T. Ton-That, *Polym. Eng. Sci. (USA)*, **44**, 1142 (2004).

43. S.C. Tjong and S.P. Bao, *J Polym Sci Part B*, **43**, 585 (2005).

44. S.C. Tjong, S.P. Bao and G.D. Liang, *J Polym Sci Part B*, **43**, 3112 (2005).

45. M.N. Bureau, M.T. Ton-That and F. Perrin-Sarazin, *Eng. Fract. Mech. (UK)*, **73**, 2360 (2006).

46. E.Clutton, in (Elsevier Science, 2001) pp. 177.

47. Y.W. Mai and B. Cotterell, *Int J Fract*, **32**, 105 (1986).

48. S. Hashemi, *Polym. Eng. Sci. (USA)*, **37**, 912 (1997).

49. S.C. Bellemare, M.N. Bureau, J. Denault and J.I. Dickson, *Polym. Compos. (USA)*, **25**, 433 (2004).

50. H. Li and M.A. Huneault, *Polymer*, **48**, 6855 (2007).

51. W.Y. Jang, B.Y. Shin, T.J. Lee and R. Narayan, *J. Ind. Eng. Chem*, **13**, 457 (2007).

52. C.F. Ou, M.T. Ho and J.R. Lin, *J Polym Res*, **10**, 127 (2003).

53. H. Cai, V. Dave, R.A. Gross and S.P. McCarthy, *J Polym Sci Part B*, **34**, 2701 (1996).

54. H. Wang, X. Sun and P. Seib, *J. Appl. Polym. Sci.*, **90**, 3683 (2003).

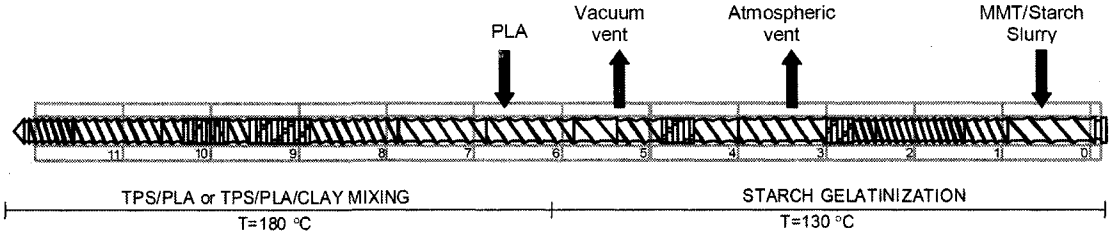

Figure 5.1 Twin-screw process configuration for TPS/PLA blending and TPS/PLA/MMT nanocomposites.

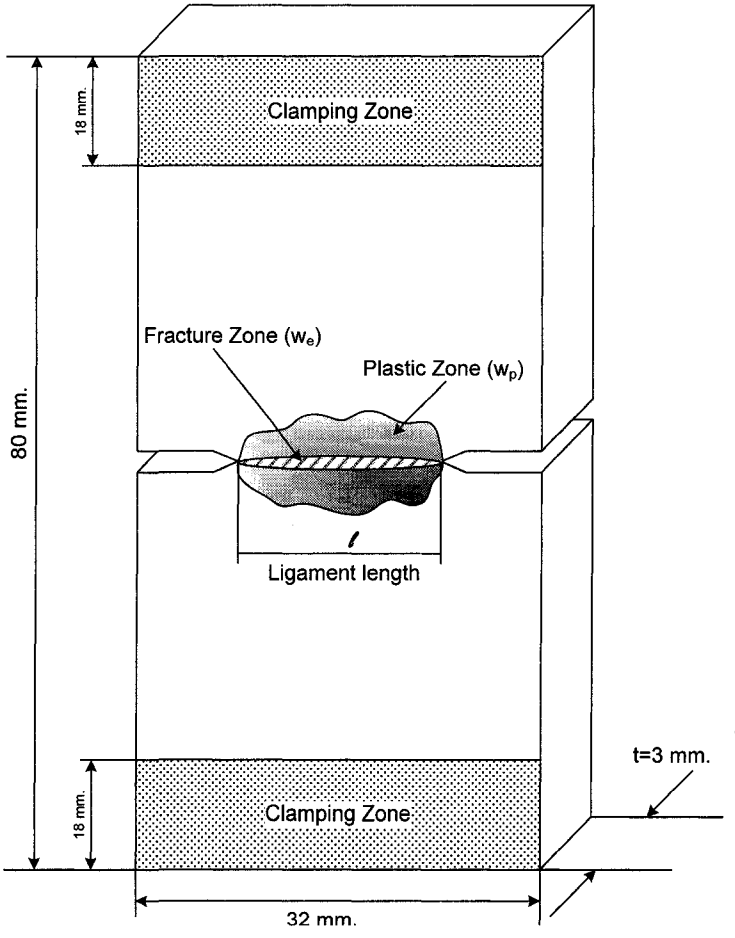

Figure 5.2. Geometry of DDENT specimens.

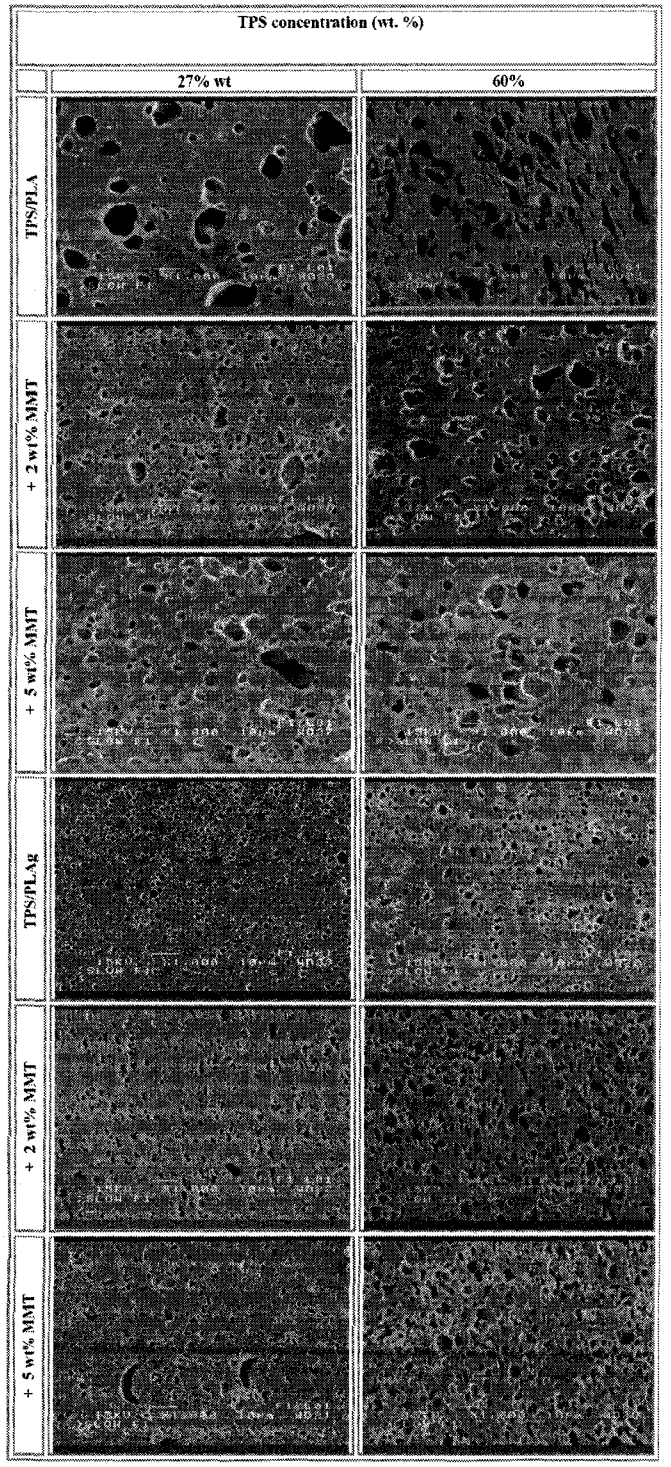

Figure 5.3. Morphology of TPS/PLA blends and Nanocomposites

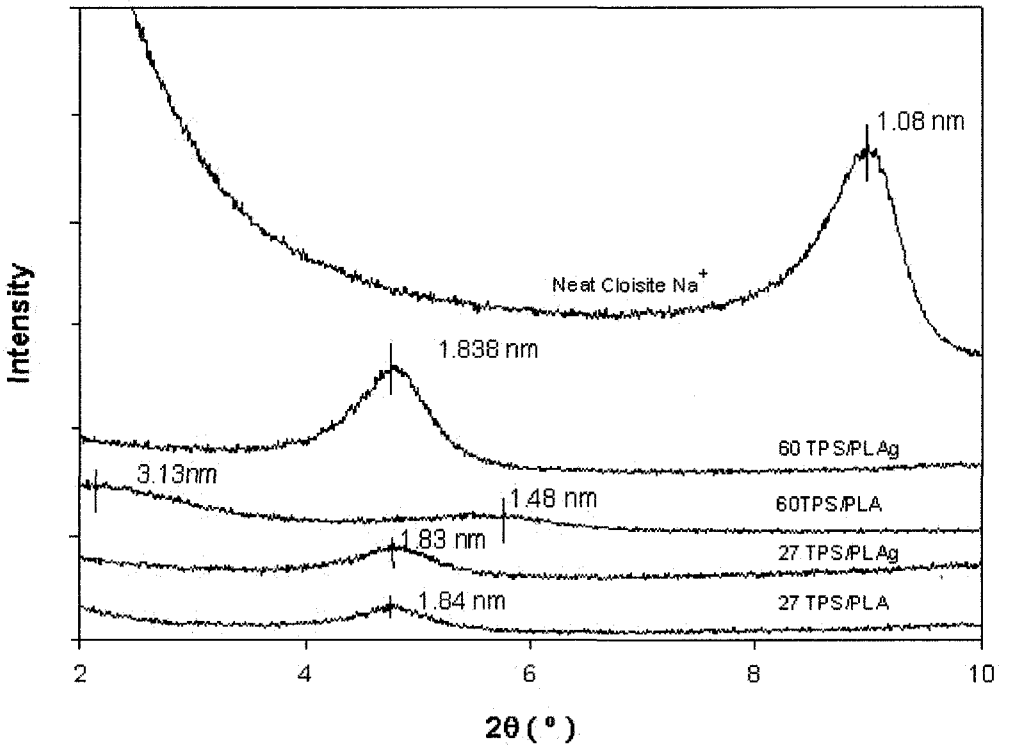

Figure 5.4. XRD spectrum for TPS/PLA nanocomposites with 2% w/w of clay. Maximum clay interlayer spacing d_{001} is shown for each nanocomposite.

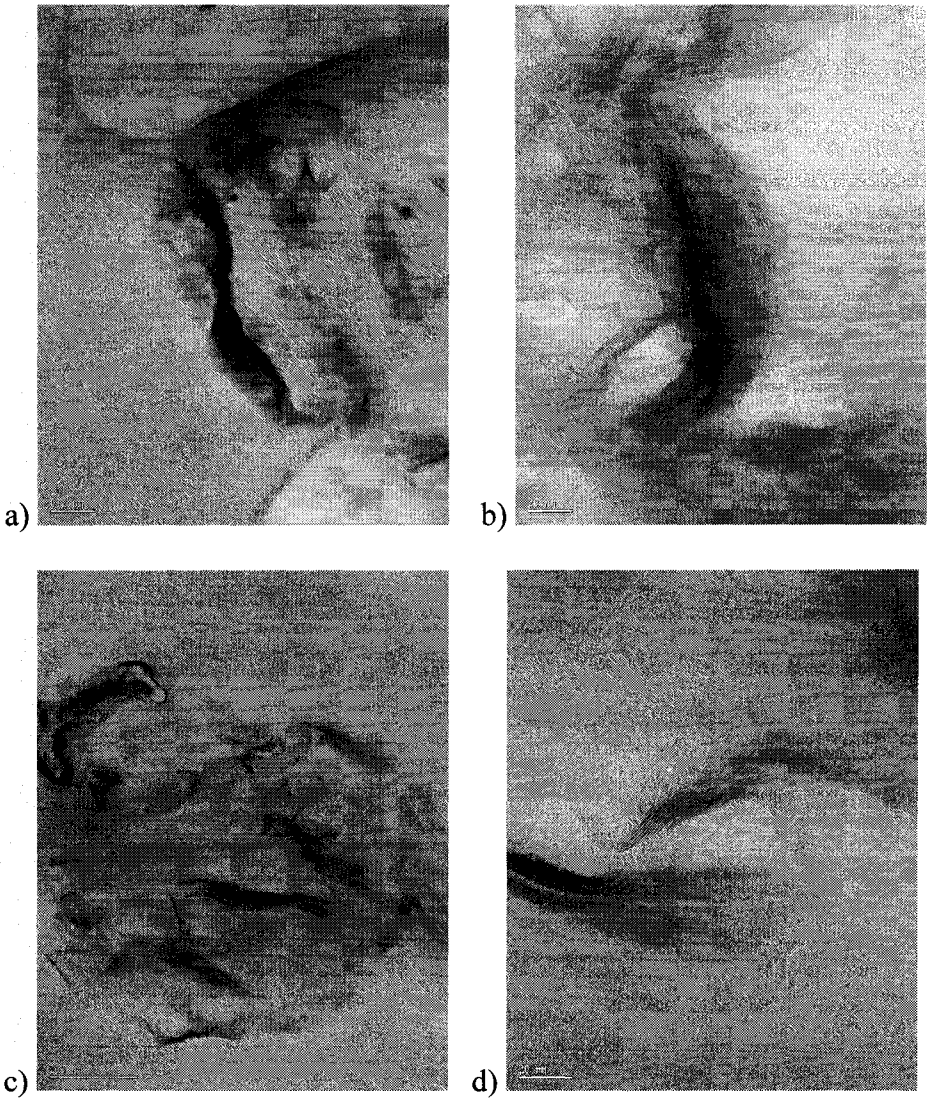

Figure 5.5. TEM micrographs of a) 27%TPS/PLA/2% MMT at low magnification and b) high magnification and of c) 27%TPS/PLAg/ 2% of MMT at low and d) high magnification.

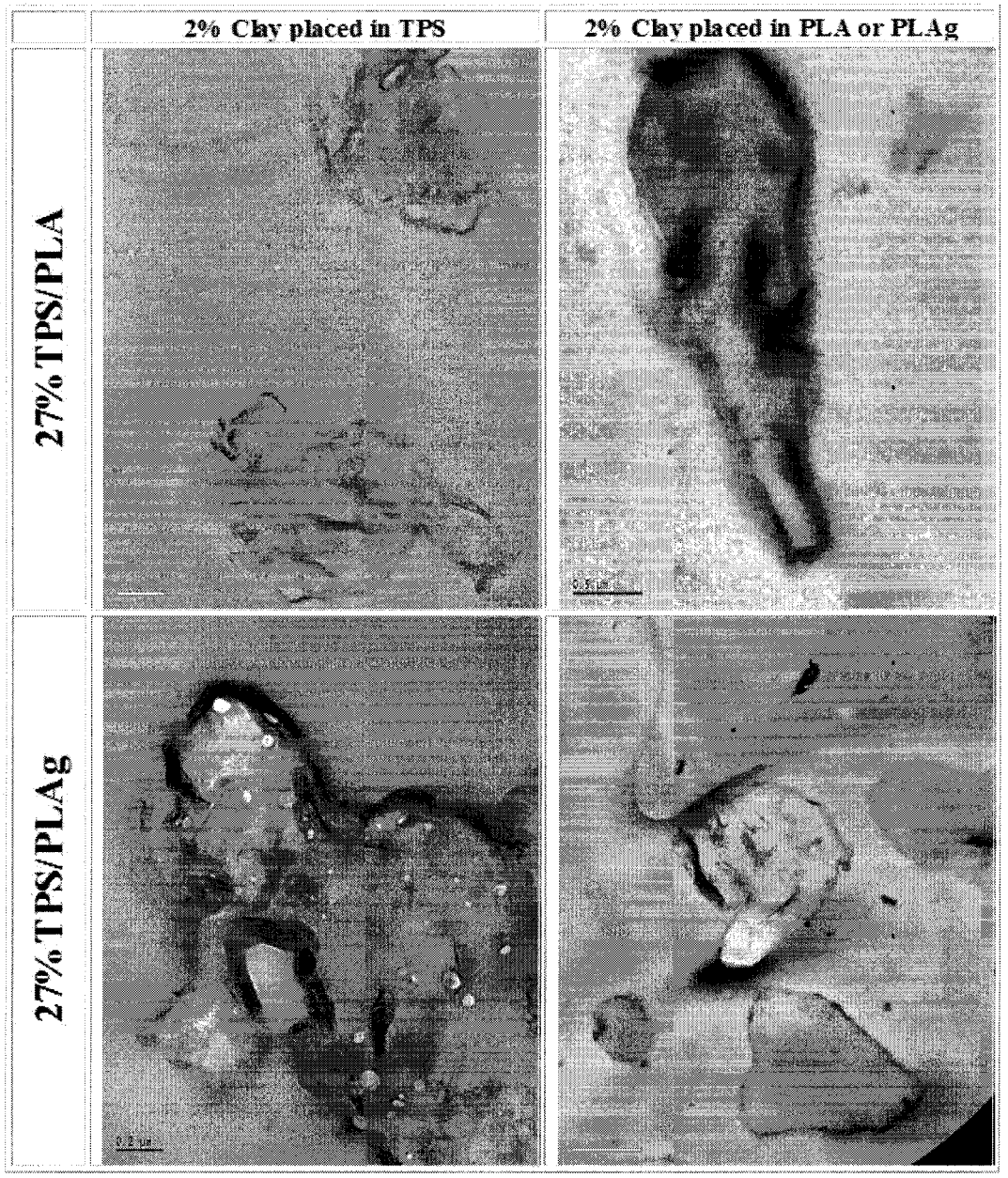

Figure 5.6. Low magnification TEM micrographs in 27% TPS/PLA/ 2% MMT blends where the MMT was initially located either in the starch suspension or in the molten PLA.

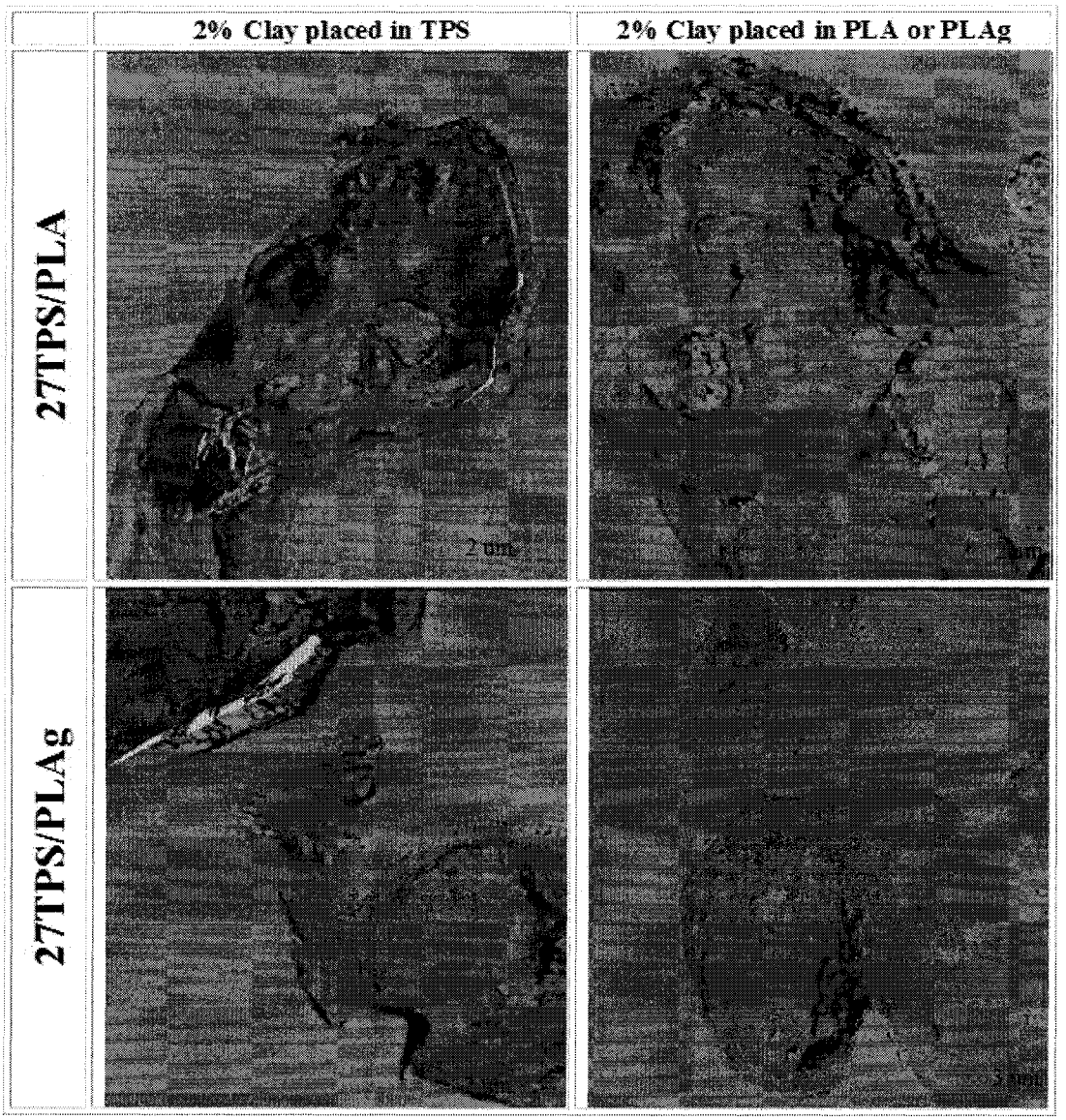

Figure 5.7. AFM micrographs 27%TPS/PLA blends with 2% Clay.

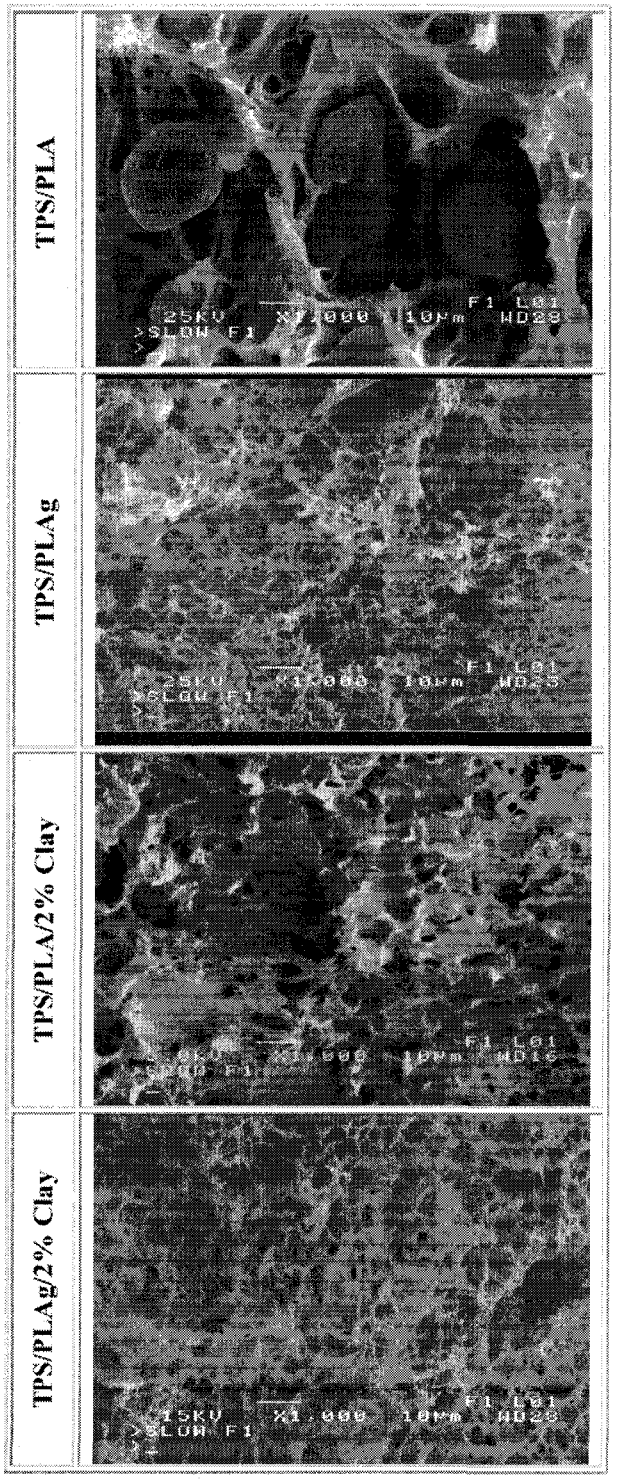

Figure 5.8. Fractographic observation of TPS/PLA blends and MMT nanocomposites based on 27% of TPS.

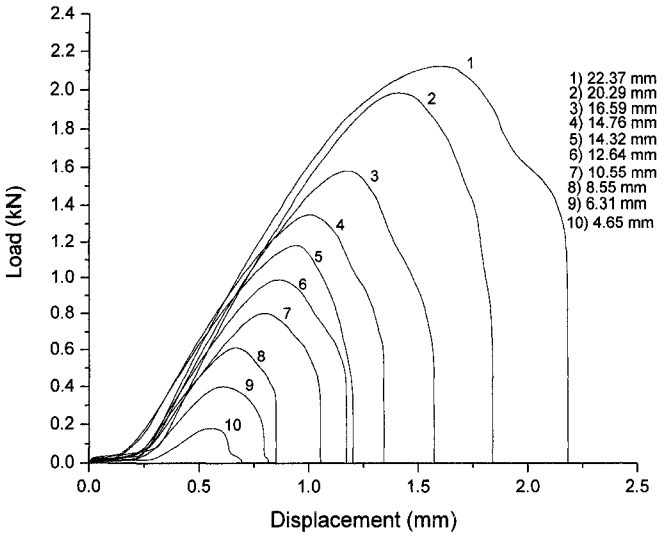

a)

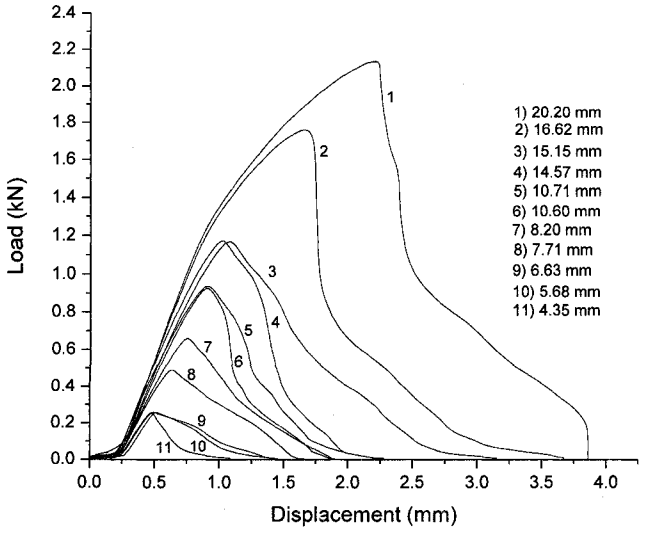

b)

Figure 5.9. Load-displacement curves of DDENT samples with different ligaments length for: a) 27TPS/PLA, b) 27TPS/PLAg, c) 27TPS/PLA/2%MMT and d) 27TPS/PLAg/2%MMT.

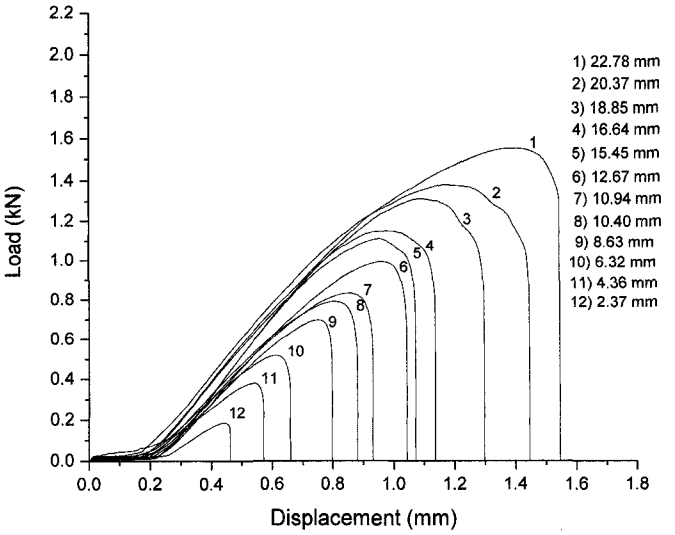

c)

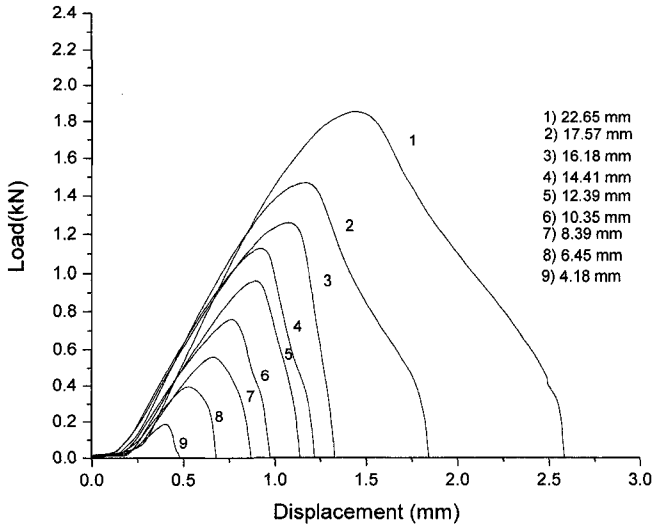

d)

Figure 5.9 (continued). Load-displacement curves of DDENT samples with different ligaments length for: a) 27TPS/PLA, b) 27TPS/PLAg, c) 27TPS/PLA/2%MMT and d) 27TPS/PLAg/2%MMT.

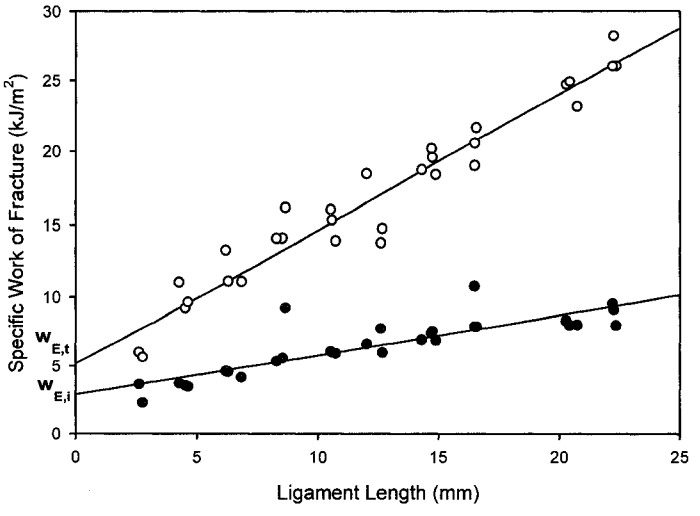

a)

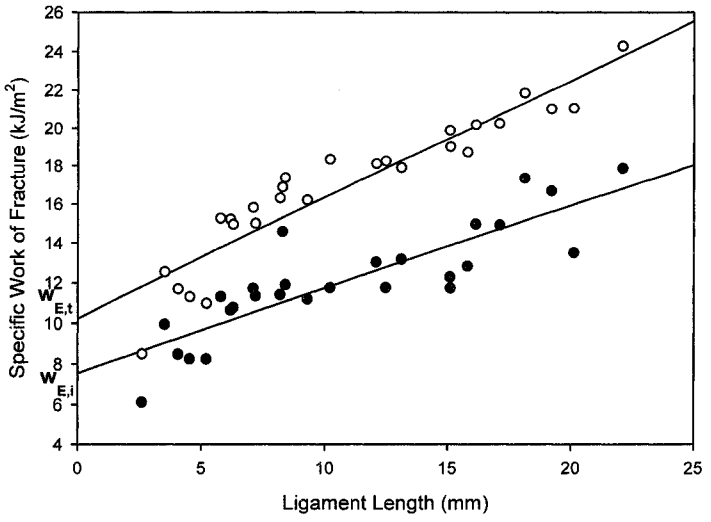

b)

Figure 5.10. Specific work of fracture for crack initiation as a function of ligaments length. $w_{E,i:}$ crack initiation specific work (closed circles) and $w_{E,t:}$ total specific work (open circles) for a) 27TPS/PLA, b) 27TPS/PLAg, c) 27TPS/PLA/2MMT and d) 27TPS/PLAg/2MMT. The lines represent least square fits.

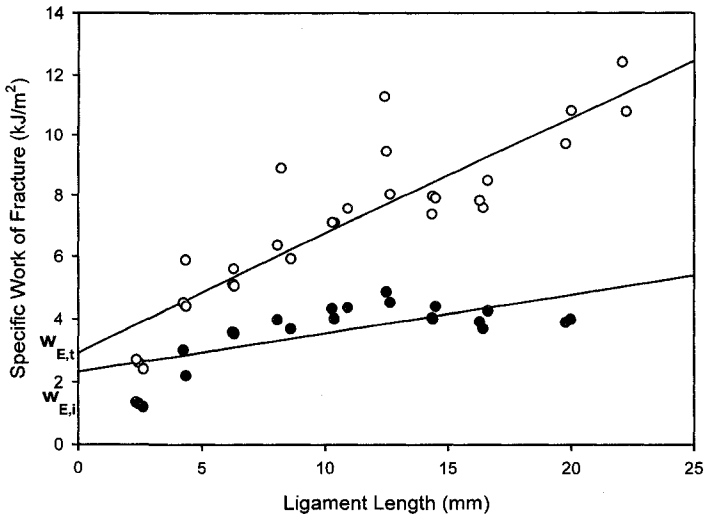

c)

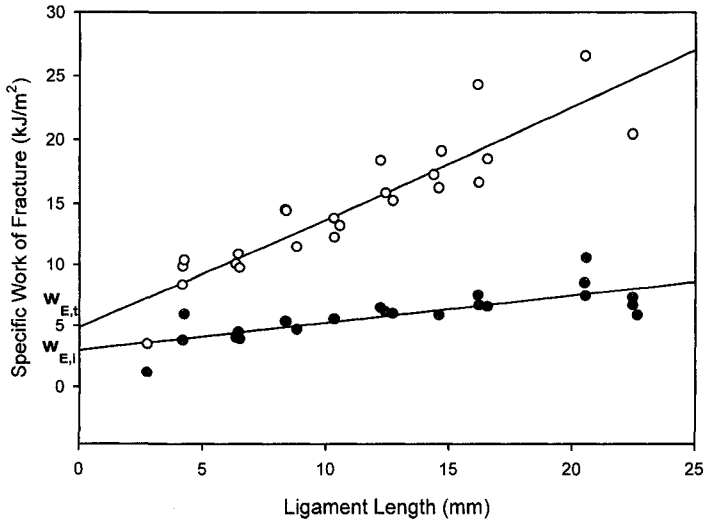

d)

Figure 5.10 (continued). Specific work of fracture for crack initiation as a function of ligaments length. $w_{E,i:}$ crack initiation specific work (closed circles) and $w_{E,t:}$ total specific work (open circles) for a) 27TPS/PLA, b) 27TPS/PLAg, c) 27TPS/PLA/2MMT and d) 27TPS/PLAg/2MMT. The lines represent least square fits.

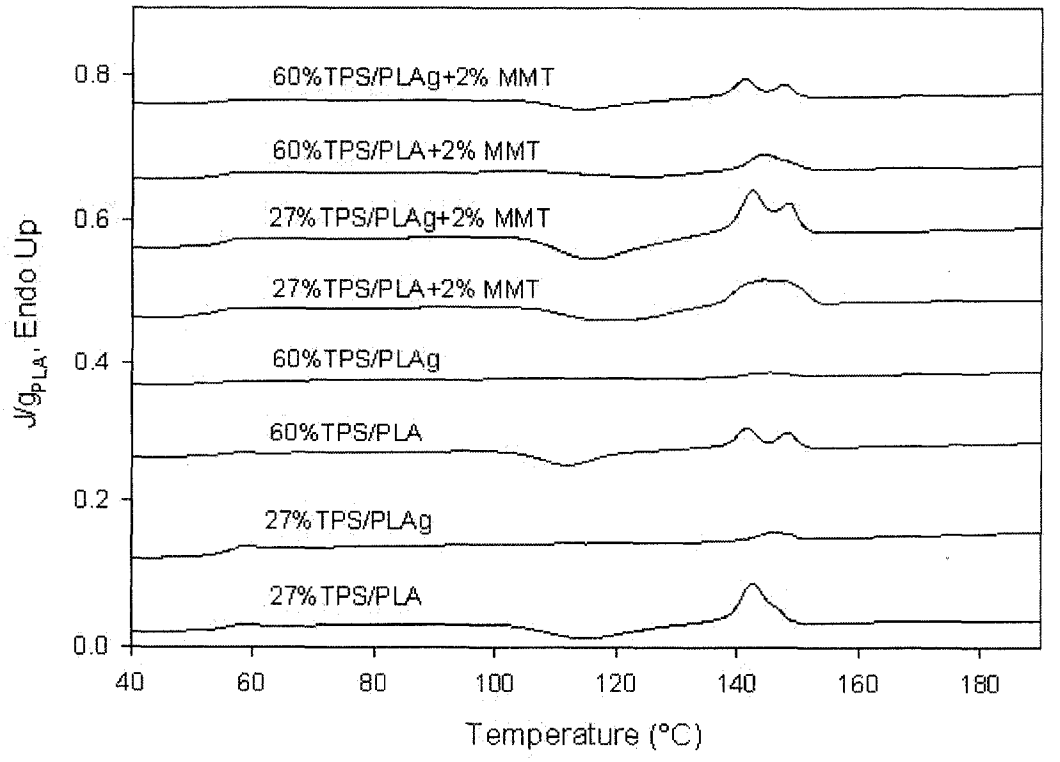

Figure 5.11. DSC Thermograms of TPS/PLA blends and nanocomposites.
a) 27TPS/PLA, b) 27TPS/PLAg, c) 60TPS/PLA, d) 60TPS/PLAg, e) 27TPS/PLA+2% MMT , f) 27TPS/PLAg + 2% MMT, g) 60TPS/PLA + 2% MMT, h) 60TPS/PLAg + 2%MMT.

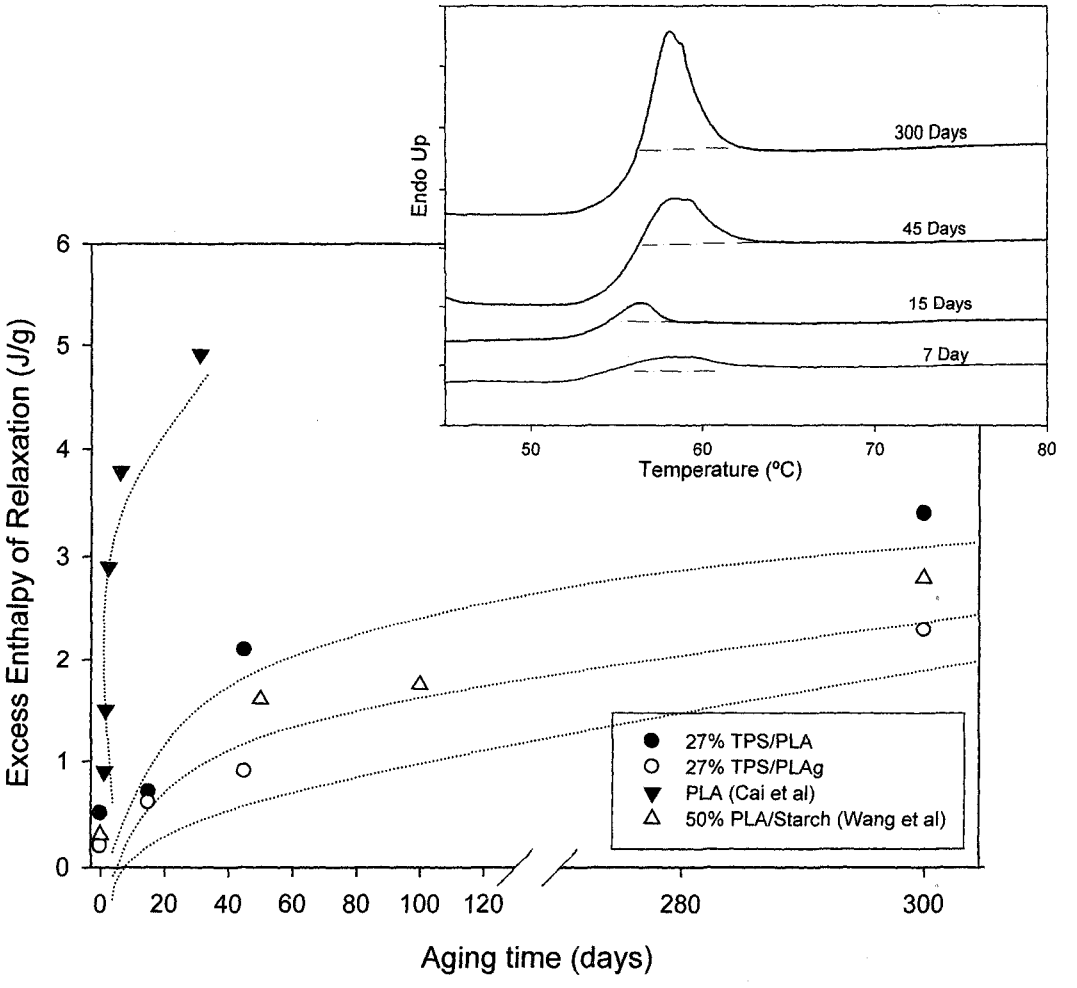

Figure 5.12. Excess enthalpy relaxation as a function of aging time for TPS/PLA blends, PLA [53] and PLA/Starch [54]. In detail: DSC Thermograms of the TPS/PLA blend (w/w, 27/73) aged at 25 °C and 50%HR for various length of time (7, 15, 45 and 300 days).

Table 5.1. Tensile mechanical properties of investigated materials after injection molding and after 300 days. Standard deviations are reported between parentheses.

Material	TPS (wt%)	E (GPa)		σ_{max} (MPa)		ε_b (%)	
		0 Day	300 Days	0 Day	300 Days	0 Day	300 Days
PLA 0% Clay	0	3.84 (0.2)	3.67 (0.7)	57.70 (3.1)	61.13 (1.4)	5.97 (1.2)	6.18 (2.9)
2% Clay	0	3.98 (0.2)	3.91 (0.3)	48.60 (1.7)	52.74 (0.9)	5.65 (1.7)	5.76 (1.4)
5% Clay	0	4.14 (0.2)	4.07 (0.2)	45.80 (1.4)	51.63 (0.9)	6.44 (1.2)	7.53 (2.0)
PLAg 0% Clay	0	3.82 (0.3)	3.80 (0.3)	45.70 (1.3)	55.23 (0.7)	8.12 (2.9)	7.43 (3.8)
2% Clay	0	3.89 (0.1)	3.81 (0.1)	45.00 (2.4)	53.14 (0.9)	9.29 (4.2)	9.88 (2.1)
5% Clay	0	4.22 (0.3)	4.03 (0.2)	46.20 (2.2)	51.83 (0.7)	8.75 (2.9)	8.55 (2.2)
27TPS/PLA 0% Clay	27	2.95 (0.3)	2.50 (0.1)	29.10 (1.2)	32.24 (0.5)	7.38 (1.1)	16.30 (3.7)
2% Clay	27	3.34 (0.1)	2.28 (0.2)	35.60 (0.7)	27.02 (0.5)	4.00 (0.3)	5.41 (1.1)
60TPS/PLA 0% Clay	60	1.44 (0.1)	1.27 (0.1)	17.10 (1.2)	17.69 (0.5)	19.09 (2.3)	28.74 (4.3)
2% Clay	60	2.21 (0.2)	2.43 (0.2)	20.21 (0.2)	22.31 (0.2)	14.42 (5.1)	21.22 (10.9)
27TPS/PLAg 0% Clay	27	2.48 (0.1)	2.51 (0.1)	39.40 (1.5)	40.02 (0.6)	50.35 (31.3)	44.97 (32.9)
2% Clay	27	2.47 (0.1)	2.24 (0.1)	28.30 (1.1)	27.81 (0.5)	4.68 (0.6)	6.69 (1.3)
5% Clay	27	2.73 (0.3)	2.01 (0.2)	30.80 (0.7)	25.86 (1.4)	4.05 (0.3)	6.28 (1.7)
60TPS/PLAg 0% Clay	60	1.28 (0.3)	1.27 (0.3)	13.21 (1.60)	15.08 (0.1)	60.07 (15.2)	67.0 (12.3)
2% Clay	60	1.34 (0.1)	1.09 (0.1)	16.20 (1.0)	15.10 (0.7)	10.91 (2.6)	13.43 (2.7)
5% Clay	60	1.89 (0.2)	1.77 (0.1)	16.37 (1.2)	19.44 (1.1)	9.48 (0.7)	10.4 (0.9)

Table 5.2. EWF test results

Materials		$w_{E,ini}$ (kJ/m^2)	$(\beta w_P)_{ini}$ (MJ/m^3)	r^2	$w_{E,total}$ (kJ/m^2)	$(\beta w_P)_{total}$ (MJ/m^3)	r^2
PLA	0% Clay	7.91	0.06	0.02	13.09	0.27	0.23
	2% Clay	2.38	0.32	0.46	2.87	0.53	0.88
	5% Clay	3.31	0.31	0.74	5.40	0.61	0.75
PLAg	0% Clay	6.11	0.06	0.04	11.83	0.30	0.39
	2% Clay	2.17	0.50	0.46	4.59	0.69	0.69
	5% Clay	4.35	0.18	0.61	4.89	0.46	0.72
27TPS/PLA							
	0% Clay	2.88	0.28	0.73	5.18	0.94	0.93
	2% Clay	2.33	0.12	0.42	2.92	0.38	0.77
60TPS/PLA							
	0% Clay	1.82	0.174	0.64	3.45	0.65	0.77
	2% Clay	3.4	0.19	0.63	7.27	0.89	0.86
27TPS/PLAg							
	0% Clay	7.56	0.41	0.73	10.22	0.61	0.87
	2% Clay	2.98	0.22	0.63	4.69	0.90	0.83
	5% Clay	2.32	0.08	0.37	1.48	0.35	0.82
60TPS/PLAg							
	0% Clay	2.95	0.18	0.74	4.84	0.44	0.79
	2% Clay	2.45	0.41	0.82	6.96	1.45	0.93
	5% Clay	2.30	0.38	0.94	7.40	1.32	0.92

r^2: squared correlation coefficient

CHAPTER 6

GENERAL DISCUSSION

This study focus on the ductility enhancement of the material resulting from montmorillonite added to polylactide thermoplastic starch blends. The following findings related to nanocomposites were observed,

- The segregation effect for MMT, which remained inside the TPS phase or along the blend interface or even crossing the interface from PLA to TPS, was unexpected. This effect manifests the strong polar affinity between TPS and MMT and the lack of it between MMT and PLA. In addition, the preferential location of MMT along the interface might be due to an effect of glycerol migration towards the interface. Glycerol is expected to form a layer along the interface, attracting the MMT towards this position. This last assumption needs to be further corroborated to this nanocomposites system. However, the attraction between MMT and glycerol has been already assumed (Chen & Evans (2005)).
- The segregation effect in the montmorillonite clay is also responsible for the localized clay concentration inside the TPS phase which was superior to the nominal concentration for the whole material. This increase of clay concentration, in some cases surpassing the 5%, obstructed the intercalation and exfoliation clay mechanics.

- The introduction of nanoparticles in polymer matrices provides evidence of enhancement in the nanocomposites properties, in particular mechanical properties for low clay concentrations. At high concentrations, the material exhibit ceramic behavior. Consequently, the reduction of clay concentration for future tests is recommendable as well as the use of a chemical agent to reach and enhance the homogeneous exfoliation in both phases, and avoid the accumulation at the TPS phase.
- Fracture toughness, studied by the essential work of fracture method, and the tensile properties of the nanocomposites seems to be negatively affected. Clay accumulation is again responsible for this behavior. The TPS was embrittled by the clay, but at high TPS concentrations, where the clay accumulation was lower, the fracture toughness and some tensile properties were improved showing the effect of addition and accumulation of clay in the TPS/PLA blends.

CHAPTER 7

CONCLUSIONS AND RECOMMENDATIONS

7.1 Conclusions

The following conclusions about processing and characterization of TPS/PLA/MMT nanocomposites were extracted from this study.

- The slurry approach combined with melt extrusion, proved to be an adequate method to incorporate Na-Montmorillonite (MMT) into PLA/TPS blends and produce TPS/PLA/MMT nanocomposites.
- In this study, water is used as a pre-dispersant of pristine untreated montmorillonite. The MMT dispersion started during the initial mixing of the starch, water and MMT, and then it continues when the starch/MMT slurry was pumped and intensively mixed across the first part of the twin-screw extruder. The water dispersion implies the water molecules pre-occupied clay interlayer positions, increasing the interlayer spacing of the natural montmorillonite, forming strong hydrogen bond interactions between water and MMT, and promoting the starch macromolecular chains to diffuse easily between the clay platelets and anchoring on the silicate surface.
- In the incorporation of MMT by starch slurry to produce TPS/PLA nanocomposites, Na-MMT showed a preferable trend to remain inside the TPS phase or along the interface. A limited migration of MMT between phases was also noticeable. However, when MMT and PLA were incorporated together, an unexpected migration of MMT from the PLA phase to the blend interface, even crossing the interface into

the TPS phase, was observed. This behavior is supposedly due to strong polar interactions between Na-MMT and TPS and the repellent forces between Na-MMT and hydrophobic PLA, creating this segregation effect.

- The tendency of MMT to remain inside the TPS phase caused the clay concentration at TPS phase to be superior to the nominal concentration (2 or 5% MMT) for the nanocomposites. This effect complicated the intercalation and exfoliation process of MMT into TPS phase and provoked reductions in the tensile properties and fracture toughness of nanocomposites in particular at low TPS concentrations, where the MMT concentration is high.
- The addition of MMT increased the tensile modulus of the material. This effect was most noticeable in TPS rich blends since the tensile modulus of the TPS is much lower than that of PLA.
- The fracture toughness in TPS/PLA blends was enhanced with the incorporation of maleic anhydride. ($w_{E,ini}$ was enhanced in 160% at 27%TPS, and 62% at 60%TPS). The incorporation of clay in TPS/PLA blends decreased the fracture toughness of nanocomposites ($w_{E,ini}$ was reduced in 60% and 70% at 27%TPS/PLAg and 17% and 22% at 60%TPS/PLAg with the addition of 2 and 5% MMT). However, the $w_{E,total}$ was enhanced only at 60%TPS, this suggest a better MMT dispersion at high starch concentrations, which is in agreement with the XRD results.
- The elongation at break in TPS/PLA blends was improved with the addition of maleic anhydride. However, it decreases with the incorporation of MMT into the blends; the reduction was evident at low concentration of TPS, indicating embrittling of the TPS

phase by MMT. It was postulated, the clay, preferentially located at the blends interface, and the accumulation of MMT in TPS phase, specially at low concentration of TPS, could reduce the interaction between the PLA and TPS phases in compatibilizer blends resulting in lower stress transfer from the PLA matrix into the TPS dispersed phase, and thus explaining the reduction in the fracture toughness and elongation at break in our nanocomposites.

- The effect of interfacial modification with the incorporation of maleic anhydride (MA) showed effective to reduce the TPS phase size, enhance the interfacial adhesion between TPS and PLA, and improved the elongation at break in the TPS/PLA blends.
- The morphology for TPS went from a coarse TPS domain structure with poor dispersion to a round fine TPS with good dispersion, confirming PLAg is effective in reducing the TPS phase size. The addition of MA also diminished the effects produced in the morphology by the addition of MMT in TPS/PLA blends. However the effect on fracture toughness, elongation at break and the MMT dispersion/intercalation in our nanocomposites was not significant.
- In TPS/PLA blends the TPS phase increased the crystallization rate of PLA, but not when the TPS was added to the PLAg. The incorporation of MMT provoked a slight increase in non-isothermal crystallization of PLA. The MMT aggregates acted as nucleation agents during PLA crystallization.
- Finally, increments in the excess enthalpy of relaxation in time were observed by DSC in TPS/PLA blends. The tensile properties in TPS/PLA blends and nanocomposites were tested over a period of 300 days and showed marginal

increments in the elongation at break and the elastic modulus while the tensile strength remained stable for the compatibilized and uncompatibilized TPS/PLA blends and their nanocomposites. Thus, it was shown the TPS/PLA blends and their nanocomposites have stable mechanical properties over a period of 300 days, the detected increment of the excess enthalpy of relaxation has no significant effect on the tensile properties and, the TPS particles are sufficiently well encapsulated in the PLA matrix to prevent changes in plasticization or significant increase in humidity level.

7.2 Recommendations

- Based on our results, the slurry-approach/melt-extrusion method seems to be a viable alternative to prepare nanocomposites of pristine montmorillonite with other non-water soluble polymer matrices.
- The observed tendency of MMT to remain into the TPS phase or along the blend interface causes a high concentration of clay in TPS. Therefore, it was necessary to decrease clay concentrations (e.g. 0.5% and 0.2%) in order to reach a better degree of intercalation/exfoliation and improvement in terms of fracture toughness and elongation at break.
- The biodegradability of the bio-based materials developed in this study and the effects on the biodegradation of TPS/PLA blends with addition of natural clay should be investigated.

- The materials studied have potential application in the food packaging industry. With this application in mind, the water vapor transmission rate with clay concentration should be assessed.
- The search and incorporation of an agent containing an active group, which reacts with starch molecules and PLA chains promoting the clay intercalation exfoliation joint to maleic anhydride grafted, is necessary to improve the fracture toughness and better stress transfer between domains.
- Alternative ways to improve the clay intercalation and exfoliation degrees are varying the sonication time, or/and the use of hot water at different temperatures during the preliminary mixing of water, starch and MMT.

REFERENCES

Alexandre M., Dubois P. (2000). Polymer-layered silicate nanocomposites: Preparation, properties and uses of a new class of materials. *Mater Sci Eng R Rep,* 28:1-2, 1-63

Anderson K.S., Schreck K.M., Hillmyer M.A. (2008). Toughening polylactide. *Polymer Reviews,* 48:1, 85-108

Auras R.A., Singh S.P., Singh J.J. (2005). Evaluation of oriented poly(lactide) polymers vs. existing PET and oriented PS for fresh food service containers. *Pack Technol Sci,* 18:4, 207-216

Barany T., Czigany T., Karger-Kocsis J. (2003). Essential work of fracture concept in polymers. *Period Polytech Mech Eng,* 47:2, 91-102

Bastioli C. (2005). *Handbook of Biodegradable polymers*. Shawbury: Rapra Technology Limited.

Bharadwaj R.K. (2001). Modeling the barrier properties of polymer-layered silicate nanocomposites. *Macromolecules,* 34:26 9189 -9192

Broberg K.B. (1968). Critical review of some theories in fracture mechanics. *Int J Fract,* 4, 11-18

Broberg K.B. (1975). On stable crack growth *J Mech Phys Solids,* 23:3, 215-237

Broberg K.B. (1982). The foundations of fracture mechanics. *Eng. Fract. Mech.,* 16:4, 497-515

Broek D. (1984). *Elementary engineering fracture mechanics*. The Hague: Martinus Nijhoff Publishers.

Bucknall C.B. (2007). New criterion for craze initiation. *Polymer,* 48:4, 1030-1041

Bui H.D. (2006). *Fracture Mechanics. Inverse Problems and Solutions.* Dordrecht: Springer.

Bureau M.N., Perrin-Sarazin F., Ton-That M.T. (2004). Polyolefin nanocomposites: Essential work of fracture analysis. *Polym. Eng. Sci.,* 44:6, 1142-1151

Bureau M.N., Ton-That M.T., Perrin-Sarazin F. (2006). Essential work of fracture and failure mechanisms of polypropylene-clay nanocomposites. *Eng. Fract. Mech,* 73:16, 2360-2374

Capkova P., Votinsky J. (2000). Molecular mechanics simulations of intercalates. *Mol Cryst Liq Cryst Sci Technol Sect A Mol Crys Liq Cryst,* 341, 301-307

Chen B., Evans J.R.G. (2005). Thermoplastic starch-clay nanocomposites and their characteristics. *Carbohydr Polym,* 61:4, 455-463

Chen B., Evans J.R.G. (2006). Elastic moduli of clay platelets. *Scripta Mater,* 54:9, 1581-1585

Ching E.C.Y., Poon W.K.Y., Li R.K.Y., Mai Y.-W. (2000). Effect of strain rate on the fracture toughness of some ductile polymers using the essential work of fracture (EWF) approach. *Polym. Eng. Sci.,* 40:12, 2558-2568

Chiu C.-W., Cheng W.-T., Wang Y.-P., Lin J.-J. (2007). Fine dispersion of hydrophobic silicate platelets in anhydride-cured epoxy nanocomposites. *Ind. Eng. Chem. Res.,* 46:22, 7384-7388

Chun-Hsin L., Nairn J.A. (1998). Using the essential work of fracture method for studying physical aging in thin, ductile, polymeric films. *Polym. Eng. Sci.,* 38:1, 186-193

Clutton E.Q. (2000). *ESIS TC4 Experience with the essential work of fracture method.* Paper presented at the Conference on fracture of polymer, composites and adhesives.

Clutton E.Q. (2001). *Fracture Mechanics Testing Methods for Polymer, Adhesives and Composites.* In D. R. More, A.Pavan & J. G. Williams, (pp. 177-195). Oxford: Elsevier Science.

Cotterell B., Reddel J.K. (1977). The essential work of plane stress ductile fracture. *Int J Fract,* 13:3, 267-277

Di Y., Iannace S., Di Maio E., Nicolais L. (2005). Poly(lactic acid)/organoclay nanocomposites: Thermal, rheological properties and foam processing. *J Polym Sci Part B,* 43:6, 689-698

Fasce L., Bernal C., Frontini P., Mai Y.-W. (2001). On the Impact Essential Work of Fracture of Ductile Polymers. *Polym. Eng. Sci.,* 41:1, 1-14

Favis B.D., Rodriguez-Gonzalez F., Ramsay B.A. (2003). Polymer Compositions Containing Thermoplastic Starch. *U.S. Patent 6, 605, 657*

Favis B.D., Rodriguez-Gonzalez F., Ramsay B.A. (2005). Method of Making Polymer Compositions Containing Thermoplastic Starch. *U.S. Patent 6,844,380*

Ferrer-Balas D., Maspoch M.L., Martinez A.B., Santana O.O. (1999). On the essential work of fracture method: Energy partitioning of the fracture process in iPP films. . *Polymer Bulletin,* 42, 101-108

Fischer H., Fischer S. (2001). Biodegradable Thermoplastic Material. *World Intellectual Property Organization Patent WO 01/68762 A1*

Frankowski D.J., Capracotta M.D., Martin J.D., Khan S.A., Spontak R.J. (2007). Stability of Organically Modified Montmorillonites and Their Polystyrene Nanocomposites After Prolonged Thermal Treatment *Chem. Mater,* 19:11, 2757-2767

Fung K.L., Zhao H.X., Wang J.T., Meng Y.Z., Tjong S.C., Li R.K.Y. (2004). Essential work of fracture (EWF) analysis for compression molded alternating polypropylene carbonate. *Polym. Eng. Sci.,* 44:3, 580-587

Garlotta D. (2001). A literature review of poly(lactic acid). *J. Polym. Environ.,* 9:2, 63-84

Gdoutos E.E. (2005). *Fracture Mechanics: An introduction* (2nd ed. Vol. 123). Xanthi, Greece: Springer.

Gong G., Xie B.-H., Yang W., Li Z.-M., Zhang W.-Q., Yang M.-B. (2005). Essential work of fracture (EWF) analysis for polypropylene grafted with maleic anhydride modified polypropylene/calcium carbonate composites. *Polym Test,* 24:4, 410-417

Grein C., Plummer C.J.G., Germain Y., Kausch H.H., Beguelin P. (2003). Essential work of fracture of polypropylene and polypropylene blends over a wide range of test speeds. *Polym. Eng. Sci.,* 43:1, 223-233

Guerard D., Elalem N.E., El Hadigui S., Ansari L., Lagrange P., Rousseaux F., Estrade-Szwarckopf H., Conard J., Lauginie P. (1986). Preparation and intercalation into graphite of some alkali metal hybrides. *J. Less-Common Metals,* 131, 173-180

Halpin J.C., Kardos J.L. (1976). Halpin-Tsai Equations:A Review. *Polym. Eng. Sci.,* 16:5, 344-352

Hasegawa N., Okamoto H., Kato M., Usuki A., Sato N. (2003). Nylon 6/Na-montmorillonite nanocomposites prepared by compounding nylon 6 with Na-montmorillonite slurry. *Polymer,* 44:10, 2933-2937

Hashemi S. (1993a). Ductile fracture of polyester films. *Plast. Rubber Compos. Process. Appl.,* 20:4, 229-237

Hashemi S. (1993b). Plane-stress fracture of polycarbonate films. *J. Mater. Sci.,* 28:22, 6178-6184

Hashemi S. (1997). Fracture toughness evaluation of ductile polymeric films. *J. Mater. Sci.,* 32:6, 1563-1573

Hashemi S. (2000a). Determination of the fracture toughness of polybutylene terephthalate (PBT) film by the essential work method: Effect of specimen size and geometry. *Polym. Eng. Sci.,* 40:3, 798-808

Hashemi S. (2000b). Temperature and deformation rate dependence of the work of fracture in polycarbonate (PC) film. *J. Mater. Sci.,* 35:23, 5851-5856

Hashemi S. (2000c). Temperature dependence of work of fracture parameters in polybutylene terephthalate (PBT). *Polym. Eng. Sci.,* 40:6, 1435-1446

Hashemi S., Williams J.G. (2000). Temperature dependence of essential and non-essential work of fracture parameters for polycarbonate film. *Plast. Rubber Compos.,* 29:6, 294-302

Hashemi S., Yuan Z. (1994). Fracture of poly(ether-ether ketone) films. *Plast. Rubber Compos. Process. Appl.,* 21, 151-161

Hbaieba K., Wangb Q.X., Chiaa Y.H.J., Cotterel B. (2007). Modelling stiffness of polymer/clay nanocomposites. *Polym. Bull,* 48 3, 901 -909

Herold A., Billaud D., Guerard D., Lagrange P., El Makrini M. (1980). Intercalation of metals and alloys into graphite. *Physica B,* 105:1-3, 253-260

Herrera N.N., Letoffe J.M., Putaux J.L., David L., Bourgeat-Lami E. (2004). Aqueous dispersions of silane-functionalized laponite clay platelets. A first step toward the elaboration of water-based polymer/clay nanocomposites. *Langmuir,* 20:5, 1564-1571

Huang M.F., Yu J.G., Ma X.F. (2004). Studies on the properties of Montmorillonite-reinforced thermoplastic starch composites. *Polymer,* 45:20, 7017-7023

Huneault M.A., Li H. (2007). Morphology and properties of compatibilized polylactide/thermoplastic starch blends. *Polymer,* 48:1, 270-280

Hussain F., Hojjati M., Okamoto M., Gorga R.E. (2006). Review article: polymer-matrix nanocomposites, processing, manufacturing, and application: an overview. *J. Compos. Mater.,* 40:17, 1511-1575

Jang B.Z., Uhlmann D.R., Vander Sande J.B. (1985). Crazing in polypropylene. *Polym. Eng. Sci.,* 25:2, 98-104

Jingshen W., Yiu-Wing M. (1996). The essential fracture work concept for toughness measurement of ductile polymers. *Polym. Eng. Sci.,* 36:18, 2275-2288

Kalambur S., Rizvi S.S.H. (2005). Biodegradable and functionally superior starch-polyester nanocomposites from reactive extrusion. *J. Appl. Polym. Sci.,* 96:4, 1072-1082

Karger-Kocsis J. (1996). How does 'phase transformation toughening' work in semicrystalline polymers? *Polym. Eng. Sci.,* 36:2, 203-210

Kato M., Matsushita M., Fukumori K. (2004). Development of a new production method for a polypropylene-clay nanocomposite. *Polym. Eng. Sci.,* 44:7, 1205-1211

Kausch H.H., Argon A.S., Berger L.L., Cohen R.E., Dettenmaier M., Doll W., Hara M., Ishikawa M., Konczol L., Kramer E.J., Leberger D., Narisawa I., Sauer J.A., Schirrer R., Takemori M.T. (1983). *Crazing in polymers.* Berlin: Springer-Verlag.

Ke T., Sun X. (2001). Effects of Moisture Content and Heat Treatment on the Physical Properties of Starch and Poly(lactic acid) Blends. *J. Appl. Polym. Sci.,* 81:12, 3069-3082

Ke Y.C., Stroeve P. (2005). *Polymer Layered Silicate and Silica Nanocomposites.* Amsterdam: Elsevier B.V.

Kinloch A.J., Young R.J. (1983). *Fracture Behaviour of Polymers.* London: Applied Science Publishers.

Krikorian V., Pochan D.J. (2003). Poly (L-Lactic Acid)/Layered Silicate Nanocomposite: Fabrication, Characterization, and Properties. *Chem. Mater.,* 15:22, 4317-4324

Krishnamoorti R., Vaia R.A., Giannelis E.P. (1996). Structure and Dynamics of Polymer-Layered Silicate Nanocomposites. *Chem. Mater.,* 8:8, 1728

Kubies D., Scudla J., Puffr R., Sikora A., Baldrian J., Kovarova J., Slouf M., Rypacek F. (2006). Structure and mechanical properties of poly(l-lactide)/layered silicate nanocomposites. *Eur Polym J,* 42:4, 888-899

Kwon H.J., Jar P.Y.B. (2005). Fracture toughness of polymers in shear mode. *Polymer,* 46:26, 12480-12492

Kwon H.J., Jar P.Y.B. (2007). New energy partitioning approach to the measurement of plane-strain fracture toughness of high-density polyethylene based on the concept of essential work of fracture. *Eng. Fract. Mech.,* 74:16, 2471-2480

Lauke B., Schueller T. (2001). Essential work of interfacial fracture: A method to characterize adhesion at polymer-polymer interfaces. *Int J Adhes Adhes,* 21:1, 55-58

LeBaron P.C., Wang Z., Pinnavaia T.J. (1999). Polymer-layered silicate nanocomposites: An overview. *Appl Clay Sci,* 15:1, 11-29

Lee C.H., Kim H.B., Lim S.T., Choi H.J., Jhon M.S. (2005). Biodegradable aliphatic polyester-poly (epichlorohydrin) blend/organoclay nanocomposites; Synthesis and rheological characterization. *J. Mater. Sci.,* 40:15, 3981-3985

Lee D.C., Jang L.W. (1996). Preparation and characterization of PMMA-clay hybrid composite by emulsion polymerization. *J. Appl. Polym. Sci.,* 61:7, 1117-1122

Lee S.-R., Park H.-M., Lim H., Kang T., Li X., Cho W.-J., Ha C.-S. (2002). Microstructure, tensile properties, and biodegradability of aliphatic polyester/clay nanocomposites. *Polymer,* 43:8, 2495-2500

Lepoittevin B., Devalckenaere M., Pantoustier N., Alexandre M., Kubies D., Calberg C., Jerome R., Dubois P. (2002). Poly (ε-caprolactone)/clay nanocomposites prepared by melt intercalation: mechanical, thermal and rheological properties. *Polymer,* 43:14, 4017-4023

Lim S.T., Hyun Y.H., Choi H.J., Jhon M.S. (2002). Synthetic Biodegradable Aliphatic Polyester/Montmorillonite Nanocomposites. *Chem. Mater.,* 14:4, 1839-1844

Liu X., Wu Q. (2001). PP/clay nanocomposites prepared by grafting-melt intercalation. *Polymer,* 42:25, 10013-10019

Luduena L.N., Alvarez V.A., Vazquez A. (2007). Processing and microstructure of PCL/clay nanocomposites. *Mater. Sci. Eng. A,* 460-461, 121-129

Ma J., Yu Z.Z., Kuan H.C., Dasari A., Mai Y.W. (2005). A new strategy to exfoliate silicone rubber/clay nanocomposites. *Macromol. Rapid Commun.,* 26:10, 830-833

Ma X., Yu J., Wang N. (2007). Production of thermoplastic starch/ MMT-sorbitol nanocomposites by dual-melt extrusion processing. *Macromol. Mater. Eng.,* 292:6, 723-728

Mai Y.W., Cotterell B. (1985). Effect of specimen geometry on the essential work of plane stress ductile fracture. *Eng. Fract. Mech.,* 21:1, 123-128

Mai Y.W., Cotterell B. (1986). On the essential work of ductile fracture in polymers *Int J Fract,* 32:2, 105-125

Mai Y.W., Cotterell B., Horlyck R., Vigna G. (1987). Essential work of plane stress ductile fracture of linear polyethylenes. *Polym. Eng. Sci.*, 27:11, 804-809

Mai Y.W., Powell P. (1991). Essential work of fracture and J-integral measurements for ductile polymers. *J Polym Sci Part B,* 29:7, 785-793

Mai Y.W., Yu Z.Z. (2006). *Polymer nanocomposites*. Boca Raton , Woodhead Publishing limited.

Maiti P., Yamada K., Okamoto M., Ueda K., Okamoto K. (2002). New polylactide/layered silicate nanocomposites: Role of organoclays. *Chem. Mater.,* 14:11, 4654-4661

Marks J.E. (1999). *Polymer data handbook*. New York, Oxford University Press.

Martin O., Averous L. (2001). Poly(lactic acid): Plasticization and properties of biodegradable multiphase systems. *Polymer,* 42:14, 6209-6219

Mehta R., Kumar V., Bhunia H., Upadhyay S.N. (2005). Synthesis of poly(lactic acid): A review. *J. Macromol. Sci., Polym. Rev.,* 45:4, 325-349

Moore D.R., Pavan A., Williams J.G. (2001). *Fracture Mechanics Testing Methods for Polymer Adhesives and Composites*. Amsterdam: Elsevier.

Mouzakis D.E., Karger-Kocsis J., Moskala E.J. (2000). Interrelation between energy partitioned work of fracture parameters and the crack tip opening displacement in amorphous polyester films. *J Mater Sci Lett,* 19:18, 1615-1619

Noh M.W., Lee D.C. (1999). Synthesis and characterization of PS-clay nanocomposite by emulsion polymerization. *Polymer Bulletin,* 42:5, 619-626

Ogata N., Jimenez G., Kawai H., Ogihara T. (1997). Structure and thermal/mechanical properties of poly(l-lactide)-clay blend. *J Polym Sci Part B,* 35:2, 389-396

Okada A., Fukushima Y., Kawasumi M., Inagaki S., Usuki A., Sugiyama S., Kurauchi T., Kamigaito O. (1988). *U. S Patent No. 4739007.* U. S. Patent.

Okada A., Usuki A. (2006). Twenty years of polymer-clay nanocomposites. *Macromol. Mater. Eng.,* 291:12, 1449-1476

Park H.M., Lee W.K., Park C.Y., Cho W.J., Ha C.S. (2003). Environmentally friendly polymer hybrids Part I mechanical, thermal, and barrier properties of thermoplastic starch/clay nanocomposites. *J. Mater. Sci.,* 38:5, 909-915

Park H.M., Li X., Jin C.Z., Park C.Y., Cho W.J., Ha C.S. (2002). Preparation and Properties of Biodegradable Thermoplastic Starch/Clay Hybrids. *Macromol. Mater. Eng.,* 287:8, 553-558

Paton C.A., Hashemi S. (1992). Plane-stress essential work of ductile fracture for polycarbonate. *J. Mater. Sci.,* 27, 2279-2290

Paul M.A., Alexandre M., Degee P., Henrist C., Rulmont A., Dubois P. (2003). New nanocomposite materials based on plasticized poly(L-lactide) and organo-modified montmorillonites: thermal and morphological study. *Polymer,* 44:2, 443-450

Perez N. (2004). *Fracture Mechanics.* Boston: Kluwer Academic Publisher.

Pluta M. (2006). Melt compounding of polylactide/organoclay: Structure and properties of nanocomposites. *J Polym Sci Part B,* 44:23, 3392-3405

Pluta M., Galeski A., Alexandre M., Paul M.A., Dubois P. (2002). Polylactide/montmorillonite nanocomposites and microcomposites prepared by melt blending: Structure and some physical properties. *J. Appl. Polym. Sci.,* 86:6, 1497-1506

Poon W.K.Y., Ching E.C.Y., Cheng C.Y., Li R.K.Y. (2001). Measurement of plane stress essential work of fracture (EWF) for polymer films: Effects of gripping and notching methodology. *Polym Test,* 20:4, 395-401

Poutanen K., Forssell P. (1996). Modification of strach properties with plasticizer. *Trends Polymer Sci,* 4:4, 128-132

Ray S.S., Okamoto K., Okamoto M. (2003). Structure-property relationship in biodegradable poly(butylene succinate)/layered silicate nanocomposites. *Macromolecules,* 36:7, 2355-2367

Rodriguez-Gonzalez F.J., Ramsay B.A., Favis B.D. (2003). High performance LDPE/thermoplastic starch blends: A sustainable alternative to pure polyethylene. *Polymer,* 44:5, 1517-1526

Roesler J., Harders H., Baeker M. (2007). *Mechanical Behaviour of Engineering Materials*. Berlin: Springer.

Rozin A.T., Komarov V.S., Berezutskii S.S., Akulich N.A. (1974). Nature of the hydroxyl groups in montmorillonite. *J. Appl. Spectrosc.,* 21:1, 132-135

Sanchez-Garcia M.D., Gimenez E., Lagaron J.M. (2008). Morphology and barrier properties of nanobiocomposites of poly(3-hydroxybutyrate) and layered silicates. *J. Appl. Polym. Sci.,* 108:5, 2787-2801

Semba T., Kitagawa K., Ishiaku U.S., Hamada H. (2006). The effect of crosslinking on the mechanical properties of polylactic acid/polycaprolactone blends. *J. Appl. Polym. Sci.,* 101:3, 1816-1825

Shen Z., Simon G.P., Cheng Y.-B. (2002). Comparison of solution intercalation and melt intercalation of polymer-clay nanocomposites. *Polymer,* 43:15, 4251-4260

Shih Y.F., Wang T.Y., Jeng R.J., Wu J.Y., Teng C.C. (2007). Biodegradable nanocomposites based on poly(butylene succinate)/organoclay. *J. Polym. Environ.,* 15:2, 151-158

Shin B.Y., Lee S.I., Shin Y.S., Balakrishnan S., Narayan R. (2004). Rheological, mechanical and biodegradation studies on blends of thermoplastic starch and polycaprolactone. *Polym. Eng. Sci.,* 44:8, 1429-1438

Sinha Ray S., Maiti P., Okamoto M., Yamada K., Ueda K. (2002). New polylactide/layered silicate nanocomposites. 1. Preparation, characterization, and properties. *Macromolecules,* 35:8, 3104-3110

Sinha Ray S., Okamoto M. (2003a). Biodegradable polylactide and its nanocomposites: Opening a new dimension for plastics and composites. *Macromol. Rapid Commun.,* 24:14, 815-840

Sinha Ray S., Okamoto M. (2003b). Polymer/layered silicate nanocomposites: A review from preparation to processing. *Prog Polym Sci* , 28:11, 1539-1641

Sinha Ray S., Yamada K., Okamoto M., Ueda K. (2003). New polylactide-layered silicate nanocomposites. 2. Concurrent improvements of material properties, biodegradability and melt rheology. *Polymer,* 44:3, 857-866

Souther-Clay-Products. (2008). Cloisite® Na+ Typical Physical Properties Bulletin. Retrieved 06/23, 2008, from http://www.scprod.com/product_bulletins/PB%20Cloisite%20NA+.pdf

Strawhecker K.E., Manias E. (2000). Structure and Properties of Poly(vinyl alcohol)/Na+ Montmorillonite Nanocomposites. *Chem. Mater.*, 12:10, 2943-2949

Tjong S.C. (2006). Structural and mechanical properties of polymer nanocomposites. *Mater. Sci. Eng., R,* 53, 73-197

Tjong S.C., Bao S.P. (2007). Fracture toughness of high density polyethylene/SEBS-g-MA/montmorillonite nanocomposites. *Compos. Sci. Technol.*, 67, 314-323

Tjong S.C., Bao S.P., Liang G.D. (2005). Polypropylene/montmorillonite nanocomposites toughened with SEBS-g-MA: Structure-property relationship. *J Polym Sci Part B,* 43:21, 3112-3126

Utracki L.A. (2004). *Clay-containig polymeric Nanocomposites*. Shawbury: Rapra Technology limited.

Vaia R. A., Ishii H., Giannelis E.P. (1993). Synthesis and properties of two-dimensional nanostructures by direct intercalation of polymer melts in layered silicates. *Chem. Mater.*, 5, 1694-1696.

Vaia R.A., Giannelis E.P. (1994). Interlayer Structure and molecular environment of alkylammonium layered silicates. *Chem. Mater,* 6, 1017-1022

Van Soest J.J.G., Hulleman S.H.D., de Wit D., Vliegenthart J.F.G. (1996). Changes in the mechanical properties of thermoplastic potato starch in relation with changes in B-type crystallinity. *Carbohydr Polym,* 29:3, 225-232

Votinský J., Kalousová J., Benescaron L. (1992). Molecular intercalates. *J. Inclusion Phenom.Macrocyclic Chem.,* 14, 19-24

Wang C.H. (1996). *Introduction to Fracture Mechanics* Melbourne: DSTO Aeronautical and Maritime Research Laboratory.

Wang K., Chen L., Kotaki M., He C. (2007). Preparation, microstructure and thermal mechanical properties of epoxy/crude clay nanocomposites. *Compos Part A Appl Sci Manuf,* 38:1, 192-197

Wang K., Wang L., Wu J.S., Chen L., He C.B. (2005). Preparation of highly exfoliated epoxy/clay nanocomposites by "slurry compounding": Process and mechanisms. *Langmuir,* 21:8, 3613-3618

Wilhelm H.M., Sierakowski M.R., Souza G.P., Wypych F. (2003). Starch films reinforced with mineral clay. *Carbohydr Polym,* 52:2, 101-110

Wong S.C., Mai Y.W. (1999). Essential fracture work of short fiber reinforced polymer blends. *Polym. Eng. Sci.* , 39:2, 356-364

Yamakawa R.S., Razzino C.A., Correa C.A., Hage Jr E. (2004). Influence of notching and molding conditions on determination of EWF parameters in polyamide 6. *Polym Test,* 23:2, 195-202

Yoo Y., Shah R.K., Paul D.R. (2007). Fracture behavior of nanocomposites based on poly(ethylene-co-methacrylic acid) ionomers. *Polymer,* 48:16, 4867-4873

Yu L., Dean K., Dong Yang W. (2007). Preparation and characterization of melt-extruded thermoplastic starch/clay nanocomposites. *Compos. Sci. Technol.,* 67:3-4, 413-421

Yu Z.Z., Hu G.H., Varlet J., Dasari A., Mai Y.W. (2005). Water-assisted melt compounding of nylon-6/pristine montmorillonite nanocomposites. *J Polym Sci Part B,* 43:9, 1100-1112

Zhang H., Zhang Z., Yang J.-L., Friedrich K. (2006). Temperature dependence of crack initiation fracture toughness of various nanoparticles filled polyamide 66. *Polymer,* 47:2, 679-689

Zhang J.F., Sun X. (2004). Mechanical properties of poly(lactic acid)/starch composites compatibilized by maleic anhydride. *Biomacromolecules,* 5:4, 1446-1451

Zhu J., Morgan A.B., Lamelas F.J., Wilkie C.A. (2001). Fire Properties of Polystyrene-Clay Nanocomposites. *Chem. Mater.,* 13:10, 3774-3780